PhD degree in Molecular Medicine (curriculum in Molecular Oncology)

European School of Molecular Medicine (SEMM),

University of Milan and University of Naples "Federico II"

Settore disciplinare: Bio/11

Genome-wide analysis of p53-dependent programs in tumor suppression

Claudia Tonelli

IEO, Milan

Matricola n. R09387

Supervisor: Dr. Bruno Amati

IEO, Milan

Added Supervisor: Dr. Stefano Campaner

IEO, Milan

Anno accademico 2013-2014

Table of contents

List of Abbreviations

ARF: alternate open reading frame

BAX: Bcl2-associated X protein

BAK: Bcl2-antagonist/killer

BBC3: Bcl2 binding component 3

BCL2: B cell leukemia/lymphoma 2

BID: BH3 interacting domain death agonist

BSA: bovine serum albumine

CDKN1A: cyclin-dependent kinase inhibitor 1A

CypD : cyclophilin D

DBD: DNA binding domain

DDR: DNA damage response

DNA: deoxyribonucleic acid

EGR1: early growth response protein 1

ESC: embryonic stem cell

FOXP1: forkhead box protein P1

G6PD: glucose-6-phosphate dehydrogenase

GADD45: growth arrest and DNA damage inducible gene 45

GFP: green fluorescent protein

GLS2: glutaminase 2

GOF: gain-of-function

GPX1: glutathione peroxidase 1

GTP: guanosine triphosphate

hnRNP-K: heterogeneous nuclear ribonucleoprotein K

HSPC: haematopoietic stem and progenitor cell

IPA: Ingenuity Pathway Analysis

KLF: Krüppel-like factor

KO: knock-out

LFS: Li-Fraumeni syndrome

LIF: leukaemia inhibitory factor

lincRNA: long intergenic non-coding RNA

LOH: loss of heterozygosity

LSL: Lox-Stop-Lox

MDM2: mouse double minute 2

MOMP: mitochondrial outer membrane permealization

MnSOD: manganese superoxide dismutase

mRNA: messenger RNA

MYC: myelocytomatosis oncogene

NADPH: nicotinamide adenine dinucleotide phosphate

ncRNA: non-coding RNA

NFY: nuclear transcription factor Y

p53ER: p53 Estrogen Receptor

PBS: phosphate buffered saline

PI: propidium iodide

PMAIP1: phorbol-12-myristate-13-acetate-induced protein 1

PTM: post-translational modification

PPP: pentose phosphate pathway

PRD: proline-rich domain

PTP: permeability transition pore

PUMA: p53 up-regulated modulator of apoptosis

PWM: position weight matrix

Rb: retinoblastoma protein

RBP: RNA binding protein

RE: response element

RNA: ribonucleic acid

RNAi: RNA interference

ROS: reactive oxygen species

shRNA: short hairpin RNA

SNP: single nucleotide polymorphism

TAD: transcriptional activation domain

Tet: tetramerization domain

TIGAR: TP53-induced glycolysis and apoptosis regulator

TP53: tumor protein p53

TSS: transcription start site

Index of the Figures

1 Abstract

The transcriptional programs triggered by p53 during tumor suppression and in response to DNA damage remain to be clarified. Using whole genome mapping of p53 binding and gene expression profiling, we investigated the transcriptional circuitry induced by p53 in suppressing cancer development and in response to genotoxic injury. We studied the progression of Myc-induced lymphomas in Eμ-*myc* transgenic mice, as well as the regression of these lymphomas following restoration of p53 function, by either pharmacological or genetic means. In parallel, we determined the p53-dependent transcriptional program in splenic cells from mice exposed to ionizing radiation. We thus expanded our understanding of the p53 response to oncogenic and genotoxic stress and identified a set of novel components of the p53 transcriptional program. Currently, we are testing the impact of these new p53 target genes on tumorigenesis using an RNA interference (RNAi)-based functional genetic screen. Altogether our data represent an extensive characterization of the p53-regulated network in response to different stimuli and will hopefully highlight new tumor suppressive mechanisms, paving the way for their therapeutic application.

2 Introduction

The evolution of a normal cell towards a cancerous one involves stepwise accumulation of genetic and epigenetic changes that confer selective advantages to the transformed cells by disrupting the homeostatic mechanisms that govern normal cell proliferation. The alterations underlying tumorigenesis endow the neoplastic cells with several properties, including self-sufficiency of growth signals, evasion from cell cycle checkpoints and cell death, unlimited replicative potential, sustained angiogenesis, and the ability to invade and metastasize, among other tumorigenic features (1).

Importantly, two classes of genes, oncogenes and tumor suppressor genes, fuel this malignant transformation, when aberrantly regulated. Oncogenes result from mutation or overexpression of a proto-oncogene causing its hyper-activation. The protein products of proto-oncogenes normally promote proliferation or provide other pro-survival signals to the cell. Disruption of their tight regulation leads to aberrant cell cycle progression and tumorigenesis. Classical examples of oncogenes include the Ras family of GTPases and the transcription factor Myc. Conversely, tumor suppressor genes normally regulate cell proliferation and ensure genome stability, inhibiting tumor development. Tumor suppressor genes, when inactivated, increase the selective growth advantage of the tumor cell. Examples are the retinoblastoma protein (Rb), which regulates cell cycle progression, and p53, which is a central hub in a molecular network controlling cell fate. Examination of these genes will continue to provide insights in the pathways that they regulate and guide to the development of effective cancer therapies.

2.1 p53

2.1.1 p53's discovery

In 1979, six groups of investigators independently reported the discovery of a 53 kDa protein that was present in both human and mouse cells. In five of these studies, the protein was described to interact with the SV40 large T-antigen by co-precipitation using antibodies against the viral

protein (2,3,4,5,6). At the same time, Old and coworkers showed that animals immunized with chemically induced sarcomas and other transformed cells produced antisera to the same 53 kDa protein, suggesting that it was not of viral origin (7). Later, p53 was found to be expressed at high levels in a large variety of cancer cells, but not or at very low levels in normal cells (8). These initial evidences misled the scientists to believe that p53 was an oncogene with transforming capabilities. The turning point in p53 research occurred ten years after its discovery, in 1989, when in a search for a putative tumor suppressor gene on chromosome 17p, a small region that contained the *TP53* gene was identified and shown to be mutated or deleted, as initially described in colorectal tumors and then in several other tumor types (9,10). It became clear that the 'wild-type' *TP53* genes used to demonstrate p53 supposed oncogenic functions were instead mutated clones (11). It took then short time to understand that p53 was a sequence-specific transcription factor that bound DNA as a tetramer (12,13,14,15,16) and that cancer associated mutations impaired its DNA binding activity (see below).

2.1.2 *TP53* is a tumor suppressor gene

Further evidence that p53 is a *bona fide* tumor suppressor comes from patients with Li-Fraumeni syndrome (LFS), a rare familial cancer predisposition disorder associated with germline mutations of the *TP53* gene with an estimated penetrance of 90-95% (17,18,19). Children and adults are affected by a wide array of cancers that occur predominantly at younger ages, developing a characteristic tumor spectrum including sarcomas, brain tumors, breast cancers and adrenocortical carcinomas (20).

Definitive demonstration for p53's central role in tumor suppression comes from the generation of *Trp53* knock-out mice that show a dramatic, and completely penetrant predisposition to cancer development (described in more details in section 2.3.1) (21,22,23).

The importance of inactivating p53 during tumorigenesis is further confirmed by the observation that *TP53* is arguably the most frequently altered gene in human cancers. *TP53* mutations are reported to occur in almost every type of cancer at rates varying between 15% (for example, in

bone tumors) and close to 40% (for example, in ovarian, colorectal and head and neck cancers) (Fig. 1) (24).

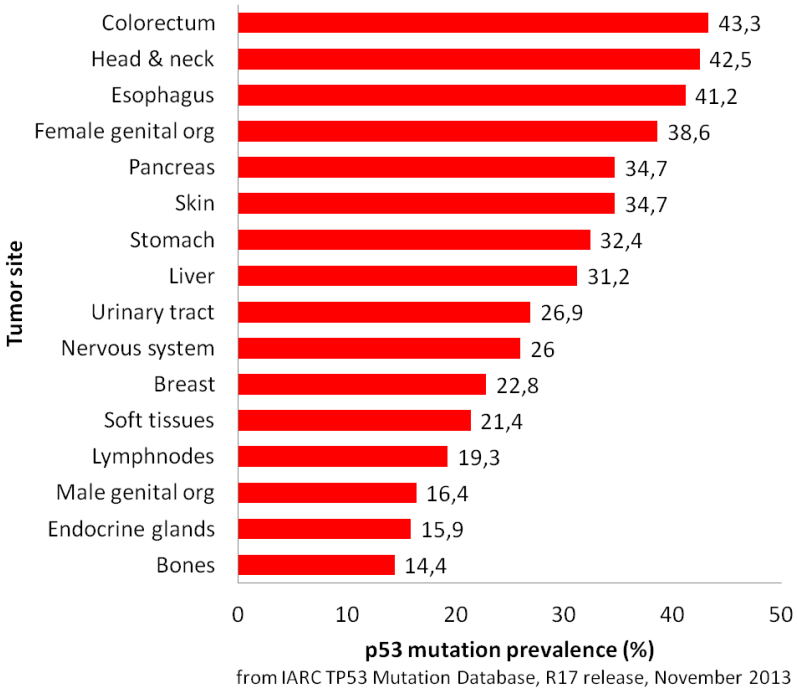

Fig. 1 - Frequency of TP53 somatic mutations in human cancers.
Data retrieved from IARC TP53 Mutation Database, R17 release, November 2013 (24).

The vast majority of *TP53* mutations identified in sporadic cancers are missense mutations that occur in all exons of the *TP53* gene, with a strong predominance in exons 4 - 9, which encode the DNA binding domain (DBD) of the protein, and in particular in six 'hot-spot' residues (Fig. 2). p53 mutants can be classified as contact mutants, which harbor mutations in p53 residues that directly contact the DNA helix, such as R248Q and R273H, and structural mutants, which carry mutations that cause either local (e.g. G245S and R249S) or global conformational distortion (e.g. R175H and R282W) (25).

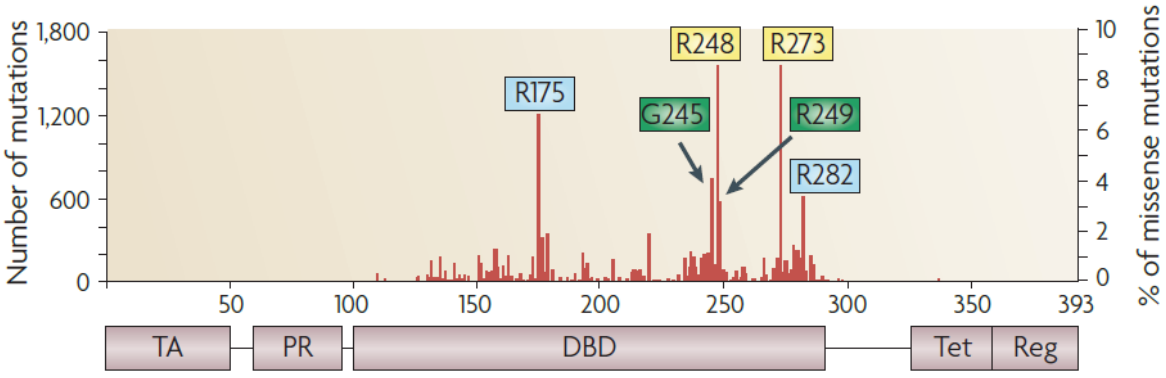

Fig. 2 - Distribution of missense mutations along the 393 amino-acid sequence of p53.
Source: Brosh R and Rotter V, Nature Reviews Cancer 2009, vol.9(10): 701-13 (25).

Ultimately, the majority of *TP53* mutations abrogate p53's ability to bind DNA in a sequence-specific manner and activate transcription of target genes, underlining how crucial p53 function as a transcription factor is for tumor suppression. p53 mutants can exert cancer-promoting effects by dominant-negative inactivation of the wild-type allele, through hetero-oligomerization of the mutant form with the wild-type form, as well as through the acquisition of gain-of-function (GOF) properties that actively promote tumor development increasing survival, proliferation, migration and invasion of the tumor cells. These GOF properties could explain why point mutations are more frequent than deletions in human cancers (25).

2.1.3 Structure of the human p53 protein

The p53 protein comprises multiple functional domains typical of transcription factors, including two transcriptional activation domains (TADs), a proline-rich domain (PRD), a sequence-specific DNA binding domain (DBD), a tetramerization domain (Tet), and C-terminal regulatory domains (Fig. 3) (26). The transactivation domains span residues 1-63 and are involved in the recruitment of histone modifying enzymes and coactivator complexes (27,28), and in the interaction with regulatory proteins, such as Mdm2 (29). C-terminal to the TADs, between residues 64-93, lies the proline-rich domain, which contains PXXP motifs, where P represents proline and X any amino acid. The main function of this domain seems to be structural, since knock-in mice carrying point mutations in the PXXP repeats appear largely normal (30), whereas complete deletion results in disruption of p53 tumor suppressive function (31). The DBD (residues 94-291) constitutes the core domain of the protein and is responsible for the sequence-specific binding to target DNA. As previously described, most cancer-associated mutations occur in this domain, underscoring the key importance of DNA binding for p53-mediated tumor suppression. The C-terminal part of p53 contains the tetramerization domain (Tet) (residues 326-354), through which p53 monomers interact to oligomerize. Finally, at the extreme C-terminus between residues 355-393, there is a basic, lysine-rich domain, which contains phosphorylation and acetylation sites and undergoes extensive post-translational modification (PTM) that modulates p53 stabilization and sequence-

specific DNA binding (32). The p53 gene is highly conserved across vertebrates, in particular the core DBD shows the highest inter-species sequence homology (33).

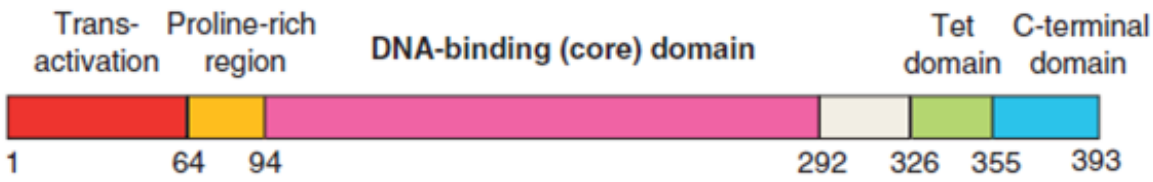

Fig. 3 - p53 structure.
Source: Joerger AC and Ferscht AR, Advances in Cancer Research 2007, vol.97: 1-23 (26).

2.1.4 p53 functions as a stress sensor

In non-transformed cells, p53 is a sensor for cellular stresses that regulates a large number of genes in response to a variety of cellular insults, including hyper-proliferative signals, DNA damage, hypoxia, nutrient deprivation, oxidative stress and many others (Fig. 4). In response to such stress signals, p53 is displaced from its negative regulators, thereby allowing its stabilization and activation through PTMs. Once activated, p53 binds its response elements and recruits diverse transcriptional coregulators such as histone modifying enzymes, chromatin remodelling factors, components of the mediator complex and of the transcription machinery to promote stress-specific and tissue-specific responses and suppress cellular transformation. As a safeguard against neoplasia, p53 drives apoptosis and senescence of irreparably damaged or malignant cells. Alternatively, p53 promotes protective, pro-survival responses such as transient cell cycle arrest and DNA repair in cells exposed to limited, reparable damage. Beyond triggering apoptosis and cell cycle arrest, p53 can regulate several additional cellular processes, including metabolic reprogramming, autophagy and signalling to the tumor microenvironment. These various responses rely primarily on p53 function as a transcription factor, but transcription-independent activities, such as direct activation of apoptosis at mitochondria, also contribute to the p53 response (32,34,35).

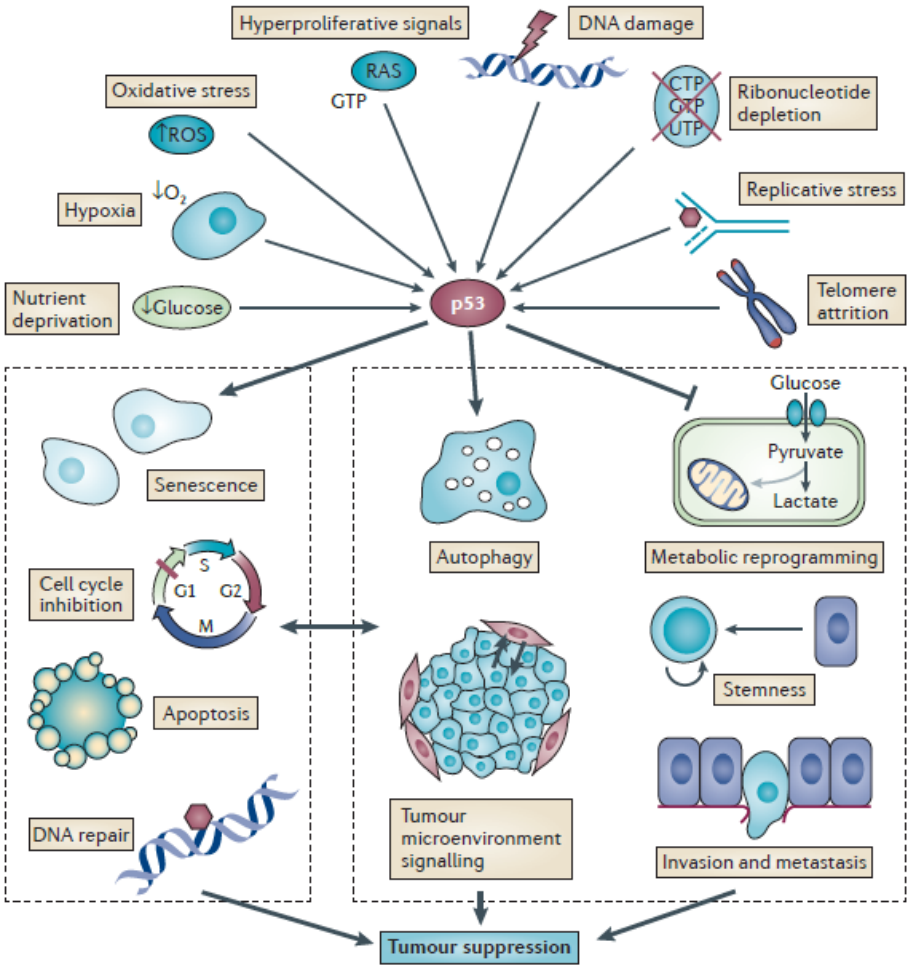

Fig. 4 - p53 activating signals and responses in mediating tumor suppression.
Source: Bieging KT, Mello SS, Attardi LD, Nature Reviews Cancer 2014, vol. 14(5): 359-70 (34).

2.1.5 The Mdm2 family controls p53 protein levels and activity

Inappropriate p53 activity can be detrimental for cell and organismal viability; therefore numerous mechanisms exist to keep p53 in check. Several E3 ubiquitin ligases - most prominently Mdm2 (29) but also others including Pirh2, Trim24, and Arf-bp1 - negatively regulate p53 protein, keeping levels low when p53 activity is not required (36). Mdm2 acts as a p53 inhibitor by binding to and sterically blocking p53 transactivation domains (37) and by serving as an E3 ubiquitin ligase to target p53 for proteasomal degradation (38,39,40). Mdm2 is a direct transcriptional target of p53, resulting in a negative-feedback loop where p53 can induce the expression of its own negative regulator (41,42). In response to stress signals, p53 is released from Mdm2 inhibitory effect, through any of several mechanisms: 1) stress-induced PTMs on both Mdm2 and p53, which disrupt the Mdm2-p53 interaction (43); 2) oncogene-induced sequestration of Mdm2 by $p14^{ARF}$ ($p19^{Arf}$ in mouse), a nucleolar protein encoded by the *INK4a/Arf* locus (44); and 3) nucleolar

stress-triggered ribosomal protein-Mdm2 interaction, that prevents Mdm2-mediated p53 ubiquitination (45). Like Mdm2, the related protein Mdm4 (also known as MdmX) binds the amino-terminal region of p53. Mdm4 does not possess E3 ubiquitin ligase activity, therefore it contributes to p53 degradation by dimerizing with Mdm2 and increasing its activity (36).

The importance of Mdm2 and Mdm4 in restricting p53 activity was shown through the generation of knock-out mice, which display early embryonic lethality. This phenotype results from uncontrolled p53 activity, as demonstrated by the complete rescue of lethality by concomitant knock-out of *Trp53* (46,47,48). Recently, the Zhang lab showed that it is the ability of Mdm2 to heterodimerize with Mdm4, which is important to suppress p53 activity, and not its E3 ligase function (49). Consistent with their central role in negatively regulating p53, Mdm2 and Mdm4 are frequently amplified in several tumor types (43).

2.1.6 Cytoplasmic functions of p53

In addition to its nuclear function as a transcription factor, p53 was shown to have additional activities (Fig. 5). The first p53 cytoplasmic function to be characterized was the induction of apoptosis in the presence of transcription inhibitors, which led to the discovery that p53 can trigger apoptosis by promoting mitochondrial outer membrane permealization (MOMP) (50,51). MOMP is controlled by the Bcl-2 family of apoptosis regulators, characterized by the presence of Bcl-2 homology (BH) domains. This family comprises three categories of proteins: 1) the pro-apoptotic effectors Bak and Bax that can oligomerize to create pores in the mitochondrial outer membrane and release pro-apoptotic factors from the intramembranous space; 2) the BH3-only proteins that stimulate Bax- or Bak-mediated pore formation, including Bim, Bid, Bad, Puma and Noxa; and 3) the anti-apoptotic proteins Bcl-2, Bcl-xL, and Mcl-1, which bind Bak and Bax to prevent their oligomerization. p53 was proposed to regulate MOMP through two main mechanisms: mitochondrial apoptosis and cytoplasmic apoptosis. The first model suggests that, upon stress signals, p53 translocates to the mitochondria where, through binding and sequestration of the anti-apoptotic effectors Bcl-2, Bcl-xL and Mcl-1, it allows derepression of Bak, prompting pore formation and cytochrome c release. The second model posits that, under normal

conditions, p53 is kept inactive in the cytoplasm in a complex with Bcl-xL; in response to stress, nuclear p53 induces the expression of several target genes, including *Bbc3/*Puma, which is then able to bind Bcl-xL and liberate p53. Free p53 activates Bax in a "hit-and-run" fashion (i.e. through transient protein-protein interactions), promoting its mitochondrial translocation and homo-oligomerization, thus inducing the MOMP and cytochrome c release. Cytochrome c binds Apaf1 (apoptotic protease-activating factor 1), inducing the assembly of seven Apaf1 monomers into an oligomeric complex termed the apoptosome that activates the initiator caspase, procaspase 9. Caspase 9 cleaves and activates the effector caspases, caspase 3 and caspase 7, which then initiate apoptosis. Both models highlight an interconnection between nuclear and cytoplasmic p53 activities, since the mitochondrial pathway components Bax, Puma, Noxa and Bid are also direct p53 target genes (52,53,54).

p53 activities at mitochondria are not only restricted to the regulation of apoptosis: in response to oxidative stress, p53 can induce necrosis, an irreversible tissue destruction characterized by cell lysis and inflammation. p53 accumulates in the mitochondrial matrix and binds cyclophilin D (CypD), triggering mitochondrial permeability transition pore (PTP) opening (55). PTP opening leads to an increase in unselective permeability to solutes and dissipates the cellular membrane potentials, leading to organelle swelling, rupture, and subsequent cell death (56).

Cytoplasmic p53 was also shown to play a role in the regulation of macroautophagy (hereafter referred to as autophagy), a catabolic process that allows the sequestration and subsequent lysosomal degradation of macromolecules for reuse. Autophagy can serve either as a pro-survival strategy under metabolic stressful conditions, or as a means to remove damaged and potentially harmful structures, hence functioning as a tumor suppressive mechanism. When taken to extremes, autophagy can lead to cell death. Conversely, autophagy can constitute an important way for tumor cells to survive to a challenging microenvironment. Given that autophagy can have both tumor suppressive and tumor promoting activities, p53 can both positively and negatively regulate it in a context-dependent manner by acting at multiple levels on the Ampk-mTor axis, an important pathway involved in modulating metabolism and growth control (57).

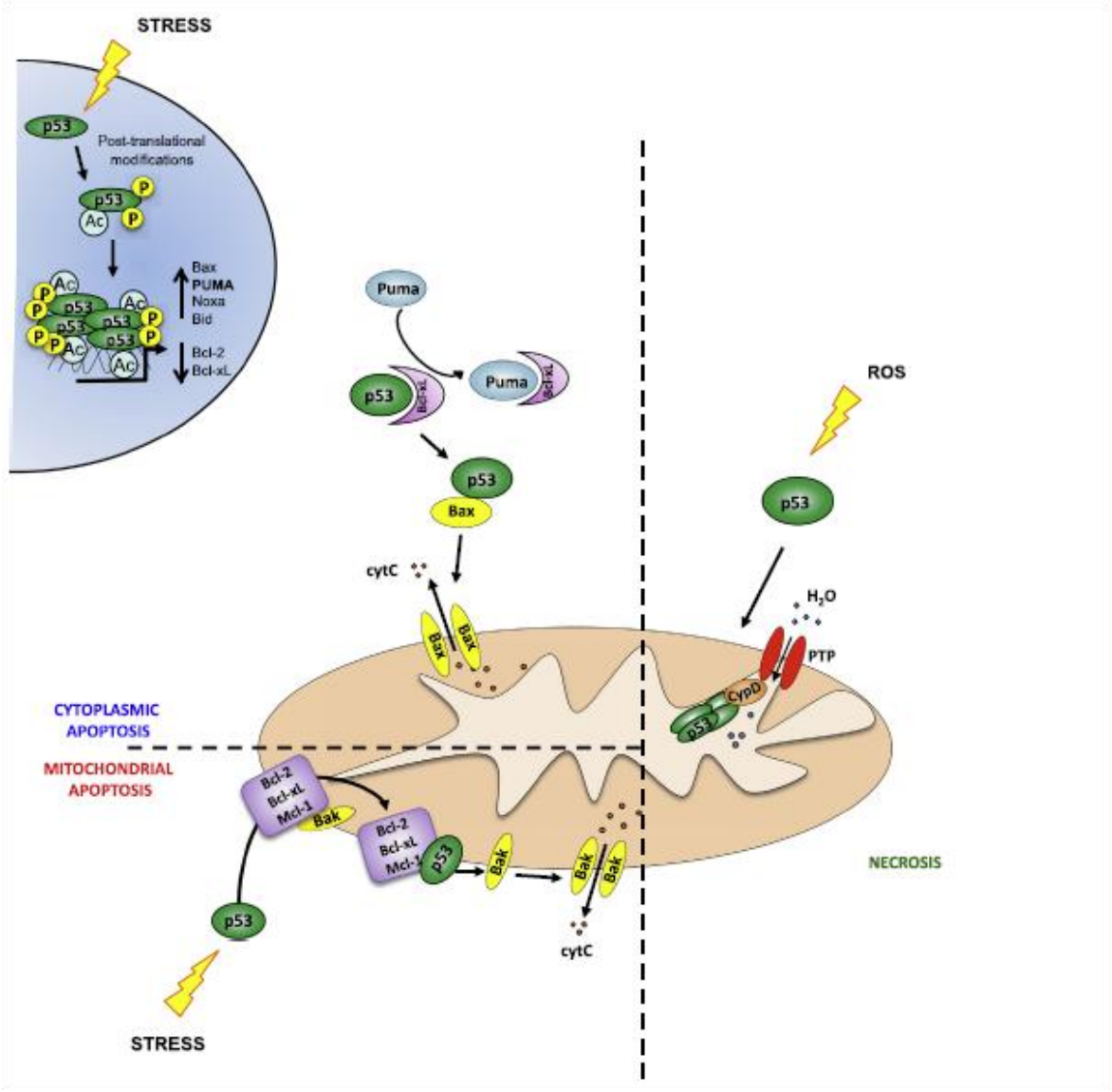

Fig. 5 - p53-induced cell death: the cytoplasmic, the mitochondrial and the necrotic program.
Source: Comel A *et al.,* FEBS Letters 2014, vol. 588(16): 2600-2609 (52)

Cytoplasmic p53 is also involved in the regulation of cell metabolism: by binding to G6PD (glucose-6-phosphate dehydrogenase), the first and rate-limiting enzyme of the pentose phosphate pathway (PPP), p53 suppresses glucose consumption and NADPH (nicotinamide adenine dinucleotide phosphate) production, preventing the glycolytic flux that is associated with malignant cell growth (58). Moreover, p53 plays a role in the regulation of oxidative stress by interacting with the primary antioxidant enzyme MnSOD (manganese superoxide dismutase) and inhibiting its activity (52,54,59,60).

2.2 Transcriptional regulation by p53

2.2.1 The p53 response element

p53 functions primarily as a tetrameric transcription factor that binds, in a sequence-specific manner, to p53 response elements (p53-RE) in DNA. The p53-RE is classically defined by the combination of two decameric half sites, each with the consensus 5'-RRRCWWGYYY-3' (R=purine, W=A or T, Y=pyrimidine), prevalently placed one next to the other or, with lower incidence, separated by a spacer of 1-13 bp (Fig. 6) (61,62). These p53 binding motifs were initially described to often reside in the 5' promoter-enhancer region or in the first intron of genes (63); recently this picture has been revised by the generation of genome-wide p53 binding maps, which show that p53 also associates with distal locations in the genome and binds DNA in a sequence-independent manner, probably through the interaction with other DNA-binding proteins (62,64).

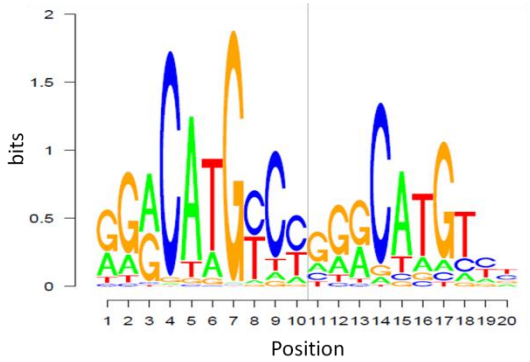

Fig. 6 - The p53 response element.
Position weight matrix (PWM) of the consensus p53-RE (JASPAR database (65)). The height of a letter at each given position is proportional to the frequency of a particular nucleotide at that position.

The p53 binding ability and its transactivation function are influenced by the sequence of the two half-sites as well as their mutual orientation (66). Using cooperativity mutants that can form weaker or stronger interactions between the p53 monomers, the Stiewe group showed that the p53 target genes can be functionally separated into two main classes based on the sequence similarity of their p53 regulatory elements to the canonical motif. Low cooperativity sites (bound by interaction-impaired mutants) are enriched for cell cycle progression genes and consist in high affinity p53 binding sites characterized by the classical consensus motif and shorter spacer length; high cooperativity sites instead (bound by strongly interacting mutants) are enriched for apoptotic genes and show reduced similarity to the p53 consensus motif and longer spacer length. The DNA

binding cooperativity of p53 is thereby important to recognize degenerate response elements and increase the spectrum of p53 target genes (67). The importance of keeping transcriptional regulation by p53 under tight control is exemplified by the observation that single nucleotide polymorphisms (SNPs) in functional p53-REs are infrequent due to negative selection, leading to the concept that such polymorphisms would likely be detrimental and are therefore purified from the population (68).

2.2.2 p53 target genes

The experimental evidence of p53 protein binding on the p53-RE close to the transcription initiation site of a gene is one of the criteria used to identify p53 target genes, and is usually coupled with the demonstration that the gene is differentially expressed when wild-type p53 is activated, but not when wild-type p53 is silenced, mutant p53 is present or the p53-RE is mutated. Several p53 direct targets associated to various tumor suppressive processes have been identified so far. The exact cell program specified by p53 activation depends on the cell type, the surrounding environment and the nature of the insult (63). In response to sustained or severe stress signals, p53 drives apoptosis of the damaged cells by up-regulating components of both the extrinsic and intrinsic death pathways, such as *Bax*, *Bid*, *Fas*, *Pmaip1/*Noxa and *Bbc3/*Puma, amongst others. In some cases, p53 responds to stress by inducing a temporary or a permanent cell cycle arrest through *Cdkn1a/*p21 expression. Beside senescence and cell death, p53 has also been shown to prevent tumor development through the regulation of cellular metabolism. Unlike normal differentiated cells, which rely primarily on mitochondrial oxidative phosphorylation to generate the energy needed for cellular processes, most cancer cells rely on glycolysis even under normal aerobic conditions, a phenomenon termed the Warburg effect. p53 has been described to counteract the Warburg effect by lowering the glycolytic rate and promoting mitochondrial respiration by regulating the expression of *Tigar*, *Sco2* and *Gls2* (57). Moreover, p53 can activate autophagy by inducing *Ulk1, Dram, Sesn1* and *2,* and a set of autophagy core machinery-encoding genes (59,69).

These are just few examples of a continuously growing list of p53 target genes, owing to the rapid progression of high throughput analyses.

2.2.3 Genome-wide analysis of the p53 network

With the advent of technologies that can reveal p53 occupancy and measure expression changes of a large number of transcripts, new p53 target genes continue to be uncovered. The first of these studies analyzed the expression profiles of cell lines with inducible *Trp53* using microarrays and observed that the p53 response depends on the levels of p53 protein, on the cell type and on the inducing agent, and involves genes belonging to different functional categories and with different kinetics in activation and repression (70). The ability to characterize p53-DNA interactions in a high-throughput manner using chromatin immunoprecipitation (ChIP) followed by hybridization on oligonucleotide arrays (ChIP-on-chip), allowed to expand the knowledge on the p53 regulatory network and led to the first indication that some p53 binding sites lie outside the promoter-proximal region (71,72). As soon as it became possible to generate whole-genome maps of p53 binding sites, initially through ChIP followed by paired-end ditag PET sequencing (ChIP-PET), and later by deep sequencing (ChIP-Seq), the p53 binding motif was better characterized, the observation that p53 binding sites also existed at large distances from transcription start sites (TSSs) was reinforced, and novel p53-regulated pathways were discovered, such as the Wnt signaling pathway or autophagy (73,74). Distal binding of p53 was associated to the regulation of non-coding RNA (ncRNA) species, such as microRNAs (75) and long intergenic non-coding RNAs (lincRNAs) (76,77), or showed chromatin features characteristic of enhancers. p53 binding at enhancer regions was shown to have opposing functions: to be one of the mechanisms underlying p53-mediated gene repression in mouse embryonic stem cells (mESC) (78) and to have enhancer activity required for efficient transactivation of the interacting target genes in fibroblasts (79); these contrasting functions could represent cell type- or gene-specific p53 regulatory activities. Another important observation that came out from these genome-wide studies is that only a minor fraction of the genes bound by p53 in the promoter-proximal region is transcriptionally regulated (69). A deeper comprehension of how p53 determines the specificity of

its responses will come from the study of p53 PTMs and cofactors at specific genomic locations. For example, there are indications that p53 phosphorylation at Serine 46 plays a role in the transactivation of several genes, in particular the apoptotic ones (80). Several other mechanisms have been described for the regulation of specific genes, but a genome-wide characterization is still missing. Finally, the p53 response can be also regulated at the post-transcriptional level by microRNAs and RNA-binding proteins (RBPs), as shown in a recent translatome analysis in MCF7 cells following Nutlin or doxorubicin treatment (81).

Initially, the activity of p53 was mainly investigated in response to cellular stress stimuli in immortalized cancer cell lines. To investigate the p53-dependent response in normal cells to stress insults, several genome-wide analyses of p53 chromatin occupancy and gene expression profiling were performed (64,69,78,82), which led to the observation that p53 is bound to DNA already in unperturbed conditions or with low levels of constitutive stress, suggesting a role for p53 in the regulation of basal processes. The study of p53 under physiological conditions is presently a growing field of investigation. One of the first reports indicated a role for p53 in regulating kidney development (83). In spite of extensive research, our understanding of the detailed molecular mechanisms activated by p53 remains incomplete. Several questions are left unanswered: for instance, what confers target gene selectivity to the p53 response and how cell fate in response to stress is determined.

2.2.4 Transcriptional repression by p53

p53's role as a transcriptional activator is well-documented. Instead, the mechanisms underlying transcriptional repression by p53 are still a matter of debate and can be grouped in direct (DNA binding-dependent) and indirect (DNA binding-independent) mechanisms (35). p53 may either displace other transcriptional activators and components of the transcriptional machinery by occluding their binding site on DNA, or recruit co-repressors and chromatin-modifying factors, such as histone deacetylases, which then block gene expression (35). Moreover, p53 has been proposed to mediate repression by interfering with distal enhancer activity (78). p53 also suppresses transcription indirectly by regulating the expression of microRNAs: in this setting, p53

facilitates not only the transcription of microRNA precursors, but also their processing into mature, active forms (75). Furthermore, p53 has been proposed to execute widespread gene repression, by activating a specific lincRNA, lincRNA-p21, which is believed to interact with hnRNP-K (heterogeneous nuclear ribonucleoprotein K) to silence target genes (76). Recently this model of lincRNAs regulating the expression of multiple genes *in trans* has been challenged by the generation of lincRNA-p21 conditional knock-out mice and the discovery that, in response to DNA damage, lincRNA-p21 acts in concert with hnRNP-K to induce p53-mediated activation of its neighboring gene *Cdkn1a*/p21, indicating a *cis* regulatory model (84). p21 mediates p53-dependent transcriptional repression by inhibiting Cdk-dependent phosphorylation of the Rb protein to keep E2f-regulated genes in an inactive state (35,85).

Recently, the model of p53 mediating repression through direct association with target promoters was questioned. Several groups reported a lack of p53 binding sites in the vicinity of most repressed genes; moreover, the Huang laboratory noted a correlation between p53 binding strength and fold induction only for the activated genes but not for the down-regulated ones (62,67,69,78), and the Espinosa group observed that very few target genes showed a diminished transcription in a Global Run-On sequencing (GRO-seq) analysis following p53 activation by Nutlin treatment (86). Altogether these findings indicate that p53-mediated repression may be largely indirect.

2.3 Dissecting p53 functions through mouse models.

2.3.1 The *Trp53* knock-out mouse

Trp53 knock-out mice were generated by three different groups, in each case through disruption of the p53 DNA binding domain (21,22,23) and provided unequivocal evidence of the fundamental role played by p53 in tumor suppression. Loss of p53 led to a dramatic, and completely penetrant predisposition to spontaneous cancer development: most *Trp53* null animals succumbing to tumors by 10 months of age. *Trp53* heterozygous mice showed increased tumor susceptibility compared to wild-type mice, although with delayed incidence compared to *Trp53* null animals. $Trp53^{-/-}$ mice most commonly died of T-cell lymphomas and a range of sarcomas, while $Trp53^{+/-}$

mice predominantly developed mesenchymal cancers (with a preponderance of osteosarcomas and soft-tissue sarcomas). The reasons for these difference in tumor spectrum are still undefined. It is clear instead that the types of tumors developed reflect an inherent predisposition of the different genetic backgrounds examined (87). In addition to providing insights to p53 tumor suppressive function, *Trp53* knock-out mice have also been used to prove the involvement of p53 in the regulation of several physiological processes. The first observation regarded an initially underestimated role of p53 during embryonal development: a fraction of *Trp53* null embryos, prevalently female embryos, displays defects in neural tube closure resulting in an overgrowth of neural tissue in the region of the mid–brain, a condition known as exencephaly (88,89). Moreover, p53 was shown to play a role in fertility by promoting embryo implantation through the induction of *Lif* (leukaemia inhibitory factor) expression (90,91).

2.3.2 p53 functions in tumor suppression: apoptosis and cell cycle arrest

Apoptosis and cell cycle arrest were the first p53 functions to be described: it was back in 1992 when p53 was named the 'guardian of the genome' for its role in maintaining genome stability and integrity in response to DNA damage (92). In this model, p53 induces a transient G_1 arrest in response to DNA damage signals, allowing cells to repair their genome before proceeding into cell cycle, and thereby limiting the propagation of potentially oncogenic mutations. One year later, two groups reported that *Trp53* null thymocytes are deficient in radiation-induced apoptosis, demonstrating the importance of p53 in the genotoxic and apoptotic responses and providing the first insights into p53 tumor suppressive mechanisms (93,94).

The general importance of p53 in preventing cancer was further demonstrated by crossing various tumor-prone mouse strains onto a p53-deficient background. In most of these studies, p53 loss correlates with acceleration of tumorigenesis, showing that p53 acts like a brake downstream of several oncogenic pathways. One of the first studies along this line analyzed a transgenic model of choroid plexus papillomas initiated by the inhibition of the Rb protein activity by a fragment of Large T-Antigen (T_{121}), leading to inappropriate cell proliferation. This hyper-proliferation activates p53 to induce apoptosis, resulting in slow-growing tumors. When the T_{121} transgenic mice are

crossed onto a *Trp53* null background, tumorigenesis accelerates dramatically, indicating that p53-dependent apoptosis is important to prevent tumor development (95).

Apoptosis is not the only means through which p53 can suppress tumorigenesis. The Lozano group studied the survival of knock-in mice expressing $p53^{R172P}$, a mutant p53 protein that is unable to induce apoptosis but can induce a partial cell cycle arrest in response to DNA damage, and corresponds to the $p53^{R175P}$ mutation that occurs in human tumors (96). $Trp53^{R172P}$ homozygous mice develop spontaneous tumors with a median of 11.5 months, while *Trp53* null mice die with a median of 5.5 months, indicating that the residual ability of $p53^{R172P}$ to initiate a cell cycle arrest plays an important role in tumor suppression. Moreover, the lymphomas and sarcomas that eventually develop in these $Trp53^{R172P/R172P}$ mutant mice remain diploid, in contrast to the aneuploid tumors that develop in $Trp53^{-/-}$ mice, suggesting that preserved cell cycle checkpoint functions can inhibit genome instability (96). The inability of $p53^{R172P}$ to suppress the development of late-onset tumors, however, also supported a role for p53-mediated apoptosis in tumor suppression. Similar conclusions were drawn by the Stiewe group with another mouse strain expressing the cooperativity mutant $p53^{E177R}$ (97). Substitution of the negatively charged glutamic acid with a positively charged arginine produces a mutant with impaired ability to bind DNA, particularly at apoptotic genes. $Trp53^{E177R/E177R}$ mutant mice show impaired apoptotic response following radiation, but retain some activity in inducing cell cycle arrest and senescence, and in the regulation of metabolism and antioxidant defense. As above for the $Trp53^{R172P/R172P}$ mutant mice, $Trp53^{E177R/E177R}$ animals are more cancer prone than *Trp53* wild-type mice, but retain some residual tumor suppressive activity when compared to *Trp53* null animals (97).

To dissect the contribution of the different p53 effectors to p53-mediated tumor suppression, several knock-out mice that lack particular p53 target genes were generated, including *Cdkn1a*- (98,99,100), *Gadd45a*- (101), *Bbc3*- (102,103), and *Pmaip1*-deficient mice (103). None of these mice can reproduce the dramatic cancer predisposition observed in *Trp53* null mice. These genes are negligible for the maintenance of genome stability and inhibition of spontaneous tumor formation; however, some of them are clearly important for p53-mediated tumor suppression in

the presence of certain oncogenic driver mutation, as their inactivation results in acceleration of carcinogenesis in tumor-prone mouse models (104,105,106,107,108).

2.3.3 p53 functions in tumor suppression: beyond apoptosis and cell cycle arrest

In an attempt to unveil the contribution of p53 transcriptional activity to tumor suppression, the Attardi team generated transactivation domain *Trp53* mutant knock-in mice, with alterations in the first ($p53^{25,26}$), second ($p53^{53,54}$), or both TADs ($p53^{25,26,53,54}$) (109). The $p53^{53,54}$ mutant retains intact transactivation function, as indicated by a global gene expression profile of HrasV12; $Trp53^{53,54}$ MEFs that is indistinguishable from that of wild-type cells, and by the ability to suppress $Kras^{G12D}$-driven lung tumors. The $p53^{25,26}$ mutant instead is severely compromised for transactivation of most p53 target genes, including *Cdkn1a*, *Bbc3* and *Pmaip1*, and cannot trigger cell cycle arrest and apoptosis in response to acute DNA damage, but can induce senescence in HrasV12 MEFs. Despite its partial impairment in transcriptional activation, $p53^{25,26}$ retains the capacity to suppress the growth of tumors that are initiated by different oncogenic lesions and in a range of tissue types (110). In contrast, the transactivation-dead $p53^{25,26,53,54}$ mutant completely lacks tumor suppressive potential, demonstrating that p53 transactivation is essential for tumor suppression, although this requirement reflects the limited transcriptional activity of $p53^{25,26}$ mutant (109,110). Gu and coworkers confirmed the observation that tumor suppression can be achieved even in the absence of full transcriptional activation of *Cdkn1a*, *Bbc3* and *Pmaip1* by generating knock-in mice expressing $p53^{3KR}$, in which three lysines known to be acetylated *in vivo* are mutated to arginines (K117R, K161R, K162R) (111). In response to DNA damage, MEFs from $Trp53^{3KR/3KR}$ mice fail to undergo apoptosis, cell cycle arrest and senescence but retain the ability to activate the metabolic genes *Gls2*, *Tigar* and *Gpx1*. $Trp53^{3KR/3KR}$ mice don't show the 100% penetrant predisposition to spontaneous tumors of $Trp53^{-/-}$ animals, suggesting that the ability to regulate energy metabolism and reduce the levels of reactive oxygen species (ROS) are crucial for tumor suppression. Moreover, these data indicate the importance of acetylation in modulating the p53 response (111). However, these studies described an impaired transcription of the classical p53 effector genes *Cdkn1a*, *Bbc3* and *Pmaip1*, but couldn't formally prove a complete

suppression, leaving the question open whether these genes could still prevent tumor development when expressed at low levels. This issue was addressed by the Strasser group through the generation of *Cdkn1a*$^{-/-}$ *Bbc3*$^{-/-}$ *Pmaip1*$^{-/-}$ mice (112). Strikingly, none of the triple knock-out animals develops spontaneous tumors up to 500 days, whereas all *Trp53*$^{-/-}$ mice succumb to lymphomas and sarcomas by 250 days. The authors noted that DNA repair upon acute DNA damage is delayed in p53-deficient cells relative to wild-type or triple knock-out cells, suggesting that p53's role in maintaining genome integrity may have protected these animals from spontaneous tumor development (112). Overall, these studies demonstrate that suppression of spontaneous tumorigenesis can still be achieved when the ability to induce apoptosis and cell cycle arrest is impaired.

2.3.4 Oncogene-driven tumor suppressive pathways: a focus on Myc

c-Myc (henceforth Myc) was initially identified as the human homologue of a retroviral oncogene of the MC29 avian tumor virus that caused myelocytomatosis in chickens (113). Several years after its discovery, it became clear that Myc is a transcription factor implicated in the control of normal cell proliferation (114). Aberrant Myc regulation is often observed in cancer and is the result of virus-mediated insertional mutagenesis, gene amplification or chromosomal translocation. In addition, Myc is deregulated by, and is an effector of, many additional mechanisms, including a variety of oncogenic signaling pathways (e.g. Wnt, Notch, Ras, ...) and activation of hormones or growth factors receptors (114). Pathological activation of Myc has two opposite and paradoxical effects: on one side Myc overexpression induces cellular transformation and hyper-proliferation, while on the other side it activates intrinsic tumor surveillance pathways aimed at restraining the expansion of pre-cancerous cells. The best characterized Myc-induced tumor suppressive arm is the p19^{Arf}/Mdm2/p53 pathway. Oncogenic Myc activates p19^{Arf}, that, as mentioned before, is able to stabilize p53 by binding and antagonizing Mdm2 (115,116). Arf accumulation and consequent p53 activation was described to be the result of Myc-induced disruption of the interaction between Arf and its E3 ubiquitin ligase Ulf (117).

The first p53-dependent response to be characterized was apoptosis: it was noticed that ectopic expression of Myc sensitizes cells deprived of extracellular survival factors to programmed cell death (118,119). Abrogation of Myc-induced cell death is crucial for cellular transformation, setting the selective pressure to inactivate Arf or p53 (116). An *in vivo* model to test the relevance of this pathway during lymphomagenesis is the Eμ-*myc* transgenic mouse model (120), in which Myc is under control of the immunoglobulin heavy chain enhancer, a genetic alteration resembling the chromosomal translocation observed in human Burkitt's lymphomas (121,122,123,124,125). Myc overexpression in B-cell progenitors leads to increased proliferation and reduced differentiation from pre-B to mature B cells (120). In the pre-tumoral stage, the high rates of cell divisions driven by Myc are counter-balanced by p53-induced apoptosis. This constitutes the main barrier against Myc's oncogenic potential and sets the selective pressure to inactivate the p53 pathway in Myc-induced lymphomas (126,127). Disruption of apoptosis by Bcl2 overexpression is sufficient to accelerate Myc-induced tumorigenesis and alleviate the pressure to inactivate p53, indicating that p53 tumor suppressive function, in this particular tumor type, relies mainly on programmed cell death (128,129). When apoptosis is disrupted, p53 retains some residual tumor suppressor activity associated to senescence (97,130,131). However, since Myc also regulates proliferation in normal cells, p53 activation should be restrained to situations wherein Myc signaling is oncogenic. Evan and coworkers showed that distinct threshold levels of Myc determine its output *in vivo*: low levels of Myc are required to drive proliferation, whereas elevated Myc levels are competent to engage the $p19^{Arf}$/p53 tumor suppressor pathway and induce apoptosis (132).

Of note, Arf loss does not always recapitulate p53 loss. For example, unlike *Trp53*$^{-/-}$ lymphomas, *Ink4a/Arf*$^{-/-}$ lymphomas are genetically stable and sensitive to chemotherapy (127), indicating that the $p19^{Arf}$/Mdm2/p53 pathway is not the only intrinsic tumor suppressive program available in the cells. Analysis of early human pre-cancerous and cancerous lesions reveals molecular marks of DNA damage, leading to a model whereby oncogene-induced hyper-proliferation results in replication stress, DNA double-strand breaks formation and ROS-associated oxidative damage

(133). Activated oncogenes can induce a DNA damage response (DDR) that signals to p53 via a phosphorylation cascade that involves the Atm and Chk2 kinases and ultimately imposes a barrier to tumor development (134,135). The $p19^{Arf}$ and the DNA damage pathway can synergize to activate p53 and this can be exploited to promote more efficiently death of tumor cells (136). However, the $p19^{Arf}$ and the DDR are not the only Myc-induced pathways upstream of p53: for example, ribosomal stress has been shown to induce ribosomal proteins-mediated inhibition of Mdm2 E3 ligase activity, resulting in p53 activation (137). Moreover, Myc can also directly induce apoptosis in the absence of $p19^{Arf}$ by regulating Bim expression (138).

2.3.5 Therapeutic promise of p53 reinstatement in tumors

Induction of p53 in pre-cancerous cells elicits several tumor suppressive mechanisms that result in the elimination of the damaged cells and, as a consequence, are selected against during tumor development. Therefore, restoration of p53 function in tumors constitutes a very attractive strategy for cancer therapy. Using transgenic mice with conditionally activatable wild-type *Trp53* alleles, three groups showed that p53 restoration induces tumor regression, based on different p53 reinstatement approaches and tumor models (136,139,140). The Evan group used the $p53ER^{TAM}$ model (141) crossed with the Eμ-*myc* lymphoma model (120,136). In the $p53ER^{TAM}$ model, the modified hormone-binding domain of the estrogen receptor is placed in-frame at the 3'-end of the coding sequence of the endogenous *Trp53* gene, to create the $p53ER^{TAM}$ allele that is activated by the oestrogen synthetic analogue 4-hydroxytamoxifen (4-OHT). Administration of 4-OHT allows a fast transition from a p53 null state to a functional p53 state (136). The Jacks laboratory inserted a transcription-translation stop casette flanked by loxP sites (LSL) in the first intron of the endogenous *Trp53* locus. p53 expression was regulated through a ubiquitously expressed tamoxifen-inducible Cre recombinase to regress radiation-induced spontaneously arising lymphomas and sarcomas (139). Finally, the Lowe lab used a doxycycline-repressible p53 short-hairpin RNA (shRNA) to conditionally regulate p53 expression in a mouse model of Ras-induced liver carcinoma (140). Interestingly, although each model show tumor regression upon restoration of p53 function, the mechanisms of p53-mediated tumor suppression depend on the

tumor type: lymphomas undergo apoptosis, while sarcomas and liver tumors show features of cellular senescence. In the liver carcinoma model, p53-induced senescent cells produce inflammatory cytokines and an innate immune response, that contributes to tumor cell clearance, providing evidence of a non-cell autonomous tumor suppressive function of p53. These results imply that p53 reinstatement has therapeutic potential for cancer treatment. However, the Evan group reported tumor relapse after p53 induction due to the selection of resistant clones that have inactivated the $p19^{Arf}$/p53 pathway (136), therefore therapies should be carefully planned.

The main strategies for re-establishing p53 activity in tumors that are currently in clinical trials are the re-introduction of p53 in cancer cells through the use of gene therapy with replication-deficient adenoviral vectors (142) and, for tumors that retain wild-type p53, small molecule drugs that mostly function by interfering with the p53 inhibitory ability of Mdm2 (143). To treat tumors with some mutant p53 proteins, scientists have developed small molecules that can refold p53 to a transcriptionally competent conformation (144). The development of such drugs raised some concerns about the potential toxicity that a systemic activation of p53 may cause in normal tissues: one can anticipate, however, that these molecules are likely to function much better in tumor cells, where upstream p53-activating signals are present and acute, compared to normal cells.

2.4 Aim of the work

The genetic programs used by the p53 tumor suppressor to direct stress-specific biological responses remain to be clarified. For example, it is still unclear whether p53 directly or indirectly represses the expression of target genes, or which are the cofactors or the effectors that cooperate with p53 to regulate gene transcription, or whether different target genes are activated in response to different stress stimuli or depending on the cellular context. To gain new insights into p53 biology, we used high-throughput sequencing to generate whole genome maps of p53 binding and gene expression profiles during tumor suppression and regression using a model of Myc-induced tumorigenesis and in response to a classical p53 activating stimulus, such as DNA damage. Through the comparison of these global p53 transcriptional programs we aim at

better understanding the regulatory mechanisms within the p53 network. Moreover, the components of p53 transcriptional programs may be critical tumor suppressor genes, paving the way for functional studies and hopefully the identification of candidate targets for future therapeutic applications.

3 Materials and Methods

3.1 Mouse breeding and genotyping

The following mouse strains were used for this study: Eμ-*myc* transgenic mice (120), p53ER^{TAM} mice (141), LSL-p53 mice (139), p53 KO (p53$^{\Delta}$) mice (21), *Arf*$^{+/-}$ mice (145) and C57/Bl6 wild-type mice (Harlan). All animals were maintained on a C57/Bl6 background (except p53ER^{TAM} mice that were on a mixed background) and bred to obtain the various genotype combinations described in this thesis.

Primers used for genotyping were listed below.

Strain	Primers
Eμ-*myc*	GGTTTAATGAATTTGAAGTTGCCA TTCTTGCCCTGCGTATATCAGTC
p53ER^{TAM}	CCTCCAGCCTAGAGCCTTCCAAGC GGTGAGATTTCATTGTAGGTGCC GCACACAAACTCTTCACCCTGC
LSL-p53	CTTGGAGACATAGCCACACTG AGCTAGCCACCATGGCTTGAGTAAGT CAACTGTTCTACCTCAAGAGCC
p53 KO	AGCGTGGTGGTACCTTATGAG GGATGGTGGTATACTCAGAGC GCTATCAGGACATAGCGTTGG

Experiments involving animals were performed in accordance with the Italian laws (D.L.vo 116/92 and following additions), which enforce EU 86/609 directive (Council Directive 86/609/EEC of 24 November 1986 on the approximation of laws, regulations and administrative provisions of the Member States regarding the protection of animals used for experimental and other scientific purposes).

3.2 Primary mouse B and non-B cells and lymphomas

B cells were extracted as described. Briefly, for control (C) and pre-tumoral (P) samples, spleens of 6–7 weeks old Eμ-*myc* transgenic mice with no infiltration of peripheral lymph nodes were used. Spleens from C57/Bl6 wild-type mice were collected four hours after exposure to 7 Gy whole-body irradiation and from a control cohort of mice. Single-cell suspensions were obtained by

pressing the spleens through nylon cell strainers and subsequent hypotonic lysis of red blood cells. To isolate B cells, we incubated single-cell suspensions with B220 MicroBeads (Miltenyi Biotech) and enriched them by magnetic cell sorting (MACS), according to the manufacturer instructions (Miltenyi Biotech). The column flow through was kept to represent the non-B cell population.

Lymphoma samples (or tumors, T) composed primarily of tumor cells, were dissected from infiltrated lymph nodes and not purified further. At this stage, samples were directly processed for the different assays.

Lymphoma cells were grown in 1:1 ratio of irradiated NIH-3T3 conditioned medium and fresh medium (DMEM and IMDM (1:1), 10% fetal bovine serum, 2mM L-Gln, 1% penicillin/streptomycin, 1% non-essential amino acids and 0,2% β-mercaptoethanol) and maintained at 37°C with 5% CO2.

Retroviral-mediated gene transfer was performed using Phoenix packaging cells. Eμ-*myc* LSL-p53 lymphoma cells were infected with pMI CreERT2-ires-Puro (146) and Eμ-*myc* $Arf^{-/-}$ $Trp53^{+/+}$ lymphomas cells with pLEPG shp53.1224 (147).

3.3 Lymphoma Transplantation and In Vivo Treatment

For transplants, lymphoma cells were thawed immediately before use, washed, counted, and injected intravenously (0.5 x 10^6 cells/mouse in 300 μl phosphate-buffered saline [PBS]) into multiple genetically matched wild-type mice (for Eμ-*myc* $p53ER^{TAM}$ lymphomas, recipient mice were immunosuppressed with 4 Gy 3–6 hr prior to transplantation). For short-term p53 restoration studies, tamoxifen (1 mg/300 μl of peanut oil/mouse) or carrier was administered once by intraperitoneal injection, when tumors were palpable.

3.4 Chemicals

Doxorubicin hydrochloride was purchased from Sigma-Aldrich Srl, dissolved in water and used 1 mM (0.6 mg/ml). (+)-and (-)-Nutlin were purchased from Cayman Chemical, dissolved in DMSO and used at 10 mM. 4-Hydroxytamoxifen was purchased from Sigma-Aldrich Srl, dissolved in

ethanol and used 0.1 mM. Tamoxifen was dissolved in peanut oil (Sigma-Aldrich Srl) and used 3 mg/ml.

3.5 Western blotting

5-10 x 10^6 cells were lysed with RIPA Buffer (20 mM HEPES at pH 7.5, 300 mM NaCl, 5 mM EDTA, 10% Glycerol, 1% Triton X-100, supplemented with protease inhibitors (Mini, Roche) and phosphatase inhibitors 0.4 mM Ortovanadate, 10 mM NaF) and sonicated. Cleared lysates were electrophoresed and immunoblotted with the indicated primary antibodies: p53 (NCL-p53-CM5p) from Novocastra laboratories and Vinculin (V9264) from Sigma. After incubation of the membranes with appropriate secondary antibodies, infrared imaging was performed with LiCor Odyssey System.

3.6 Flow citometry: cell cycle and apoptosis analysis

To analyze cell cycle and apoptosis, 1 x 10^6 live cells were resuspended in 1 ml of PBS and fixed by adding 2 ml of ice-cold absolute ethanol and kept at 4°C for at least 30 minutes. Cells were washed once with 1 ml of PBS 1% BSA and stained overnight with 1 ml 50 µg/ml propidium iodide (PI) and 250 µg/ml RNaseA at 4°C. 50000 total events were analyzed by FACS. All the FACS data were acquired using a FACSCalibur machine (Becton Dickinson) and then analyzed by using FlowJo software (TreeStar).

3.7 Chromatin Immunoprecipitation

Cells were processed as described above.

To minimize inter-individual variation we decided to process ChIP samples of Eµ-*myc* control and pre-tumoral mice, and C57/Bl6 wild-type mice (Harlan) in pools of ten age- and sex-matched animals, while, due to the clonal nature of lymphomas, we kept tumor samples separated and analyzed four Eµ-*myc* p53ER^{TAM} lymphomas, three Eµ-*myc* *Arf*$^{-/-}$ *Trp53*$^{+/+}$ and three Eµ-*myc* LSL-p53 lymphomas. For ChIP-Seq analysis of p53, lysates from 50 x 10^6 B cells were immunoprecipitated with 10 µg p53 antibody (NCL-p53-CM5p - Novocastra laboratories). p53

antibody specificity was tested by ChIP-Seq analysis in total splenic cells from *Trp53*$^{-/-}$ mice four hours after 7 Gy of X-ray radiation.

Cells were fixed by addition of 1% formaldehyde for 10 min. Fixation was stopped by addition of 0,125 M glycine. Cells were washed three times in PBS, resuspended in SDS buffer (50 mM Tris at pH 8,1, 0,5% SDS, 100 mM NaCl, 5 mM EDTA, and protease inhibitors) and stored at -80 °C before further processing for ChIP. Cells were pelleted by centrifugation, and suspended in 4 ml of IP Buffer (100 mM Tris at pH 8.6, 0.3% SDS, 1.7% Triton X-100, and 5 mM EDTA). Cells were disrupted by sonication with a Branson 250 sonicator, performing 5 cycles of 30 sec 30% amplitude, yielding genomic DNA fragments with a bulk size of 100–400 bp. 1 ml of diluted lysate was precleared by addition of 25 µl of blocked protein A beads (50% slurry protein A-Sepharose, Amersham; 0.5 mg/ml fatty acid-free BSA, Sigma; and 0.2 mg/ml tRNA,Sigma, in TE). Samples were immunoprecipitated overnight at 4°C with polyclonal antibodies. Immune complexes were recovered by adding 50 µl of blocked protein A beads and incubated for 4 hr at 4°C. Beads were washed with successive washes in 1 ml of Mixed Micelle Buffer (20 mM Tris at pH 8.1, 150mMNaCl, 5mMEDTA, 5% w/v sucrose, 1% Triton X-100, and 0.2% SDS), Buffer 500 (50 mM HEPES at pH 7.5, 0.1% w/v deoxycholic acid, 1% Triton X-100, 500 mM NaCl, and 1 mM EDTA), LiCl Detergent Wash Buffer (10 mM Tris at pH 8.0, 0.5% deoxycholic acid, 0.5% NP-40, 250 mM LiCl, and 1 mM EDTA), and TE (pH 7.5). DNA was eluted in TE 2% SDS and crosslink reversed by incubation overnight at 65 °C. DNA was then purified by Qiaquick columns (Qiagen) and quantified using PicoGreen (Invitrogen). 2-10 ng ChIP DNA was prepared for HiSeq2000 sequencing with TruSeq ChIP Sample Prep Kit (Illumina) following manufacturer instructions. For ChIP-qPCR analysis, DNA was amplified in Real-time PCR reactions with FAST SYBR Green Master Mix (Applied Biosystems).

3.8 RNA extraction and analysis

Total RNA was purified onto RNeasy columns (Qiagen) and treated on-column with DNase (Qiagen). Complementary DNA (cDNA) was produced using the reverse transcriptase ImPromII

(Promega). 10 ng of cDNA were used for Real-time PCR reactions with FAST SYBR Green Master Mix (Applied Biosystems).

For RNA-Seq, total RNA from 10^7 cells was purified using Trizol (Invitrogen), treated with Turbo DNase (Ambion) and purified with RNA Clean XP (Agencourt). 5 µg of purified RNA were then treated with Ribozero rRNA removal kit (Epicentre) and ethanol precipitated. RNA quality and removal of rRNA were checked with the Agilent 2100 Bioanalyzer (Agilent Technologies). Libraries for RNA-Seq were then prepared with the TruSeq RNA Sample Prep Kits v2 (Illumina) following manufacturer instruction (except for skipping the first step of mRNA purification with poly-T oligo-attached magnetic beads).

3.9 NGS data filtering and quality assessment

ChIP-seq and RNA-seq NGS reads sequenced with the Illumina HiSeq2000 were filtered using the fastq_quality_trimmer and fastq_masker tools of the FASTXToolkit suite (http://hannonlab.cshl.edu/fastx_toolkit/). Their quality was evaluated and confirmed using the FastQC application (www.bioinformatics.babraham.ac.uk/projects/fastqc/).

3.10 Analysis of ChIP-seq data

ChIP-seq NGS reads were aligned to the mm9 genome through the BWA aligner (148) using default settings. Peaks were called using the MACS software (v1.4)38 (149). Only peaks with p-value < 1e-8 were retained. Peak enrichment was determined as $\log_2(ChIP_w - input_w)$, where $ChIP_w$ and $input_w$ is the normalized count of reads in the peak region in the ChIP and in the corresponding input sample.

3.11 Genome annotation

Refseq mm9 gene model was used in the present study. The corresponding gtf and bed files were downloaded from the UCSC Table Browser.

3.12 RNA-seq data analysis

RNA-Seq NGS reads were aligned to the mm9 mouse reference genome using the TopHat aligner (version 2.0.6). In case of duplicated reads, only one read was kept. Read counts were associated to each exon using the HTSeq software (http://www.huber.embl.de/users/anders/HTSeq/doc/overview.html).

3.13 Identification of differentially expressed genes

Differentially expressed genes (DEGs) were identified using the Bioconductor package DESeq2 (30). In order to call DEGs over-genes when multiple isoforms are present, the rounded mean of counts over the isoforms is used. DEGs are defined as genes whose q-value relative to the control is lower than 0.05. Quantification of relative levels of total mRNA was calculated on B and non-B cells RNA-Seq data from 4 *Trp53*$^{+/+}$ and 2 *Trp53*$^{-/-}$ mice in each condition, 4 Eμ-*myc* p53ER^{TAM} lymphomas treated with 4-OHT and 3 Eμ-*myc Arf*$^{-/-}$ *Trp53*$^{+/+}$ lymphomas following (-)-Nutlin and doxorubicin treatment relative to controls. All RNA-Seq experiments in Eμ-*myc* lymphoma samples were performed on biological and technical replicates.

3.14 Other bioinformatic and statistical analyses

Statistical analysis, heatmaps, hierarchical clustering of RNA-seq data and other visual representations of the data were performed using R and Bioconductor packages (150). Two-tailed Student's t-test was used to calculate p-values.

3.15 Motif search

Sequences from the reference genome were extracted and subjected to a *de novo* motif search using MEME-ChIP (151). The discovered motifs were compared with known motifs from the JASPAR database using TOMTOM (152). The occurrence of the p53 motif at the genomic intervals analyzed was calculated by the FIMO (Find Individual Motif Occurences) algorithm (153) (p-value<1 x 10^{-5}).

3.16 Gene ontology biological process analysis

Functional annotation analysis to determine enriched Gene Ontology Biological Processes was performed using DAVID (154,155), GREAT (156) or GO terms in the biological process ontology, as specified in the figure legends.

3.17 Primer Design and List of Primers

Primers for ChIP and mRNA analysis were designed by using primer design software (Primer-BLAST).

Gene	**Primers for ChIP-PCR**
Cdkn1a	TAGCTTTCTGGCCTTCAGGA GGGGTCTCTGTCTCCATTCA
Bbc3	CCGTTAGTCTGAGCGTACTCC CGCTTGACACACTGACACACT
AchR	AGTGCCCCCTGCTGTCAGT CCCTTTCCTGGTGCCAAGA
Gene	**Primers for RT-PCR**
Cdkn1a	CTGGGAGGGGACAAGAG GCTTGGAGTGATAGAAATCTG
Bbc3	GAGACAAGAAGAGCAGCATCG AAGAGATTGTACATGACCCTCCA
Pmaip1	CAGAGCTACCACCTGAGTTCG TACACTTTGTCTCCGATCTTCCT
Trp53	CGCTGCTCCGATGGTGAT TGGCGAAAAGTCTGCCTGTC
Tbp	TAATCCCAAGCGATTTGCTG CAGTTGTCCGTGGCTCTCTT

3.18 Ingenuity pathway analysis (IPA)

Upstream Regulator Analysis was performed using QIAGEN's Ingenuity Pathway Analysis (IPA, QIAGEN Redwood City, www.qiagen.com/ingenuity). Statistical significance and p-values were determined by IPA using a Fisher's Exact Test.

3.19 Vector and shRNA library construction

A miR-30-based shRNA library was designed to target 330 p53 target genes, that were strong candidates for mediating tumor suppression. 97-base-pair gene-specific hairpins were selected from the Hemann lab shRNA database (http://euphrates.mit.edu/cgi-bin/shRNA/index.pl) to generate an shRNA library subdivided into 30 pools of 55 shRNAs each targeting 11 genes (5

shRNA/gene). 121-base-pair oligonucleotides (including the miR-30-shRNA precursor, the EcoRI site and a pool-specific barcode) were synthesized on a 12k customized oligonucleotide array (CustomArray). Pool-specific PCR products were individually cloned in MLS vector. Viruses were produced by transient transfection of Phoenix ecotropic packaging cell line.

3.20 Haematopoietic stem and progenitor cell isolation and *in vivo* adoptive transfer

Single-cell suspensions of Eμ-*myc* HSPCs were prepared by resuspending ED 12.5-14.5 fetal livers in stem cells medium (DMEM and IMDM (1:1), 10% stem cell serum (Stem Cell Technologies), 2mM L-Gln, 1% penicillin/streptomycin, 0,2% β-mercaptoethanol, 0,4% WEHI-3B conditioned medium) supplemented with 2 ng/ml IL-3, 2 ng/ml IL-6 and 20 ng/ml SCF. Cells were retrovirally transduced with shRNA pools or individual shRNAs. After short-term *in vitro* expansion, $1\text{-}2 \times 10^6$ HSPCs were transplanted by tail-vein injection into sublethally irradiated (7 Gy) 8- to 10- week-old syngenic C57/Bl6 females. Recipient mice were administered neomycin (1 mg/ml, Sigma-Aldrich) in the drinking water for 2 weeks after transplantation.

3.21 Tumour sequencing

DNA was extracted from lymphoma cell pellets with Puregene A Core Kit (Qiagen). shRNAs were amplified by PCR, from the genomic tumor DNA, with vector-specific primers (forward primer, 5'-AATGATACGGCGACCACCGACTAAAGTAGCCCCTTGAATTC -3', barcoded reverse primer, 5'-CAAGCAGAAGACGGCATACGA-NNNNNN-TAGTGAAGCCACAGATGTA -3'). The primers also contained the P5 and P7 adaptor sequences required for sequencing on the Illumina HiSeq 2000 platform. After amplification, PCR products from individual tumor samples amplified with specific barcodes were purified, quantified and pooled. Approximately 2×10^6 50-base-pair reads were acquired for each sample. By reading 50 nucleotides into the amplicon starting from the shRNA guide strand, we were able to deconvolute the different tumour samples according to the sample-specific barcode. The specific sequences were subsequently identified by comparing the reads

with the original library sequences using the BWA algorithm, and the relative distribution was calculated.

4 Results

4.1 Characterization of the p53-dependent response to acute DNA damage

4.1.1 Genome-wide analysis of p53 binding following ionizing radiation

DNA damage is one of the best characterized p53 activating stimuli. *Trp53* null thymocytes are deficient in radiation-induced apoptosis, demonstrating the importance of p53 in the response to genotoxic stress (93,94). Given the pivotal role played by p53 in the response to genotoxic injury, we explored the transcriptional activity of p53 following ionizing radiation (IR)–induced DNA damage *in vivo* with a combination of ChIP-Seq and RNA-Seq experiments in wild-type and *Trp53*-deficient mice: we thus compared p53 binding and mRNA expression profiles in different cell types, including mature splenic B cells, defined by the presence of the surface marker B220 (henceforth "B cells"), and a myeloid-enriched population, constituted by the rest of the cells in the organ (B220-negative, "non-B cells"). Four hours after exposure to 7 Gy whole-body irradiation, cells were isolated and processed for the different assays immediately after purification without any *in vitro* culture. We first analyzed the genomic distribution of p53 *in vivo* in unperturbed and irradiated wild-type B and non-B cells, and in irradiated total splenic cells from *Trp53*$^{-/-}$ mice as a negative control for the specificity of the p53 antibody (Fig. 7). Stress stimulation greatly increased the total number of binding sites both in B and non-B cells (from around 2,000 sites in control to 20,000 in irradiated samples) (Fig. 7, Fig. 8). All p53 peaks identified in control samples were retrieved in the irradiated samples where they constituted some of the most enriched peaks (Fig. 7). Upon stress stimulation, p53 binding sites increased by ten-times and the overlap between p53 peaks in B and non-B cells went from 50% in controls up to 85% in irradiated samples. Moreover, all the binding sites in unperturbed samples were retrieved in either B and non-B cells upon irradiation.

In all conditions, 30-40% of the p53 binding sites were located nearby an annotated transcription start site (-5 to +2kb from the TSS, henceforth referred to as "promoter"). The remaining peaks

were distal, and equally distributed among intra-and intergenic regions. With the increase in p53 levels following acute DNA damage, the new binding sites distributed roughly proportionally on promoters, gene bodies and extragenic locations, resulting in a similar genomic distribution of p53 peaks as in control samples (Fig. 8).

We then performed motif analysis on the p53-bound sites and checked for the occurrence of the canonical p53 consensus motif (Jaspar database (65)): the p53-RE could be identified in approximately 10% and 30% of the promoter-proximal and distal p53 binding sites, respectively (Fig. 7, Fig. 9). At the remaining sites, p53 could be bound to weak variant sites or in a non-sequence specific manner, through protein-protein interactions or chromatin looping. This notion was also supported by the observation that sites containing the p53 motif represented the high affinity sites as indicated by a clear correlation between the presence of the p53-RE and p53 binding strength (Fig. 10). However, it should be noted that this was a preliminary analysis that didn't take into consideration weaker variant sites or p53 motifs with a spacer or half sites, therefore we could be underestimating the number of p53-REs identified.

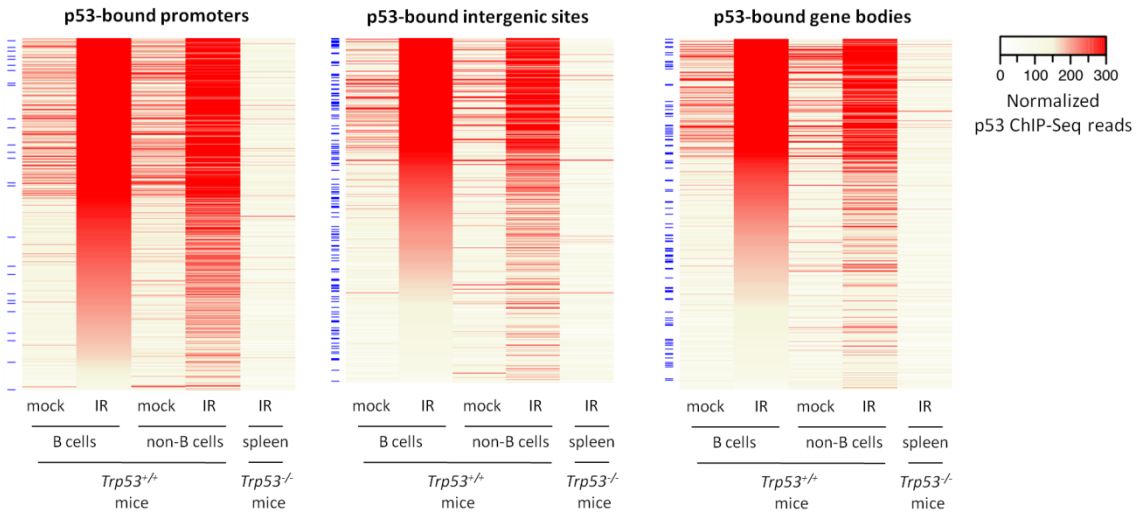

Fig. 7 - IR exposure increased both the binding intensity and the total number of p53 binding sites.
Heatmaps showing library size-normalized ChIP-seq read counts for all p53-bound promoters (-5/+2 kb from the TSS), gene bodies (+2 kb from the TSS through 3'UTR) and intergenic regions (everything else) at chromosome 1 in B and non-B cells from control (mock) and irradiated (IR) *Trp53*$^{+/+}$ mice and total splenic cells from irradiated *Trp53*$^{-/-}$ mice, as indicated. Peaks are ranked from top to bottom by reads density in irradiated B cells. The occurrence of the p53 motif at the genomic intervals analyzed is calculated by the FIMO (Find Individual Motif Occurences) algorithm (153) (p-value<1 x 10^{-5}) and indicated with blue lines on the left side of the heatmaps.

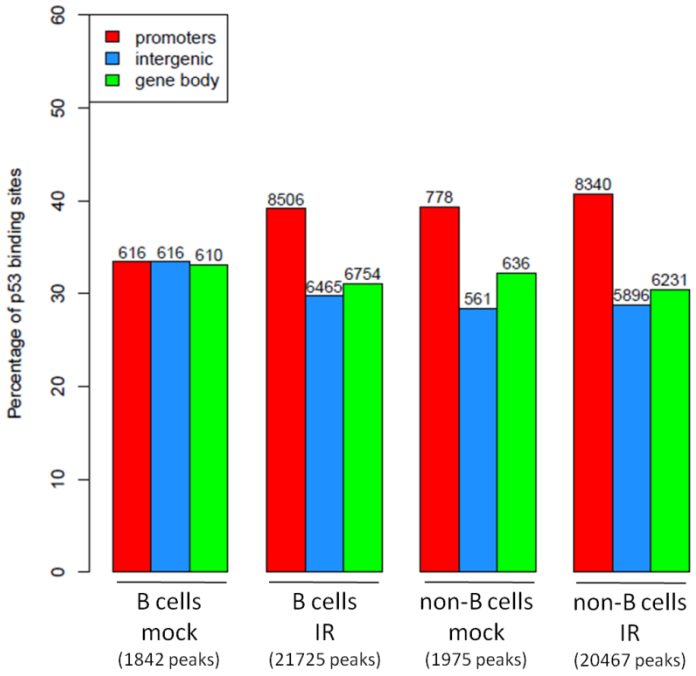

Fig. 8 - Genomic distribution of p53 binding sites.
Percentages of p53 binding sites at promoters (-5/+2 kb from the TSS, red bar), gene bodies (+2 kb from the TSS through 3'UTR, green bar) and intergenic regions (everything else, blue bar) in B and non-B cells from control (mock) and irradiated (IR) wild-type mice. Absolute numbers of peaks are indicated above the bars and total numbers of peaks in the sample below the labels.

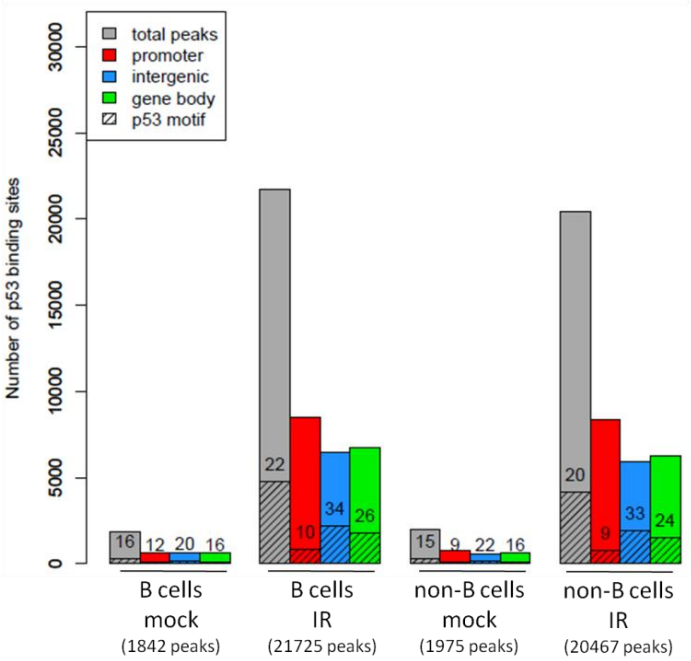

Fig. 9 - Motif analysis and genomic distribution of p53-binding sites.
Characterization of all p53-bound sites at promoters (-5/+2 kb from the TSS, red bar), gene bodies (+2 kb from the TSS through 3'UTR, green bar) and intergenic regions (everything else, blue bar) in B cells and non-B cells from control (mock) and irradiated (IR) wild-type mice, for the occurrence of the p53 motif as calculated by the FIMO algorithm (p-value<1 x 10^{-5}). The percentage of p53-bound sites containing the p53-RE is indicated.

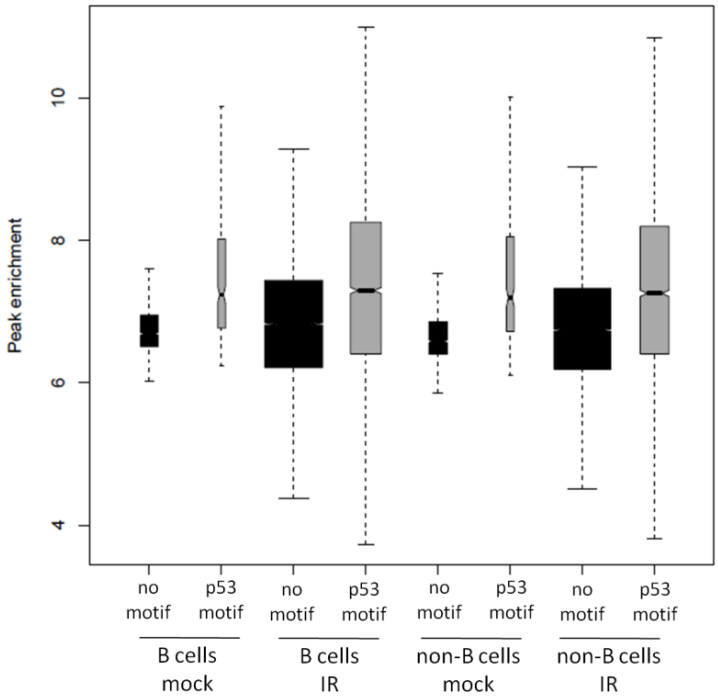

Fig. 10 - Stronger p53 binding sites are more likely to contain the consensus p53 motif.
Peak enrichment of p53 binding sites that contain (grey boxes) or not (black boxes) the p53 motif in control (mock) and irradiated (IR) B and non-B cells. The boxes are drawn with widths proportional to the square-roots of the number of observations in the groups.

To chart p53 binding sites at active promoters and enhancers, we characterized them for the co-localization with the active promoter mark H3K4me3, the enhancer mark H3K4me1 and the activation mark H3K27ac, using our recently published ChIP-Seq dataset in mouse B cells (157). All p53-bound promoters were characterized by the presence of H3K4me3 and H3K4me1; moreover, the H3K27ac mark was identified at most promoter-proximal sites, indicating that p53 associated with regulatory elements that pre-existed in an active state in non-irradiated B cells (Fig. 11A). A major fraction of the p53-bound distal sites showed chromatin features characteristic of enhancers (high H3K4me1/H3K4me3 ratios) and were similarly partitioned on intra-and intergenic regions (Fig. 11B). The H3K27ac mark co-occurred at most of these sites, indicative of active enhancers. Distinct subsets of p53-bound promoters and enhancers, however, lacked H3K27ac: it would be interesting to study whether these elements would acquire the mark upon irradiation. There are few contrasting reports in the literature about the role played by p53 at enhancers, suggesting an activating and a repressing role on gene expression (78,79). Moreover, accurate assignment of an enhancer element to a given gene requires knowledge of long-range interactions, based on chromosome conformation capture technology. Therefore, further

investigation is needed to understand how and to what extent long-distance transcriptional regulation contributes to shape the p53 response. It should also be noted that a small fraction of the distal p53 binding sites showed the occurrence of the H3K4me3 mark, suggesting that they were erroneously assigned to distal regions and may instead be linked to the promoters of unannotated transcripts or ncRNAs. Finally, some of the distal sites didn't bear any of the chromatin features investigated so far: more extensive characterization of the chromatin signature of these regions may unravel yet unknown aspects of p53 activity.

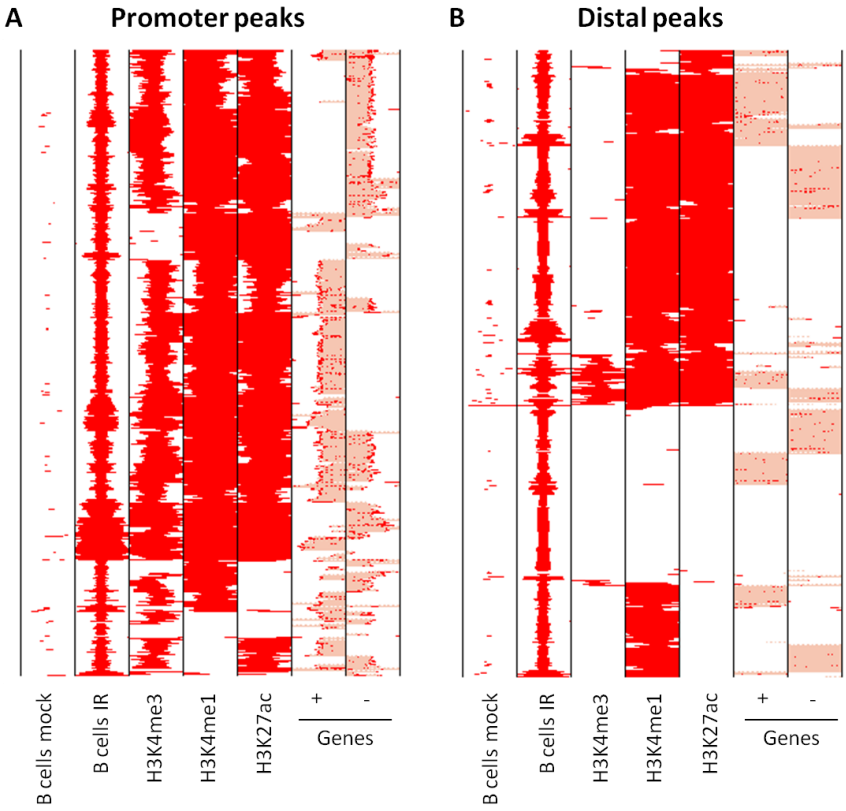

Fig. 11 - Distribution of p53 peaks at annotated promoters and at distal binding sites.
Heatmaps showing the distribution of p53 at annotated promoters (panel A) and at distal binding sites (panel B). Each row represents a different genomic interval (5 kb width centred on p53 peaks). The panels include every annotated promoter and every distant location in chromosome 1 that is identified as p53-associated by ChIP-seq in at least one of the experimental samples: unperturbed (mock) and irradiated (IR) B cells. For the same intervals, the distribution of H3K4me3, H3K4me1, H3K27ac in B cells is shown (157). Genes: RNA transcripts are indicated, based on annotation (exons in red, introns in pink; + sense, - antisense strand).

4.1.2 Expression profiling following acute DNA damage in primary splenic cells.

We used RNA-Seq to determine total RNA profiles before and after IR exposure. RNA-Seq samples were ordered in a dendrogram by unsupervised hierarchical clustering according to similarity in gene expression: the shorter the connecting branch, the more similar the expression profiles

among the samples (Fig. 12). B and non-B cells were clearly separated in the dendrogram, indicating that cell type was the major determinant of expression profiles. Radiation exposure and genotype also contributed in shaping the transcriptome: this was particularly evident for B cells, which showed very homogeneous profiles, with irradiated and control samples forming distinct clusters further sub-divided in clusters of *Trp53*$^{+/+}$ and *Trp53*$^{-/-}$ samples. The result was less clear for non-B cells, with higher inter-mixing among genotypes and treatment, possibly owing to the heterogeneous composition of this cell population (Fig. 12). We will henceforth concentrate mainly on the B cell data.

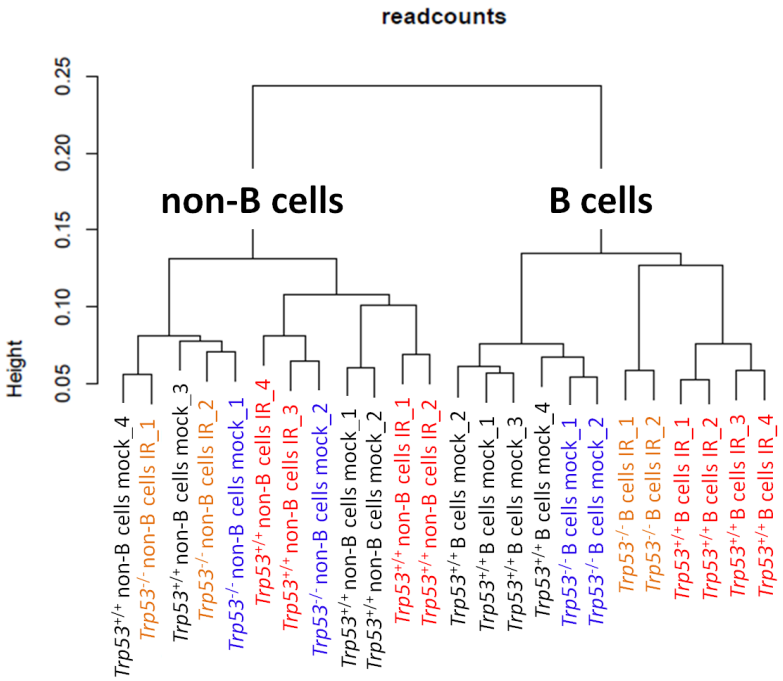

Fig. 12 - Unsupervised hierarchical clustering of RNA-Seq data identifies the cell type as the major determinant of expression profiles.
Unsupervised hierarchical clustering based on RNA-Seq read counts of all expressed genes (read counts>10) in splenic B and non-B cells. Cells were isolated from either control (mock) or irradiated animals (IR) 4 hours after γ-radiation. Data are from 4 *Trp53* wild-type mice and 2 *Trp53* knock-out mice in each condition.

Normalizing the mean expression values of irradiated samples relative to those of unstressed controls yielded 3908 and 2123 differentially expressed genes (DEGs) in B and non-B cells, respectively (Table 1). In either cell type, approximately half of the DEGs were up- and half down-regulated. Based upon loss of the response in *Trp53* knock-out animals, expression of 1308 and 1113 up-regulated genes, 476 and 624 down-regulated genes in B and non-B cells, respectively, was considered as p53-dependent (Table 1, Fig. 13). Hence, the p53-regulated program

constituted a large part of the response to acute DNA damage. p53-dependent and -independent genes could be clearly visualized in the scatter plots in Fig. 13, which confronted the fold-change values of all DEGs following IR exposure in wild-type cells (x-axis) to *Trp53*-deficient cells (y-axis). In B cells, 54% of the DEGs were p53-independent and formed a neat cloud along the bisector of the plot, while the p53-dependent genes grouped separately along the x-axis (Fig. 13A). In non-B cells, instead, most DEGs were p53-dependent and the few that were classified as p53-independent showed smaller fold changes (Fig. 13B). One possible interpretation for this observation was that the cell types that constituted the non-B cell population had different p53-independent responses to IR that opposed each other resulting, on average, in smaller expression changes, while retaining similar p53-regulated programs.

Ionizing radiation-regulated genes							
B cells							
3908 DEGs							
p53-independent 2124 (54%)				p53-dependent 1784 (46%)			
DEG up 780 (37%)		DEG down 1344 (63%)		DEG up 1308 (73%)		DEG down 476 (27%)	
non p53-bound 416 (53%)	p53-bound 364 (47%)	non p53-bound 725 (54%)	p53-bound 619 (46%)	non p53-bound 920 (70%)	p53-bound 388 (30%)	non p53-bound 325 (68%)	p53-bound 151 (32%)
p53 motif 23 (6%)	p53 motif 40 (12%)	p53 motif 39 (5%)	p53 motif 34 (6%)	p53 motif 40 (4%)	p53 motif 168 (43%)	p53 motif 34 (11%)	p53 motif 8 (5%)
non-B cells							
2123 DEGs							
p53-independent 386 (18%)				p53-dependent 1737 (82%)			
DEG up 198 (51%)		DEG down 188 (49%)		DEG up 1113 (64%)		DEG down 624 (36%)	
non p53-bound 119 (60%)	p53-bound 79 (40%)	non p53-bound 118 (63%)	p53-bound 70 (37%)	non p53-bound 837 (75%)	p53-bound 276 (25%)	non p53-bound 399 (64%)	p53-bound 225 (36%)
p53 motif 3 (3%)	p53 motif 17 (22%)	p53 motif 3 (3%)	p53 motif 4 (6%)	p53 motif 17 (2%)	p53 motif 104 (38%)	p53 motif 4 (1%)	p53 motif 12 (5%)

Table 1 - Ionizing radiation-regulated genes in B and non-B cells.
Summary of total numbers and percentages of p53-dependent and -independent IR-regulated genes (q-value<0.05; -0.58>$\log_2$ of fold-change>0.58) in B and non-B cells, further distinguished in induced and repressed genes, and having or not a p53 binding site in the promoter-proximal region containing the p53-RE. In case a gene is bound by p53, we analyze the DNA sequence covered by the p53 peak for the presence of the p53 motif; in case a gene is not bound by p53, we analyze the DNA sequence from -600 bp to +400 bp around the TSS, because the promoter-proximal peaks in this setting are on average 1 kb wide and peak 100 bp upstream of the TSS. p53-dependent genes are defined as follows: all up-regulated genes in *Trp53*$^{+/+}$ cells with a fold induction upon IR at least 1.5 times higher than in *Trp53*$^{-/-}$ cells and all down-regulated genes in *Trp53*$^{+/+}$ cells with a fold repression upon IR at least 1.5 times lower than in *Trp53*$^{-/-}$ cells.

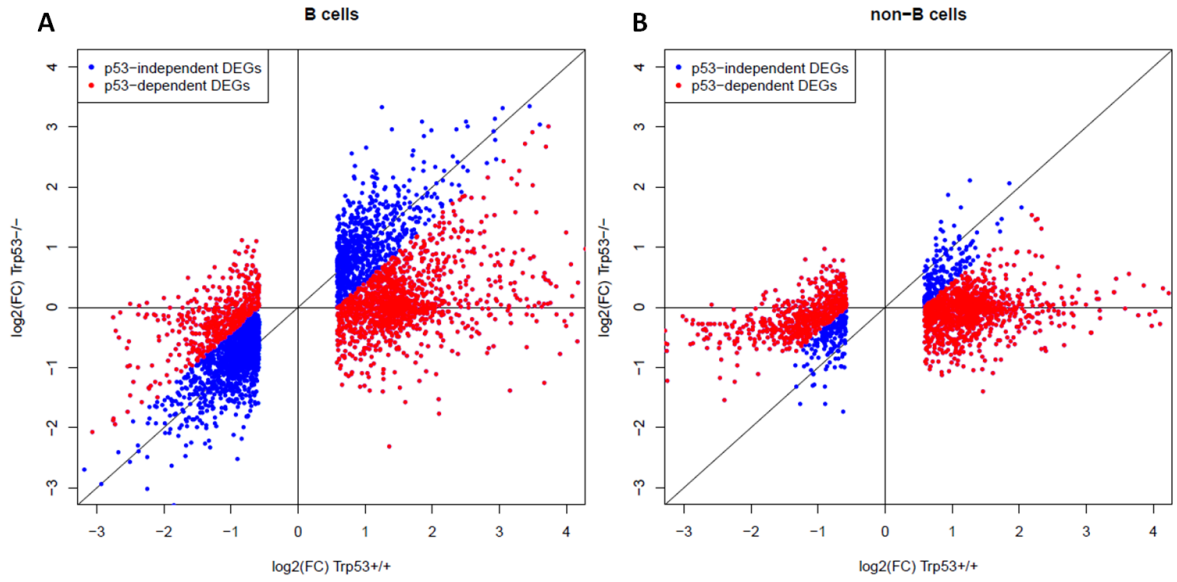

Fig. 13 - Scatter plot of expression changes following IR in Trp53$^{+/+}$ and Trp53$^{-/-}$ B and non-B cells.
Scatter plot opposing the $\log_2$(FC) ($\log_2$ of fold-change) values of all DEGs as estimated by RNA-Seq analysis in irradiated B cells (panel A) and non-B cells (panel B) relative to controls in wild-type mice (x-axis) and the $\log_2$(FC) in *Trp53*-deficient mice (y-axis). Blue dots indicate p53-independent DEGs, red dots p53-dependent DEGs.

Radiation exposure resulted in the activation of programs that were, in part, cell type-specific, as already suggested by the hierarchical clustering of the RNA-Seq data (Fig. 12) and as exemplified in the plot showing ratios of gene expression changes of all DEGs in B cells (x-axis) versus non-B cells (y-axis) (Fig. 14). Thus, many genes were preferentially activated or repressed in one cell type or the other, but only a small fraction of genes changed expression in opposite direction in the two cell types and with smaller fold changes compared to the rest of the DEGs (Fig. 14). The DEGs in common were 32% and 52% of the up-regulated genes, 18% and 41% of the down-regulated in B and non-B cells, respectively (Table 2). Of note, p53-dependent genes were the most negatively and positively-regulated genes in irradiated B and non-B cells, suggesting that these genes were probably the main effectors of the p53 response (Fig. 14).

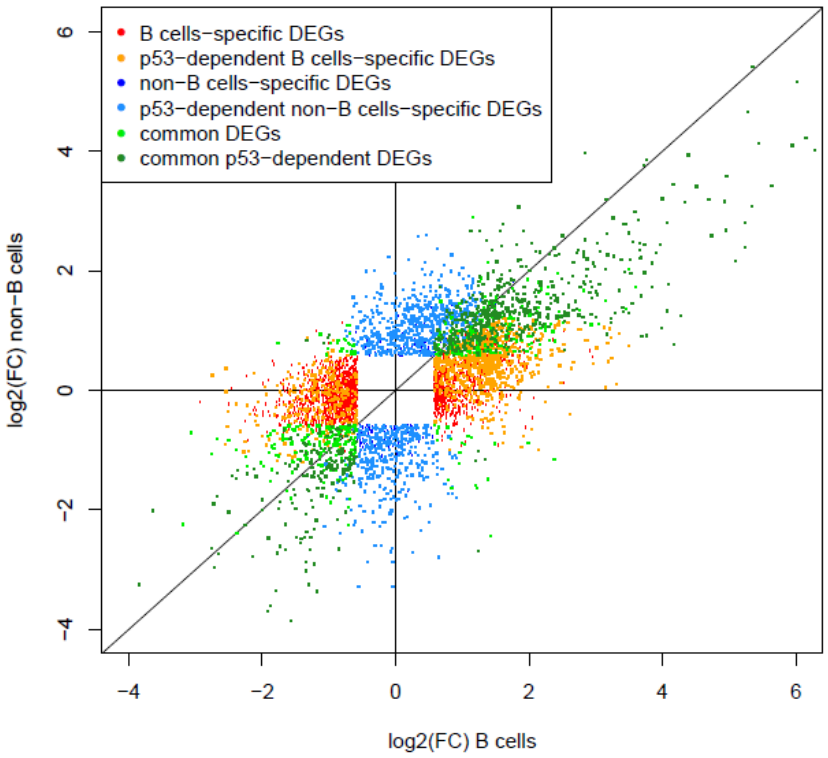

Fig. 14 - Comparison of IR-regulated and p53-dependent genes in B and non-B cells.
Scatter plot opposing the $\log_2$(FC) ($\log_2$ of fold-change) values of all DEGs as estimated by RNA-Seq analyses in both irradiated B and non-B cells relative to controls. Red dots indicate B cells-specific IR-regulated DEGs, orange dots B cells-specific IR-regulated and p53-dependent DEGs, blue dots non-B cells-specific IR-regulated DEGs, light blue dots non-B cells-specific IR-regulated and p53-dependent DEGs. Green dots represent common DEGs between B and non-B cells, with the p53-dependent ones colored in dark green.

To determine which of the IR-regulated genes were direct p53 targets, we combined p53 binding and gene expression profiles (Fig. 15). Approximately 30% of the p53-dependent DEGs in either B and non-B cells had a p53-binding site nearby the TSS (Table 1, Fig. 15), indicating that most of the p53-dependent response was indirectly regulated. We also detected p53 peaks at the promoter of p53-independent DEGs, implying that mere p53 binding to the promoter-proximal region of a gene was not predictive of transcriptional regulation (Table 1, Fig. 15). Moreover, even though the genome-wide p53 DNA-binding patterns were almost identical upon acute DNA damage in B and non-B cells (Fig. 7), we observed substantial differences in the transcriptional response to stress, further supporting that binding was not predictive of transactivation and implying the involvement of other factors, such as cofactors recruited or PTMs of p53, in determining the transcriptional outcome in a cell type-specific manner (Fig. 15).

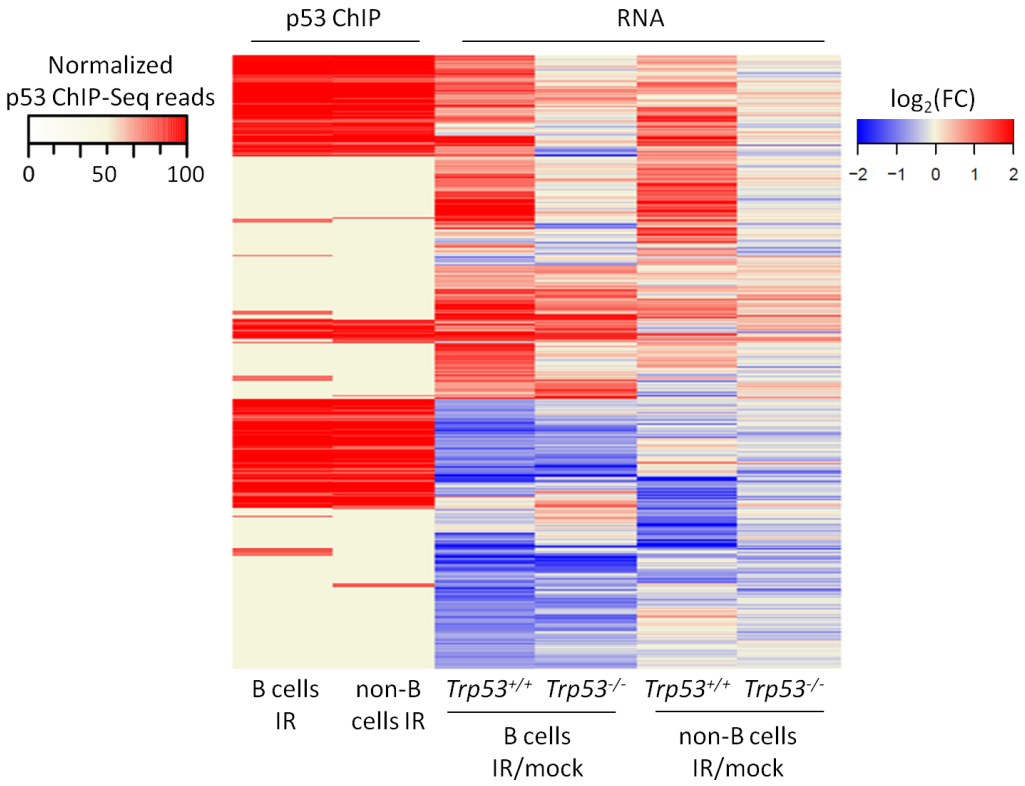

Fig. 15 - Heatmap of IR-regulated genes in B and non-B cells together with the indication about enrichment of p53 binding at the corresponding promoter.
Heatmap of the log2(FC) (log2 of fold-change) values of all DEGs (n=4966) as estimated by RNA-Seq analyses in both irradiated B and non-B cells relative to controls from *Trp53*$^{+/+}$ and *Trp53*$^{-/-}$ animals, together with the indication about enrichment of p53 binding at the corresponding promoter (-600/+400 bp from the TSS).

To determine whether the transcriptional response correlated with sequence-specific DNA binding, we determined the frequency of the p53-RE in the promoters of p53-bound DEGs. To correct for the probability of identifying the p53 motif by chance, we analyzed the DNA sequence of the promoter region (-600 bp to +400 bp from the TSS) of the DEGs not bound by p53 as negative control (Table 1). Remarkably, the motif was significantly enriched among 40% of the p53-dependent up-regulated genes compared to less than 5% of the unbound ones, but not among the p53-dependent down-regulated genes (Table 1), indicating that only gene induction, but not gene repression, was directly regulated by p53 via binding to the p53-RE.

We tested whether p53 binding on the p53-RE nearby the TSS of a gene would be predictive of gene transactivation: we observed that the percentage of up-regulated p53-bound genes increased from 5-10% of induced genes, when we considered any gene with a p53 binding site nearby the TSS, to 20-30%, when we analyzed only genes with a p53 peak on the p53-RE (Fig. 16). Moreover, more than 80% of the DEGs bound by p53 on the p53-RE were also p53-dependent,

suggesting that p53 regulated the expression of the genes that it directly bound. Differently from other transcription factors, such as Myc, p53 didn't bind the RE at the promoter of genes that were not under its direct control. The remaining direct p53 targets containing the p53 motif may not increase significantly the transcript levels at this time point or require other factors for their regulation (Fig. 16).

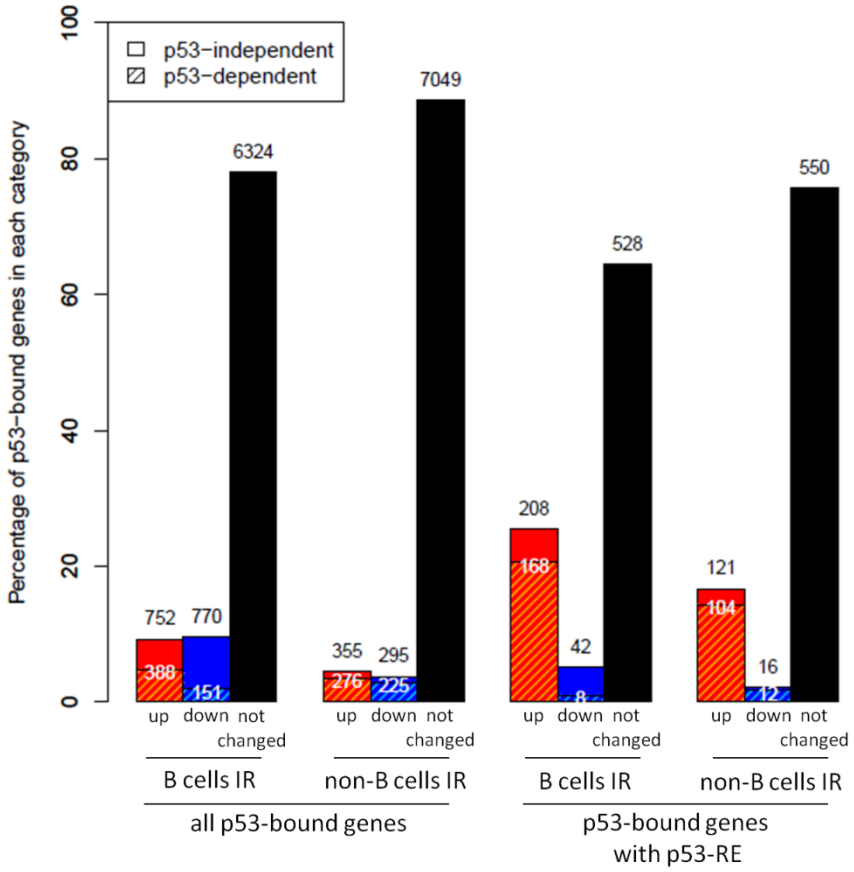

Fig. 16 - Expression changes of p53-bound genes following IR.
Bar plot showing the percentage and the absolute number of all p53-bound genes and of p53-bound genes containing the p53-RE in irradiated (IR) B and non-B cells that don't change expression (black bar), or that are up-regulated (red bar) or down-regulated (blue bar) in response to DNA damage in a p53-dependent or -independent way, as indicated.

To gain more insights into how p53 regulated transcription, we inspected p53 binding strength in the promoter-proximal regions (Fig. 17). As previously observed (Fig. 10), higher p53 binding strength correlated with the presence of the p53-RE. However, among the binding sites on the p53 motif, the peak enrichment of those at the promoter of up-regulated genes was significantly higher compared to genes that didn't change their expression in response to acute DNA damage (p-value: 4×10^{-9} in B cells, 2×10^{-6} in non-B cells). This correlation was not observed or less significant when we compared p53-bound genes without the p53 motif. Altogether p53 binding

strength, like the presence of the p53 motif, correlated with gene activation. Furthermore, we could speculate that the genes bound by p53 at the p53-RE that were not identified as differentially expressed in response to DNA damage, may instead be activated in a minor fraction of cells, as indicated by the lower peak enrichment, therefore resulting on average as not having changed expression. It would be worth measuring the differential expression of these genes at a later time points, to check if their steady state mRNA levels would increase.

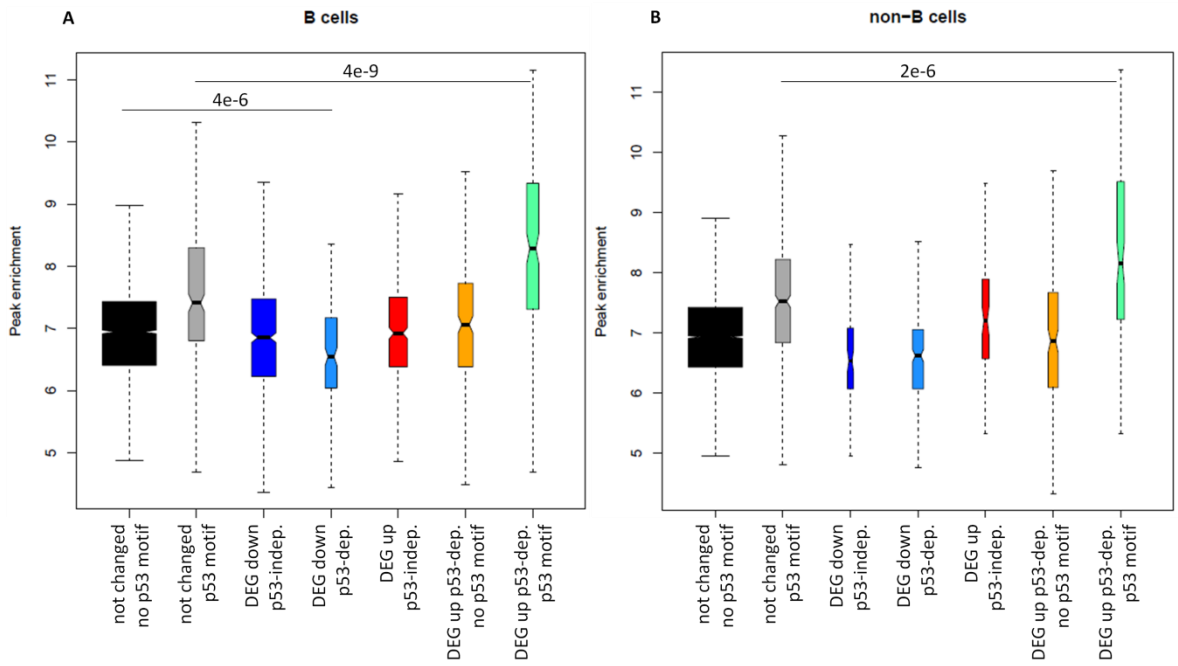

Fig. 17 - Higher p53 binding intensities are most frequently correlated with transcriptional activation. Box plots showing the enrichment of p53 peaks in irradiated (IR) B cells (panel A) and non-B cells (panel B) in the promoter region of genes containing or not the p53-RE, as indicated. Black box, no DEG no p53 motif present; grey box, no DEG p53 motif present; blue box, down-regulated p53-independent genes no p53 motif present; light blue box, down-regulated p53-dependent genes no p53 motif present; red box, up-regulated p53-independent genes no p53 motif present; orange box, up-regulated p53-dependent genes no p53 motif present; seagreen box, up-regulated p53-dependent genes p53 motif present. The boxes are drawn with widths proportional to the square-roots of the number of observations in the groups.

The p53-dependent IR-induced genes constituted the gene set with the highest percentage of common DEGs between B and non-B cells: this overlap increased when we restricted the analysis to the p53-bound ones, and even more when we considered only the subset containing the p53-RE, with almost 90% of the p53-dependent up-regulated genes containing the p53 consensus motif in non-B cells identified in B cells, as well (Table 2). Closer inspection of these gene lists indicated that some genes were defined as p53-dependent in one cell type but not in the other, indicating that some *bona fide* p53 targets may be missed in this analysis due to the stringency of

our statistical criteria. Altogether these data suggested that directly induced p53 targets constituted the core of a cell type-independent p53 response. The comparison between p53-independent genes was limited by the fact that they were very few in non-B cells.

	B cells	non-B cells	common		B cells	non-B cells	common
DEG up	2088 (32%)	1311 (52%)	675	**DEG down**	1820 (18%)	812 (41%)	334
- p53-dependent	1308 (39%)	1113 (46%)	507	**- p53-dependent**	476 (36%)	624 (27%)	171
- non p53-bound	920 (33%)	837 (36%)	299	- non p53-bound	325 (33%)	399 (27%)	107
- p53-bound	388 (45%)	276 (63%)	175	- p53-bound	151 (31%)	225 (20%)	46
- p53 motif	168 (54%)	104 (87%)	90	- p53 motif	8 (25%)	12 (17%)	2
- no p53 motif	220 (36%)	172 (47%)	80	- no p53 motif	143 (30%)	213 (20%)	43
- p53-independent	780 (8%)	198 (31%)	61	**- p53-independent**	1344 (6%)	188 (40%)	76
- non p53-bound	416 (7%)	119 (24%)	29	- non p53-bound	725 (6%)	118 (35%)	41
- p53-bound	364 (7%)	79 (32%)	25	- p53-bound	619 (4%)	70 (34%)	24
- p53 motif	40 (10%)	17 (24%)	4	- p53 motif	34 (9%)	4 (75%)	3
- no p53 motif	324 (6%)	62 (31%)	19	- no p53 motif	585 (3%)	66 (30%)	20

Table 2 - Overlap of ionizing radiation-regulated genes in B and non-B cells.
Summary of total numbers of induced and repressed IR-regulated genes, further distinguished in p53-dependent and p53-independent, and in p53-bound and -unbound and containing the p53-RE. The number and the percentage of common genes between B and non-B cells in the different categories is reported.

A biological process Gene Ontology (GO) analysis indicated that the direct p53 targets containing the p53-RE were involved in the negative regulation of cell cycle progression and in the apoptotic and DNA damage response (Fig. 18). The down-regulated p53-dependent genes, whether p53-bound or not, enriched for terms related to cell cycle and mitosis (Fig. 18). p53 was named the 'guardian of the genome' for the ability of transiently blocking cell cycle progression in response to genotoxic stress, allowing cells to repair their genome before proceeding to cell division, and thereby preventing the accumulation of mutations. In case the DNA alteration was not corrected, p53 signaled the cells to undergo apoptosis. The up-regulated genes not bound by p53 enriched for categories associated to tissue development, organ morphogenesis and cell-cell signaling in either B and non-B cells, in ion transport in the B cells only, in locomotion and response to external stimulus in the non-B cells only (Fig. 18).

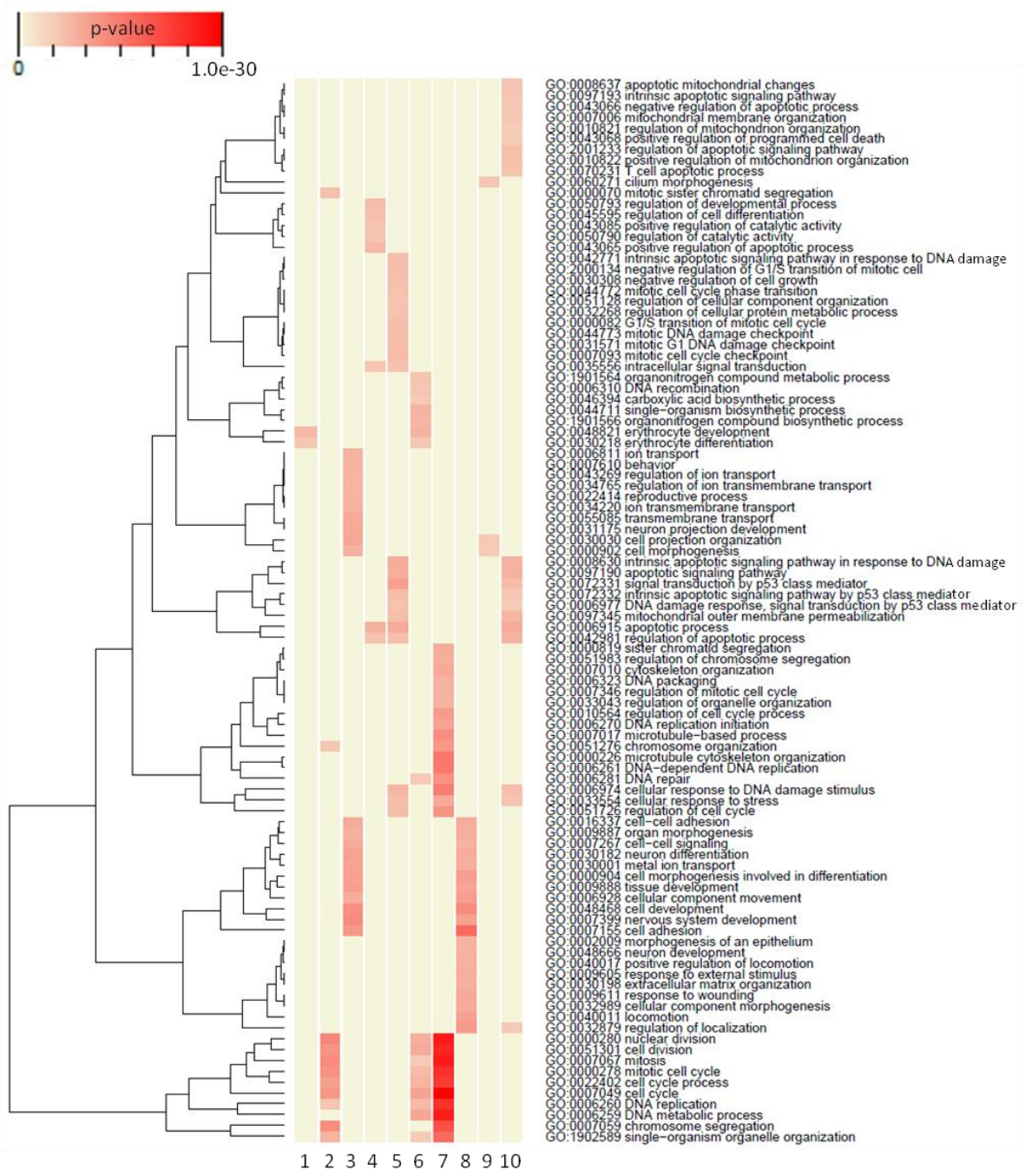

Fig. 18 - Functional annotation of IR-regulated p53-dependent DEGs.

Gene Ontology terms enriched in up- and down-regulated p53-dependent genes in B and non-B cells following IR exposure relative to controls, further distinguished in p53-bound and -unbound and containing the p53-RE. GO terms significantly enriched (Fisher test p-value<$1*10^{-5}$) in at least one gene set were selected (rows in the heatmap) and the p-values for each GO term in each gene set (columns) were colour-coded as indicated. Only GO terms in the biological process ontology that are assigned to less than 2,000 and more than 10 genes in the mouse genome are considered.

Distinct transcription factors may contribute to the IR response, in particular to the regulation of those p53-dependent genes that were not bound by p53, or were bound by p53 but in the absence of the canonical motif. To address this issue, we performed a *de novo* motif search using MEME-ChIP (151). Confirmation of the accuracy of our analysis came from the identification of the canonical p53 motif at the binding sites on the p53-RE (Table 3). Among the other motifs identified there were potential binding sites for Sp1 and Sp2, Egr1 (early growth response protein 1), FoxP1 (Forkhead box protein P1), Nfy (nuclear transcription factor Y), Klf (Krüppel-like factors), and several others (Table 3). Some of these factors were previously suggested to cooperate with p53 (74,158), however our motif analysis of random promoters and of the promoters of p53-independent genes indicated that the results were biased towards commonly identified binding sites in the TSS-proximal region and didn't highlight p53-specific effectors, whose recognition motif could have been hidden by the abundance of binding sites for more general transcriptional regulators.

	DEG up p53-bound p53 motif		DEG up p53-bound no motif		DEG down p53-bound no motif		DEG up non p53-bound		DEG down non p53-bound	
p53-dependent genes	B cells	non-B cells	B cells	non-B cells	B cells	non-B cells	B cells	non-B cells	B cells	non-B cells
	TP53 2.6e-104	TP53/TP63 1.1e-27	STAT3/STAT1/Stat5a/b 2.5e-12	EGR1/SP2/SP1 1e-9	SP1/SP2/KLF5 1.6e-28	EGR1/SP2/SP1 2.5e-69	Sp2 2.4e-99	Sp2/Zfp281/ZNF26 3 6.3e-118	Sp2/EGR1/Zfp281/ 4.6e-76	Sp1/Sp2/Egr1 1.1e-68
			SP1/SP2/EGR1 2e-8	FOXP1/FOXP2/Zfp1 05 2.2e-2	Mtf1/Zfp105/FOXP 1 3e-22	Srf/Mtf1/FOXP1 3.6e-44	Klf7 1.3e-81	Mtf1/FOXP1/IRF1 8.9e-67	Irx6/Mtf1/Sox21 1.6e-48	Klf4 2.7e-27
			IRF1/FOXP1/Mtf1 1.8e-7	SP2/SP1/Bcl6b 2.4e-2	NFYA/Barhl1/NFYB 8.3e-11	NFYA/NFYB/Nkx1-1 2e-27	NFYB 3.9e-43	Klf4 6.4e-19	Klf4 6.3e-41	NFYB 6e-26
			EGR1/Zfx/SP2 3.3e-6		ELF1/SPIB/FLI1 1.3e-6	E2F4/E2F6/E2F3 8.7e-44	GABPA 1.8e-26	EGR2/RREB1 1.1e-15	NFYB 7.6e-23	Srf/Mtf1/FOXP1 7.2e-20
			FEV/Ehf/RELA 5.1e-5		E2F4/E2F6/E2F3 9.8e-4		Srf/Mtf1/Sox7 1.1e-24	NFYB 1.3e-11	Smad3 5.3e-22	NRF1 2.5e-11
			ZEB1/Bhlhe40/T 6.7e-5				NRF1 3.4e-19	Egr1 1.9e-9	NRF1 2.5e-14	Smad3 9.1e-11

	DEG up p53-bound no motif		DEG down p53-bound no motif		DEG up non p53-bound		DEG down non p53-bound		Random promoters
p53-independent genes	B cells	non-B cells	B cells	non-B cells	B cells	non-B cells	B cells	non-B cells	
	SP1/Zfx/SP2 5.6e-19	IRF1/Mtf1/FOXP1 7.8e-6	RUNX/RREB1/Foxd3 1.7e-50	SP1/KLF5/Klf7 7.8e-1	Mtf1/FOXP1/Zfp105 3.3e-64	Mtf1/FOXP1 3.2e-14	KLF5 1.0e-77	Sp4 1.8e-11	Sp2/EGR1/Zfp281 1e-54
	Stat3/Stat5a/b/Stat4 1.8e-11		EGR1/SP2/Zfx 3.7e-44		SP2/SP1/KLF5 1.9e-59	Znf263/EGR1/Zfp740 2.8e-9	Foxj1/Zfp105/Mtf1 1.0e-60	E2F4 1.6e-5	Mtf1/FOXP1/Zfp105 4.6e-49
	GABPA/ELK4/ELF1 3.8e-6		Ets1/Spi1/Erg 6.3e-21		Klf7 1.9e-50	NRF1 1.1e-3	Gabpa 1.0e-50	Bcl6b 5.9e-5	Sp4 5.8e-19
	Mycn/Myc-Max/Bhlhb2 1.4e-2				NRF1 4.9e-27	Klf7 3.4e-3	NFYB 5.8e-49	Klf1 1.6e-4	NFYB 2.4e-16
					Egr1 9.2e-19	Myb/Zbtb3 1.2e-2	Ehf 1.6e-27	NRF1 3.2e-2	Ascl2 1.3e-7
					ELK4 2.3e-14	Irf3 2.2e-2	Egr1 3.2e-24	Gabpa 4.0e-2	NRF1 1.2e-6

Table 3 - Overrepresented transcription factor binding motifs at the promoter of p53-dependent and -independent genes.

De novo motif search by MEME-ChIP (151): the top motif (lowest E-value) are depicted. In case a gene is bound by p53, we analyze the DNA sequence covered by the p53 peak; in case a gene is not bound by p53, we analyze the DNA sequence from -600 bp to +400 bp around the TSS. The analysis of 500 randomly selected promoters is included as negative control.

As *de novo* motif search highlighted very general transcription factor binding motifs; we used Ingenuity Pathway Analysis (IPA), to identify regulators that could mediate indirect gene regulation downstream of p53 activation: this analysis pointed to the microRNA *let-7*, the E2f family of transcription factors (in particular E2f4), the cell cycle inhibitor and well-known p53 target p21 (*Cdkn1a*), cyclin D1 (*Ccnd1*), the cyclin-dependent kinase 4 (*Cdk4*) and the retinoblastoma protein (*Rb*) as possible regulators of the p53-dependent IR-repressed genes, whether p53-bound or not, and in either B- and non-B cells (Table 4). All these factors, except *let-7*, act in the same pathway: while the cyclin D-Cdk4 complex mediates Rb phosphorylation, p21 inhibits it. Unphosphorylated Rb is inactive and cannot dissociate from E2f, resulting in the repression of E2f-regulated cell cycle genes. Hence, in agreement with published findings, gene repression in our experimental model appeared to be indirect, and likely mediated by the microRNA *let-7* and by p53-mediated induction of p21, and consequent repression of the Rb/E2f axis (85,159).

B cells				non-B cells			
DEG down p53-dependent				DEG down p53-dependent			
p53-bound		non p53-bound		p53-bound		non p53-bound	
Upstream Regulator	p-value	Upstream Regulator	p-value	Upstream Regulator	p-value	Upstream Regulator	p-value
CDKN1A	3.03e-14	IKZF1	3.58e-08	E2F4	5.54e-33	let-7	1.31e-09
CCND1	5.22e-14	GATA1	4.88e-08	TP53	1.47e-24	CDKN1A	7.71e-09
E2F4	5.30e-13	EP400	5.11e-07	let-7	4.04e-23	E2F4	8.90e-09
TBX2	1.17e-12	KLF1	3.25e-06	CDKN1A	1.35e-22	CCND1	1.46e-07
PTGER2	1.81e-12	PTGER2	5.07e-06	E2F1	6.81e-22	TCF3	3.04e-07
E2F8	2.25e-11	CCND1	5.29e-06	YY1	8.79e-18	HDAC1	4.82e-07
CDK4	7.11e-11	HIPK2	5.37e-06	TBX2	9.45e-18	GATA1	7.02e-07
let-7	4.80e-10	CDK4	9.27e-06	RB1	2.43e-17	TBX2	2.10e-06
FOXM1	3.82e-09	NUPR1	1.71e-05	CCND1	4.94e-17	PTGER2	4.05e-06
Rb	1.18e-08	TBX2	3.77e-05	PTGER2	8.78e-17	KDM5B	1.18e-05
E2F7	2.39e-08	TCF3	9.19e-05	Rb	9.51e-17	NUPR1	1.18e-05
Vegf	3.46e-08	TGFB1	3.13e-04	NUPR1	2.58e-13	TP53	1.58e-05
TP53	4.01e-08	ESR1	3.74e-04	FOXM1	1.77e-12	PPARA	1.88e-05
RB1	6.76e-08	CDKN1A	3.80e-04	RBL1	2.05e-12	CDCA7L	2.40e-05
EP400	1.61e-07	HOXA10	4.14e-04	EP400	2.62e-12	RB1	4.30e-05

Table 4 - Putative upstream regulators of p53-dependent down-regulated genes.
IPA Upstream Regulator Analysis of p53-dependent down-regulated genes having or not a p53 binding site at the promoter. Statistical significance and p-values are determined by IPA using a Fisher's Exact Test.

p53, its family members p63 and p73 and its cofactor Brd7 (160), were identified as the main regulators of the p53-dependent up-regulated genes that had a p53 binding site on the p53-RE nearby the TSS in either B- and non-B cells (Table 5). p53 and NF-κB were indicated as regulators of the induced p53-dependent genes bound by p53 in the absence of the canonical motif, highlighting a pathway that was previously described to be important for the induction of

apoptosis (161) (Table 5). Finally, the putative regulators of the non p53-bound genes were different in B and non-B cells. Of note, none of the regulators identified for the p53-dependent genes was also indicated for the p53-independent genes, suggesting that these downstream effectors were specific to the p53 response (Table 6). However, we didn't identify any direct p53 target containing the p53-RE that could mediate gene activation, as p21 for gene repression.

B cells						non-B cells					
DEG up p53-dependent						DEG up p53-dependent					
p53-bound p53 motif		p53-bound no motif		non p53-bound		p53-bound p53 motif		p53-bound no motif		non p53-bound	
Upstream Regulator	p-value	Upstream Regulator	p-value	Upstream Regulator	p-value	Upstream Regulator	p-value	Upstream Regulator	p-value	Upstream Regulator	p-value
TP53	5.28e-25	TP53	2.92e-11	CTNNB1	2.25e-05	TP53	5.92e-21	TP53	9.73e-10	SMAD3	8.94e-09
TP73	1.34e-14	RELA	4.82e-07	PTK2	2.81e-05	TP73	2.81e-13	TICAM1	4.32e-06	MYD88	5.14e-08
TP63	1.99e-12	NFKB1	6.08e-07	MYOCD	3.45e-05	CHEK2	1.84e-11	RELA	2.28e-05	TBK1	2.14e-07
ANXA2	1.52e-11	EGR1	2.43e-06	MEF2C	4.38e-05	ANXA2	2.09e-11	NOD2	9.69e-05	SMAD7	3.00e-07
TOPBP1	8.29e-11	NOTCH4	2.55e-05	WNT11	5.81e-05	BRD7	4.47e-10	ERBB4	2.71e-04	CR1L	3.78e-07
CHEK2	4.41e-10	MXD1	7.76e-05	COL9A1	7.50e-05	TP63	4.97e-10	BRCA1	4.14e-04	NFKB1	3.81e-07
CDKN2A	3.65e-09	REL	1.44e-04	FOXA2	7.57e-05	TOPBP1	7.64e-10	ITGA9	6.58e-04	COL4A3	3.94e-07
BRCA1	4.26e-09	NFATC3	1.60e-04	PITX2	8.83e-05	RPL22	1.27e-09	JAK2	7.15e-04	MEF2C	4.55e-07
BRD7	6.27e-09	Map3k7	1.60e-04	REST	9.06e-05	BCL2L12	3.79e-09	TP73	7.27e-04	CREB1	5.10e-07
RPL22	1.05e-08	HIF1A	2.49e-04	TWIST1	1.66e-04	TP53BP2	3.79e-09	IRF7	8.24e-04	SAMSN1	8.02e-07
BCL2L12	3.12e-08	RPS6KA5	2.85e-04	CREB1	1.70e-04	BRCA1	6.85e-09	MYD88	8.96e-04	CREBBP	8.04e-07
TP53BP2	3.12e-08	CYR61	3.43e-04	LMX1B	3.84e-04	PHF1	6.07e-08	PRKAG3	9.06e-04	NOTCH1	9.75e-07
UIMC1	3.14e-07	GATA4	3.81e-04	TGFBR1	4.76e-04	UIMC1	6.47e-08	EGR4	9.18e-04	MERTK	1.13e-06
ID4	4.28e-07	CFL1	4.59e-04	SMAD4	4.81e-04	CDKN2A	1.13e-07	EGR1	9.35e-04	CHUK	1.22e-06
PHF1	8.21e-07	PTK2B	5.01e-04	RBPJ	6.84e-04	S100A4	1.54e-07	S100A9	1.05e-03	DOCK8	1.28e-06

Table 5 - Putative upstream regulators of p53-dependent up-regulated genes.
IPA Upstream Regulator Analysis of p53-dependent up-regulated genes having or not a p53 binding site at the promoter containing the p53-RE. Statistical significance and p-values are determined by IPA using a Fisher's Exact Test.

B cells							
DEG up p53-independent				DEG down p53-independent			
p53-bound		non p53-bound		p53-bound		non p53-bound	
Upstream Regulator	p-value	Upstream Regulator	p-value	Upstream Regulator	p-value	Upstream Regulator	p-value
MYC	2,01E-11	NFAT5	4,75E-02	TP53	3,85E-06	MAPK1	7,06E-06
BRD4	7,34E-06	GATA6	4,75E-02	TFEB	1,02E-04	STAT6	1,47E-05
EIF2AK3	1,03E-05	PLAG1	4,64E-02	TRIM24	1,56E-04	ERBB2	1,98E-05
CLOCK	4,93E-05	MAP2K7	4,64E-02	mir-223	2,12E-04	SP1	8,80E-05
MYCBP	9,90E-05	TCF4	4,64E-02	SATB1	2,52E-04	miR-328-3p	8,87E-05
MTBP	9,90E-05	KDM2B	4,40E-02	NKX2-3	2,59E-04	CLDN7	1,99E-04
EPAS1	2,93E-04	ZNF219	4,32E-02	PRKAG3	2,83E-04	PDLIM2	2,79E-04
IRS	6,13E-04	KDM4D	4,32E-02	SIN3A	2,94E-04	IFN α/β	4,31E-04
KRT5	6,13E-04	NPAS4	4,32E-02	STAT4	3,68E-04	STAT1	4,58E-04
MYCN	8,10E-04	HSPBP1	4,32E-02	SERTAD2	4,21E-04	STAT4	4,67E-04
MAX	1,11E-03	RSPO2	4,32E-02	FOXP3	1,01E-03	TP53	4,92E-04
MXI1	1,18E-03	KDM4A	4,32E-02	RFX2	1,16E-03	mir-223	6,19E-04
GTF2B	1,39E-03	LPXN	4,32E-02	MAPK1	1,46E-03	SOCS1	6,64E-04
E2F1	1,46E-03	ADRBK2	4,32E-02	WWC1	1,63E-03	HNRNPA2B1	6,96E-04
IRAK3	1,73E-03	RPL13A	4,32E-02	miR-293-5p	1,64E-03	IRF3	8,29E-04

Table 6 - Putative upstream regulators of p53-independent genes in B cells.
IPA Upstream Regulator Analysis of p53-independent up-and down-regulated genes in B cells having or not a p53 binding site at the promoter. Statistical significance and p-values are determined by IPA using a Fisher's Exact Test. The limited number of p53-independent genes in non-B cells prevented the analysis.

In conclusion, our observations could be summarized in the following model: upon acute DNA damage, p53 binds, in a selective way, the p53-REs in the genome and induces the transcription of several p53 effectors, which then extend the p53-dependent network in a cell type-specific way; moreover, it up-regulates p21 and indirectly let-7, which then mediate repression of cell cycle genes (Fig. 19).

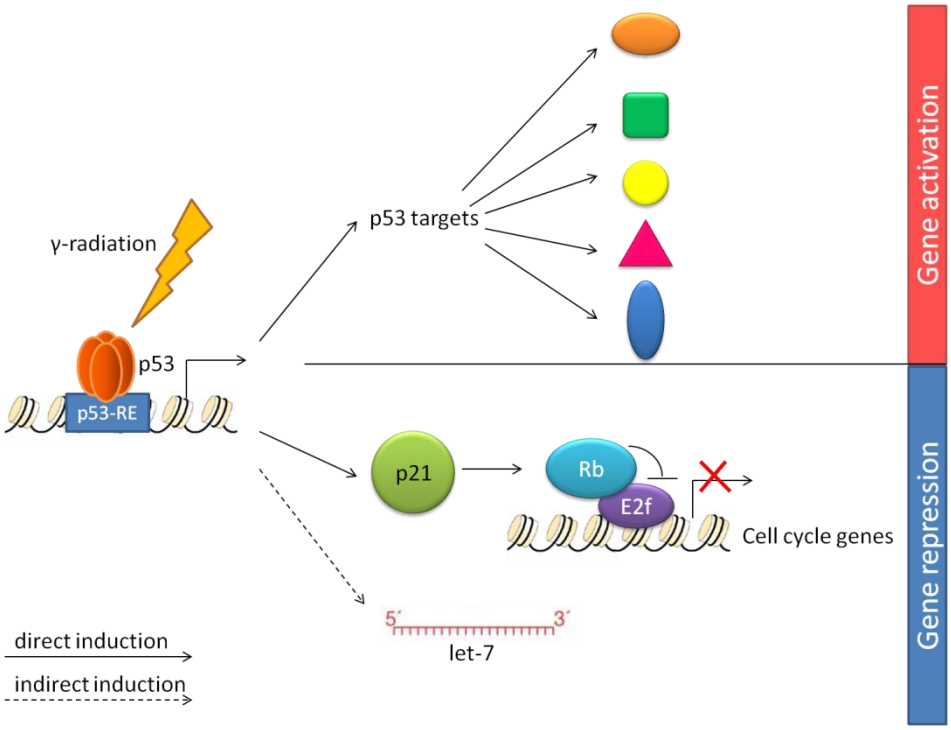

Fig. 19 - Model of p53-mediated gene regulation.

4.1.3 p53 in unperturbed conditions

Under normal unperturbed conditions, p53 is a very unstable protein with a half life of 5-20 minutes (162), therefore it was relatively surprising to detect it bound to chromatin *in vivo*, in cells fixed immediately after purification from the spleen. Previous studies had reported p53-DNA interactions in unstressed cells; however, they were all performed in immortalized cancer cell lines or upon prolonged culturing *in vitro*, conditions that are known to activate p53 (69,78,82). Recently, El-Dahr and coworkers described the p53-regulated program in developing mouse kidney, demonstrating a role for p53 in a physiological process, such as organ development (83).

We previously showed that, in B cells, p53 affected the expression profile not only following IR exposure, but also in unperturbed conditions (Fig. 12). To identify the biological processes regulated by p53 at basal levels, we searched for genes differentially expressed between

unstressed *Trp53*$^{+/+}$ and *Trp53*$^{-/-}$ B cells. We identified 296 genes, with a median of fold induction of 1.5 (Fig. 20). A biological process Gene Ontology (GO) analysis on these basal p53-regulated genes most significantly enriched for terms related to regulation of cellular component size, in particular membrane and cytoskeleton organization, Ras signalling and amino acid import (Table 7). We analyzed published RNA-Seq data (69) using the same parameters as for our analysis and observed that 38% of these basal regulated genes were differentially expressed between *Trp53*$^{+/+}$ and *Trp53*$^{-/-}$ mouse embryonic fibroblasts (MEFs), suggesting that, at least in part, this was not a cell type-specific program. Of note, only four of the basal regulated genes (*Pla2g4a*, *Trpm2*, *Slc39a9*, *9030617O03Rik*) were bound by p53 in unstressed conditions. As previously observed in MEFs, we confirmed that this basal p53 program was mainly indirectly regulated.

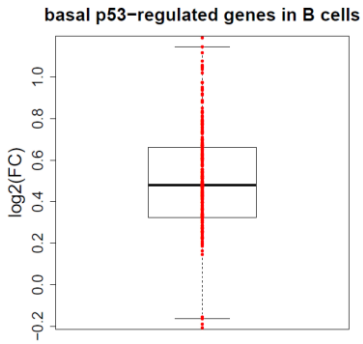

Fig. 20 - Differential expression of basal p53-regulated genes between unstressed Trp53$^{+/+}$ and Trp53$^{-/-}$ B cells.
Box plot showing the $\log_2$(FC) ($\log_2$ of fold-change) values of basal p53-regulated genes in Trp53$^{+/+}$ relative to Trp53$^{-/-}$ unstressed B cells.

GO term biological process	p-value	Genes
GO:0032535~regulation of cellular component size	0.0011	Trp53, App, Lima1, Limk1, Zmat3, Cyfip1, Rictor, Cln8, Epb4.9, Vill
GO:0046578~regulation of Ras protein signal transduction	0.0024	Agap1, Rasgrf2, Rictor, Arhgef5, Tbc1d2b, Tbc1d9, Abr, Asap2, Dgki, Arhgef12
GO:0043090~amino acid import	0.024	Slc11a1, Slc1a3, Cln8
GO:0016044~membrane organization	0.0041	Trp53, Slc11a1, App, Myo6, Dysf, Snca, Sort1, Pmaip1, Cln8, Lrp4, Myh10, Hip1
GO:0007010~cytoskeleton organization	0.0057	Akap2, Lima1, Ptk2, B230120H23Rik, Rictor, Cln8, Dst, Epb4.1l1, Epb4.1l3, Epb4.9, Fmnl2, Myh10, Vill
GO:0007268~synaptic transmission	0.0074	Atxn1, Ptk2, App, Kif1b, Myo6, Clstn1, Snca, Cln8, Dlg2
GO:0030003~cellular cation homeostasis	0.0106	Trp53, Slc11a1, App, Clstn1, Nr3c2, Tgm2, Epor, Prnp
GO:0008088~axon cargo transport	0.0120	App, Kif1b, Dst
GO:0008202~steroid metabolic process	0.0430	Apob48r, Hdlbp, Cyp39a1, Osbpl1a, Hsd11b1, Pbx1, Cln8

Table 7 - Functional annotation of p53 basal regulated genes in B cells.
Biological process GO terms enriched in the list of genes differentially regulated between unstressed *Trp53*$^{+/+}$ and *Trp53*$^{-/-}$ B cells, with p-values as calculated by DAVID (154,155) using a modified Fisher exact test.

Since the basal regulated genes were not direct p53 targets, we performed a biological process GO analysis on the gene set bound by p53 in unstressed cells to understand its function. The p53-bound genes in unperturbed B and non-B cells enriched for multiple terms related to leukocyte

activation and regulation of immune response, and for cell type-specific categories like B lymphocytes activation in B cells and granulocyte, T cell and myeloid cell differentiation in non-B cells (Fig. 21).

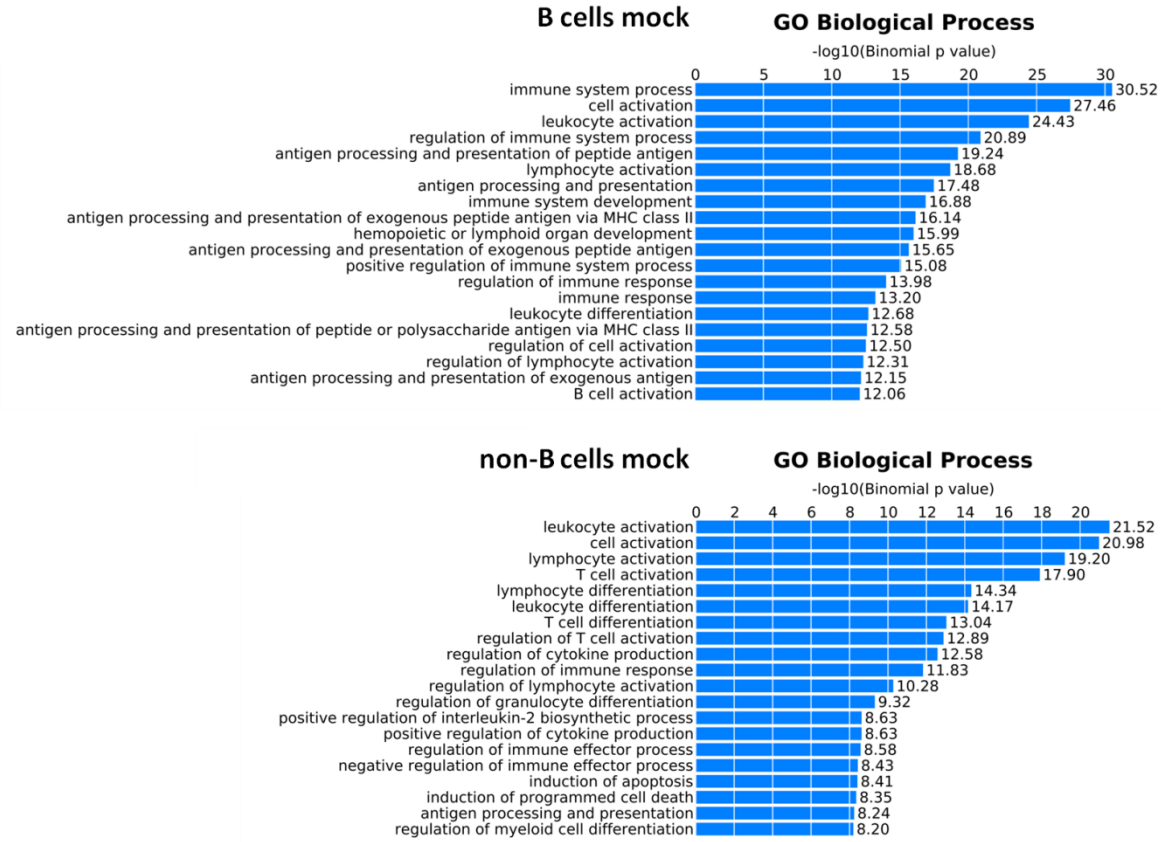

Fig. 21 - p53 binding sites in unperturbed cells are associated with genes involved in immune cell activation and cell type-specific functions.
Biological process GO terms enriched in p53-bound genes in unstressed B and non-B cells, with binomial p-values as calculated by GREAT (156).

To test if p53 was poised for activation on these basally bound genes, we checked whether they changed their expression following IR. Approximately 10% of these genes became differentially expressed both in B and non-B cells following IR exposure, and the percentage increased to 30-40% when we considered only the binding sites containing the p53 motif (Fig. 22). p53 seemed to be poised for activation at its response elements, in the absence of stress stimuli, on cell type-specific genes involved in basic cellular functions, ready to be triggered by PTMs or the recruitment of cofactors to direct a fast response to the insult.

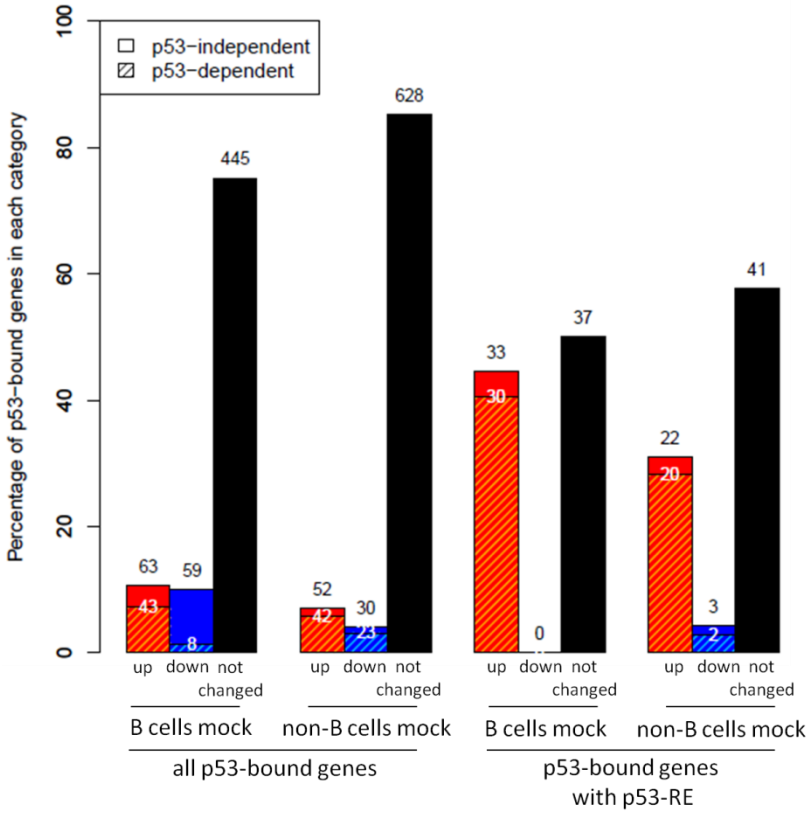

Fig. 22 - Expression changes of p53-bound genes in control samples following IR.
Bar plot showing the percentage of p53-bound genes in unperturbed (mock) B cells and non-B cells that don't change expression (black bar), or that are up-regulated (red bar) or down-regulated (blue bar) in response to DNA damage in a p53-dependent or -independent way, as indicated.

4.2 Characterization of the p53-dependent response to Myc oncogenic stress

In the literature, there are numerous evidences of the fundamental role played by p53 in preventing cancer development; nevertheless, how p53 regulates tumor suppressive programs is still not completely understood. To gain more insight into this process, we generated whole genome maps of p53 binding and gene expression profiles during tumor progression in Eμ-*myc* transgenic mice, as well as during the regression of Myc-driven lymphomas following restoration of p53 function, by either pharmacological or genetic means.

4.2.1 Eμ-*myc* pre-tumoral mice

The Eμ-*myc* mouse model is characterized by a temporally defined pre-tumoral phase, during which the high rates of cell divisions driven by Myc are counter-balanced by the activation of intrinsic tumor suppressive mechanisms that effectively restrain clonal expansion of pre-cancerous cells: the major compensatory mechanism triggered by oncogenic Myc in this setting is apoptosis (128,129), but evidence emerged for a contribution of senescence (130,131).

Remarkably, both of these responses are mediated by p53, and loss of p53 activity is the major selected event in lymphomagenesis (126,127).

To dissect the p53-dependent program during tumor development, we generated ChIP-seq profiles in B cells from young non-transgenic (control, C) and Eμ-*myc* transgenic littermates (pre-tumoral, P): this yielded around 230 peaks both in C and in P, of which 80% were identified in both samples. p53 binding intensity increased from C to P, indicating that a bigger fraction of cells had p53 bound to those genomic regions in P (Fig. 23). Half of the binding sites were at distal intergenic loci, and the remaining ones were distributed between promoters and gene bodies (Fig. 24). Approximately, half of the peaks both in C and P enriched for the p53 consensus motif (Fig. 23, Fig. 24).

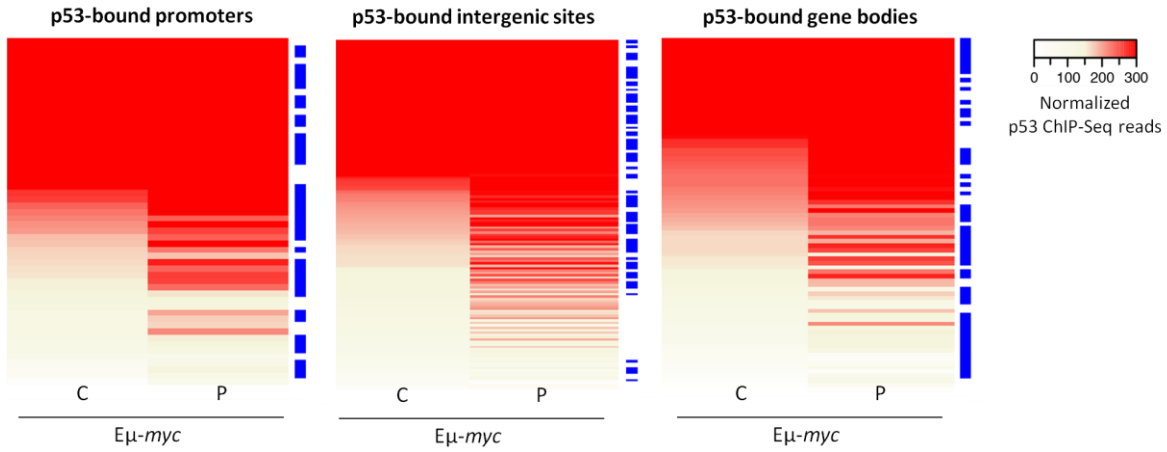

Fig. 23 - Heatmap of p53 binding sites in control and pre-tumoral B cells.
Heatmaps showing library size-normalized ChIP-seq read counts for all p53-bound promoters (-5/+2 kb from the TSS), gene bodies (+2 kb from the TSS through 3'UTR) and intergenic regions (everything else) in control (C) and Eμ-*myc* pre-tumoral (P) B cells. Peaks are ranked from top to bottom by reads density in sample C. The occurrence of the p53 motif at the genomic intervals analyzed is calculated by the FIMO algorithm (153) (p-value<1 x 10^{-5}) and indicated with blue lines on the right side of the heatmaps.

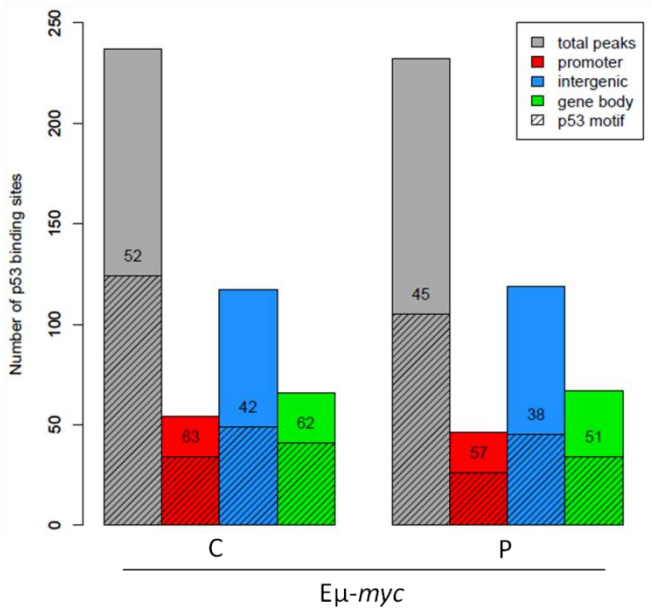

Fig. 24 - Motif analysis and genomic distribution of p53-binding sites in control and pre-tumoral B cells.

Characterization of all p53-bound sites at promoters (-5/+2 kb from the TSS, red bar), gene bodies (+2 kb from the TSS through 3'UTR, green bar) and intergenic regions (everything else, blue bar) in control (C) and Eμ-*myc* pre-tumoral (P) B cells, for the occurrence of the p53 motif as calculated by the FIMO algorithm (p-value<1 x 10^{-5}). The percentage of p53-bound sites containing the p53-RE is reported.

The readers may have noticed that in control B cells from C57/Bl6 mice in our irradiation experiments (Fig. 7) we identified 10-times more peaks than in control B cells from non-transgenic mice of the Eμ-*myc* cohort (C). To test if these two mouse strains would respond differently to a genotoxic insult, we profiled RNA expression in non-transgenic mice of the Eμ-*myc* cohort before and four hours after exposure to 7 Gy whole-body irradiation and compared the RNA-Seq read counts for all genes obtained in the two mouse strains. We observed a very high correlation of gene expression (Fig. 25). Hence, despite a different p53 binding pattern in control cells, the transcriptional response to stress was substantially identical between the two mouse strains. We surmise that basal p53 activity can vary between mouse cohorts of similar genetic background, highlighting the sensitivity of p53 to subtle genetic and/or environmental cues, which remain to be characterized.

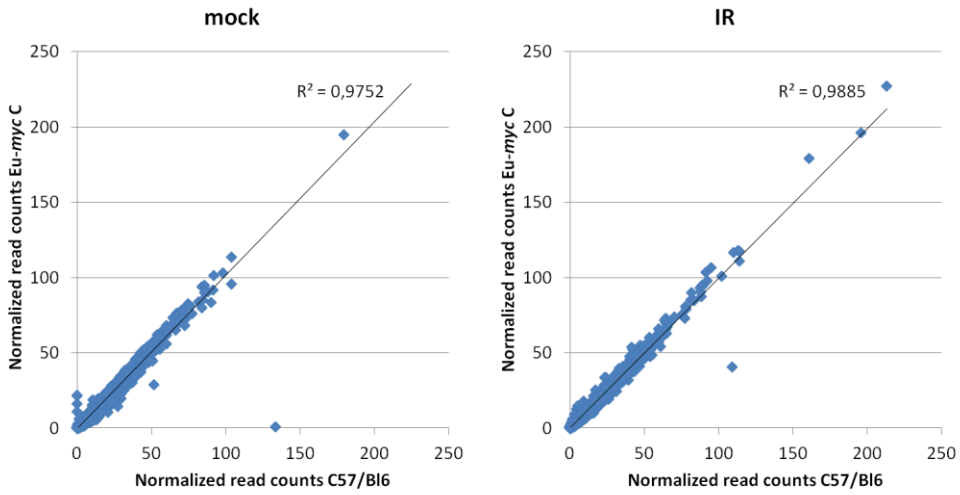

Fig. 25 - The transcriptional profiles in B cells from control and irradiated C57/Bl6 and Eμ-myc C mice are substantially identical.
Scatter plot of library size normalized RNA-Seq read counts for all annotated genes in B cells from control (mock) and irradiated (IR) C57/Bl6 mice and non-transgenic mice of the Eμ-*myc* cohort (C). The correlation coefficient is reported on the graphs.

4.2.2 p53 restoration in Eμ-*myc* lymphomas (i.): p53ER^{TAM} knock-in

The p53 pathway is impaired in tumors, but its reinstatement has been shown to induce tumor regression (136,139,140). Here, we characterized the cellular and transcriptional responses induced upon p53 restoration in lymphomas arising from Eμ-*myc* mice heterozygous for a knock-in allele expressing the conditional p53ER^{TAM} fusion protein (Eμ-*myc* p53ER^{TAM}) (136). Administration of tamoxifen (TAM) *in vivo* allowed a fast transition from a p53 null state to a functional p53 state; once activated, p53 became competent to sense pre-existing stimuli and mount a response. Eμ-*myc* p53ER^{TAM} mice developed lymphomas by 50 days of age; the lymphomas were collected, serially transplanted into syngeneic mice and allowed to develop in the absence of tamoxifen. When the tumors were palpable, p53ER^{TAM} was activated by intraperitoneal injection of 1 mg of tamoxifen, triggering rapid and massive apoptosis of the lymphoma cells (measured as sub-G1 fraction) (Fig. 26). The expression of known p53 target genes increased 2.5 hours after tamoxifen administration, preceding the increase in apoptosis (Fig. 26, Fig. 27).

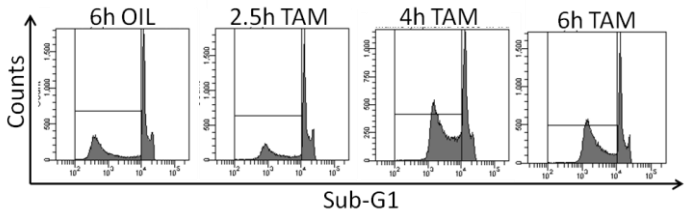

Fig. 26 - p53 restoration in Eμ-myc p53ER^{TAM} lymphomas in vivo triggers rapid apoptosis.
Representative flow cytometric analysis of DNA content (PI staining) of Eμ-myc p53ER^{TAM} lymphoma cells harvested at different time points after vehicle or TAM injection.

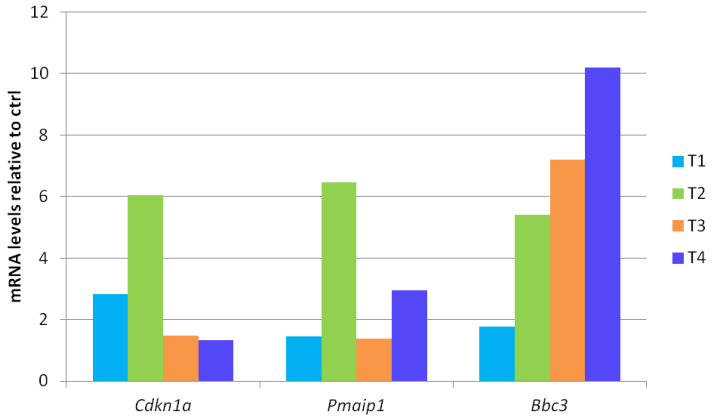

Fig. 27 - p53 restoration in Eμ-myc p53ER^{TAM} lymphomas in vivo induces the expression of p53 target genes.
The expression of p53 target genes (*Cdkn1a/*p21, *Pmaip1/*Noxa, *Bbc3/*Puma) is measured by real-time PCR 2.5 hr after TAM or vehicle *in vivo* treatment in four different Eμ-*myc* p53ER^{TAM} lymphomas.

A similar response was observed when p53ER^{TAM} was reactivated *in vitro* in cultured lymphomas, with cell death starting 4 hours after p53 restoration (Fig. 28). For *in vitro* analyses, we chose to treat the lymphoma cells for 2 hours with 4-OHT: at this time point we could measure an induction in p53 target genes (Fig. 29) with no substantial increase in apoptosis above the basal levels seen in untreated cells (Fig. 28).

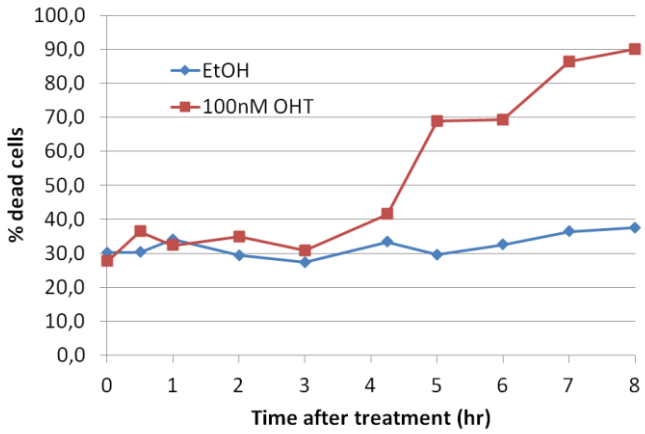

Fig. 28 - p53 restoration in Eμ-myc p53ER^{TAM} lymphomas in vitro triggers rapid apoptosis.
Percentage of dead cells measured by Trypan blue assay was reported at each time point for 100 nM 4-OHT- and vehicle-treated Eμ-*myc* p53ER^{TAM} lymphoma cells.

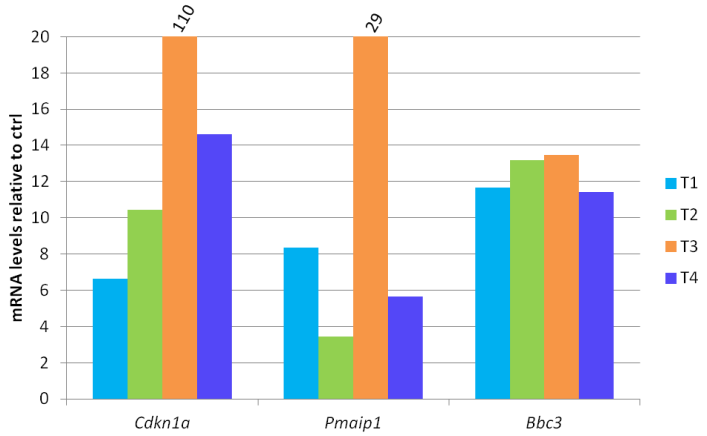

Fig. 29 - p53 restoration in Eμ-myc p53ER^{TAM} lymphomas in vitro induces the expression of p53 target genes.
The expression of p53 target genes (*Cdkn1a/*p21, *Pmaip1/*Noxa, *Bbc3/*Puma) is measured by real-time RT-PCR 2 hr after 100 nM 4-OHT or vehicle *in vitro* treatment in four different Eμ-*myc* p53ER^{TAM} lymphomas.

As assayed by ChIP, the p53ER^{TAM} chimera was a bit leaky: we could detect p53-DNA interactions slightly above background already in vehicle-treated cells, which then increased upon p53 restoration by 4-OHT treatment (Fig. 30).

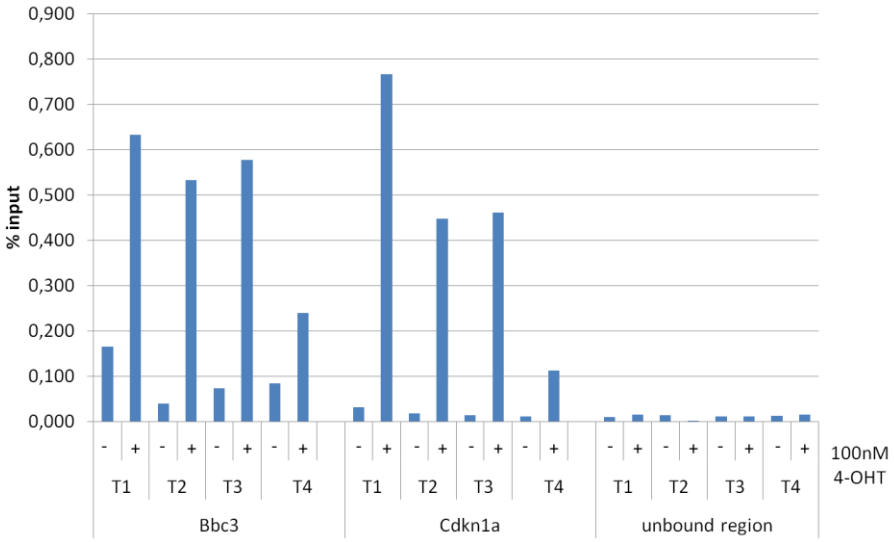

Fig. 30 - ChIP-qPCR analysis of p53 binding.
qPCR analysis of p53 ChIP in four 100 nM 4-OHT- or vehicle-treated Eμ-*myc* p53ER^{TAM} lymphomas at the promoters of two known p53 target genes *Cdkn1a/*p21 and *Bbc3/*Puma. Acetylcholine receptor is analyzed as a negative control. ChIP data are quantified as percentage of input DNA.

We performed p53 ChIP-sequencing in four Eμ-*myc* p53ER^{TAM} lymphomas upon p53 restoration by 4-OHT treatment *in vitro* in cultured lymphomas and *in vivo* by TAM injection in mice with palpable tumors (Fig. 31). The *in vivo* restoration samples had narrower peaks because of technical problems that resulted in lower sequencing depth. Nonetheless, the promoter-proximal

and distal binding sites with the highest enrichment levels in the *in vitro* treated samples were also identified upon *in vivo* restoration of p53. In the *in vivo* data we identified more distal sites, not observed in the *in vitro* data, that were also only partially overlapping between the different lymphomas (Fig. 31B). Since the sequencing quality of the *in vitro* data was better and the other experiments of p53 reinstatement were performed on cultured lymphomas (see below), we continued the analysis only on the *in vitro* data.

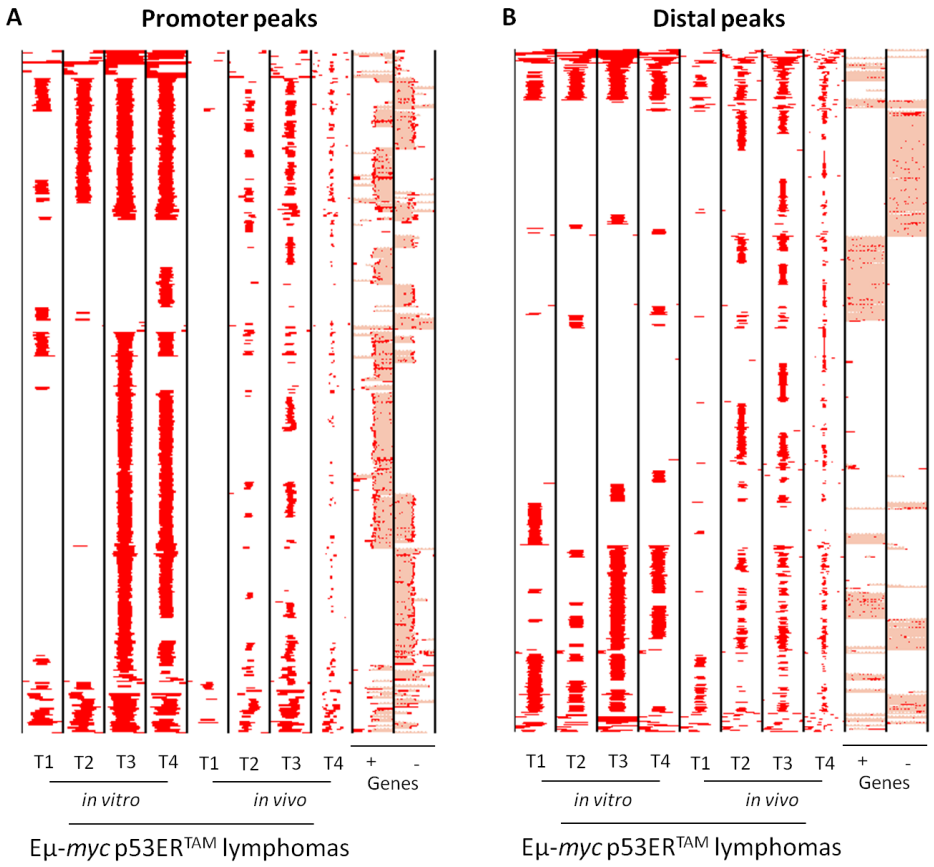

Fig. 31 - Distribution of p53 peaks at annotated promoters and at distal binding sites upon p53 restoration in vivo and in vitro in Eμ-myc p53ER^{TAM} lymphomas.
Heatmaps showing the distribution of p53 at annotated promoters (panel A) and at distal binding sites (panel B) in four Eμ-*myc* p53ER^{TAM} lymphomas (T) treated *in vitro* with 100 nm 4-OHT or *in vivo* with 1 mg of TAM. Each row represents a different genomic interval (4 kb width centred on p53 peaks). The panels include every annotated promoter and every distant location at chromosome 1 that is identified as p53-associated by ChIP-seq in at least one of the experimental samples. Annotated genes (exons in red, introns in pink; + sense, - antisense strand) are also shown.

We observed that both the binding intensity and total number of binding sites increased upon p53 restoration, reaching up to 3500 p53 peaks in lymphomas 1 and 2, 9000 and 8000 in lymphomas 3 and 4, respectively (Fig. 32, Fig. 33). The binding sites with the highest enrichment levels were identified in all tumors and most of the weaker ones were retrieved in at least two samples, confirming their specificity (Fig. 33). In all the lymphomas, the binding sites at promoter-

proximal regions were the most abundant, but only around 10% contained the canonical p53-RE (Fig. 34). Moreover, most of the new p53 binding sites identified only in lymphomas 3 and 4 were located at annotated promoters and few in distant regions (Fig. 31, Fig. 32). Distal binding sites were around 3000 to 4000 in the different lymphomas and approximately one third of these sites had a p53 consensus motif. As previously observed in B and non-B cells, binding to the p53-RE correlated with higher peak enrichment (Fig. 35).

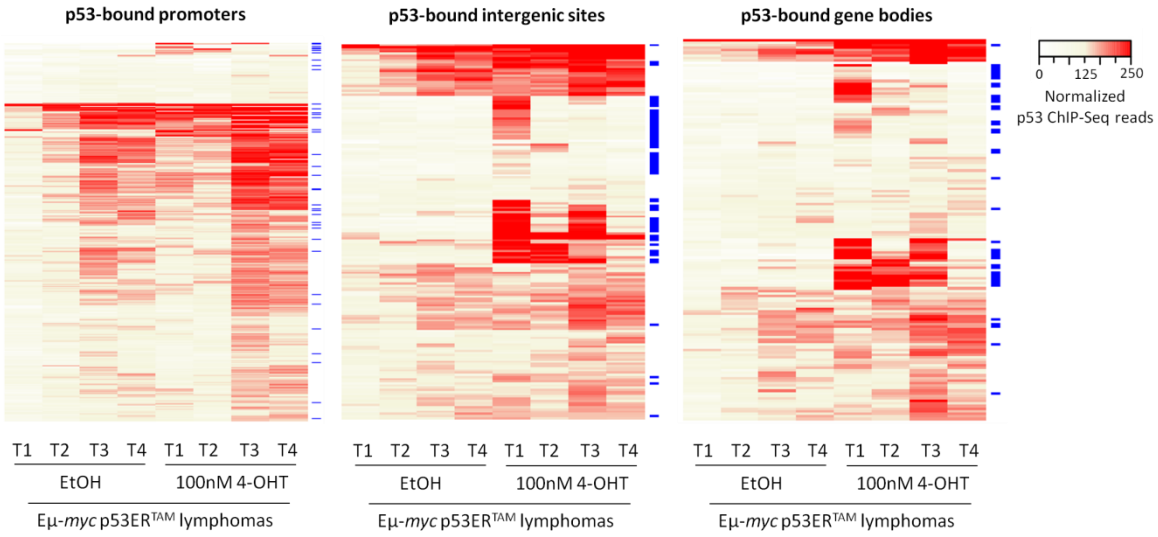

Fig. 32 - Heatmaps of p53 binding sites in vehicle- and 4-OHT-treated Eμ-myc p53ER^{TAM} lymphomas.
Heatmaps showing library size-normalized ChIP-seq read counts for all p53-bound promoters (-5/+2 kb from the TSS), gene bodies (+2 kb from the TSS through 3'UTR) and intergenic regions (everything else) at chromosome 1 in control and 4-OHT-treated Eμ-*myc* p53ER^{TAM} lymphoma cells (T). Peaks are hierarchically clustered. The occurrence of the p53 motif at the genomic intervals analyzed is calculated by the FIMO algorithm (153) (p-value<1 x 10^{-5}) and indicated with blue lines on the right side of the heatmaps.

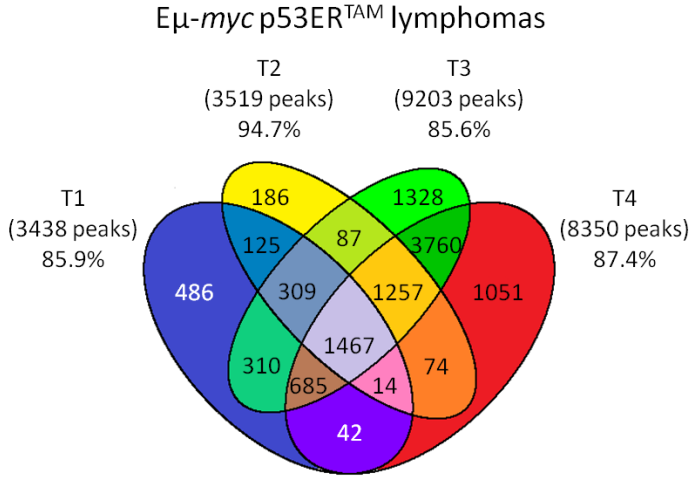

Fig. 33 - Overlap of p53 binding sites between four 4-OHT-treated Eμ-myc p53ER^{TAM} lymphomas.
Venn diagrams of p53 binding sites in four 4-OHT-treated Eμ-*myc* p53ER^{TAM} lymphoma cells (T). Percentages indicate the number of peaks for each lymphoma present in at least another sample.

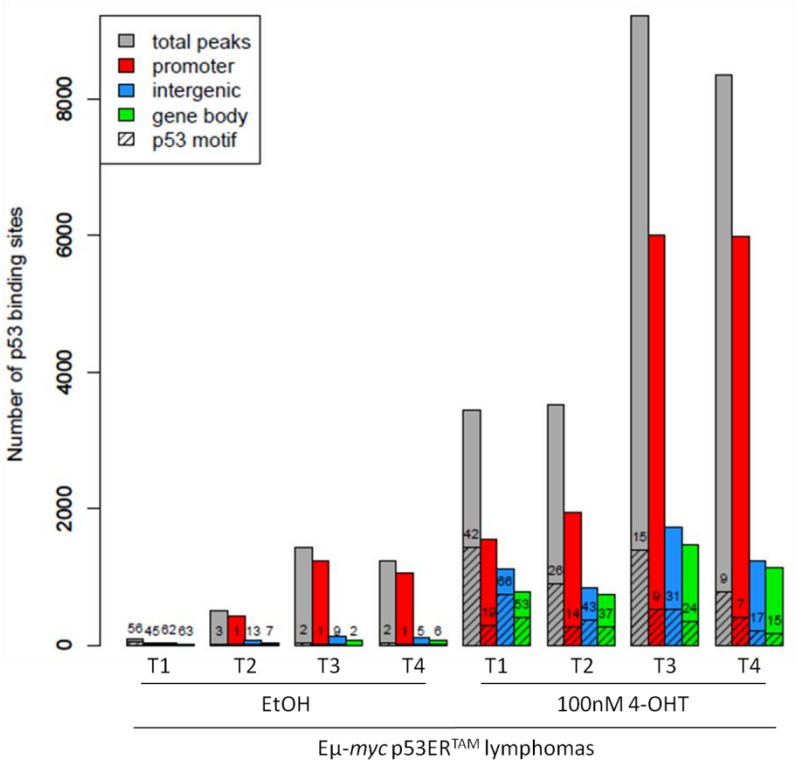

Fig. 34 - Motif analysis and genomic distribution of p53-binding sites in vehicle- and 4-OHT-treated Eμ-myc p53ER^{TAM} lymphomas.

Characterization of all p53-bound sites at promoters (-5/+2 kb from the TSS, red bar), gene bodies (+2 kb from the TSS through 3'UTR, green bar) and intergenic regions (everything else, blue bar) in control and 4-OHT-treated Eμ-*myc* p53ER^{TAM} lymphoma cells (T), for the occurrence of the p53 motif as calculated by the FIMO algorithm (p-value<1 x 10^{-5}). The percentage of p53-bound sites containing the p53-RE is reported.

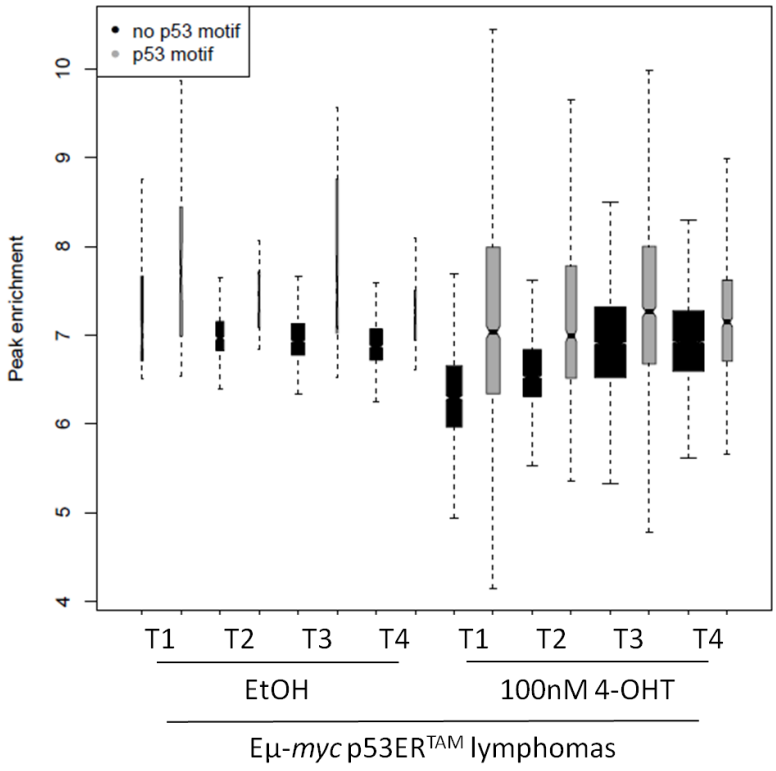

Fig. 35 - Stronger p53 binding sites are more likely to contain the consensus p53 motif.

Peak enrichment of p53 binding sites that contain (grey boxes) or not (black boxes) the p53 motif in control (EtOH) and 100 nM 4-OHT treated Eμ-*myc* p53ER^{TAM} lymphoma cells (T).

4.2.3 p53 restoration in Eμ-*myc* lymphomas (ii.): LSL-p53

As a second model of tumor regression, we generated tumors carrying a reactivatable *Trp53* allele by crossing Eμ-*myc* mice with LSL-p53 mice (139). The LSL-p53 mice carry a transcription–translation stop cassette flanked by loxP sites (LSL) in the first intron of the wild-type *Trp53* locus. The STOP element efficiently silences *Trp53* expression and can be excised by Cre recombinase, thus restoring the expression of the endogenous *Trp53* gene. Eμ-*myc* mice heterozygous for LSL-p53 developed lymphomas by 35 days of age, with every lymphoma analyzed showing loss of heterozygosity (LOH) for the wild-type *Trp53* allele (Fig. 38), as expected according to previous observation in Eμ–*myc* lymphomas arising in $Trp53^{+/-}$ animals (126,127). To temporally control p53 reactivation, we infected lymphoma cells with a selectable retroviral vector expressing a Cre-recombinase-Estrogen-Receptor-T2 (Cre-ER^{T2}) fusion protein (146). The ER^{T2} moiety caused retention of the Cre recombinase in an inactive form in the cytoplasm until tamoxifen administration released this inhibition, thus permitting the recombination of the genomic loxP sites. Release of the transcription–translation block by provision of tamoxifen did not itself activate p53 but simply restored the expression of the wild-type p53 protein which was then competent to become activated by appropriate signals in the cell, in this particular case by Myc-induced oncogenic stress and elevated levels of $p19^{Arf}$ (116,126).

The STOP element efficiently prevented gene expression, with no detectable p53 mRNA or protein in vehicle-treated cells (Fig. 36, Fig. 37). *Trp53* mRNA levels peaked eight hours after Cre activation by 4-OHT treatment, along with the mRNAs of two well-known p53 targets *Cdkn1a* and *Bbc3* (Fig. 36). Western blot analysis showed accumulation of the p53 protein (Fig. 37) and excision of the STOP element, even though incomplete, was also detected by PCR on genomic DNA (Fig. 38). Restoration of p53 function selected for the rapid outgrowth of undeleted clones, as indicated by the decrease in the intensity of the band of the recombined LSL cassette over time after Cre activation. The presence of undeleted clones together with the fact that recombination of the LSL casette was not synchronous in all cells, causing that the cells that recombined first were lost by apoptosis before the others started to recombine the locus, prevented the detection

of cell death that was instead observed in Eμ-*myc* p53ER^{TAM} lymphomas. For these reasons, the analysis of p53-dependent responses was confined within 8 hours.

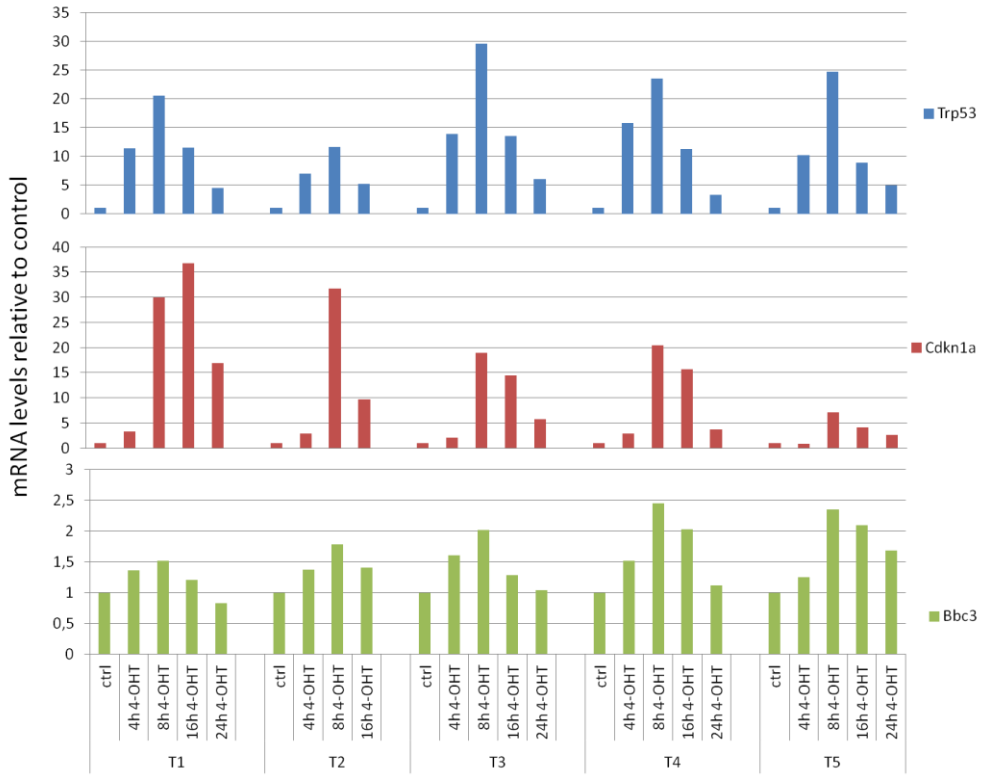

Fig. 36 - Conditional reactivation of p53 in vitro in Eμ-myc LSL-p53 lymphomas induces the expression of p53 target genes.
Real time RT-PCR analysis shows induction of expression of *Trp53* and p53 target genes *Cdkn1a*/p21 and *Bbc3*/Puma in five different Eμ-*myc* LSL-p53 lymphomas (T) at different time points after *in vitro* treatment with 250 nM 4-OHT or vehicle.

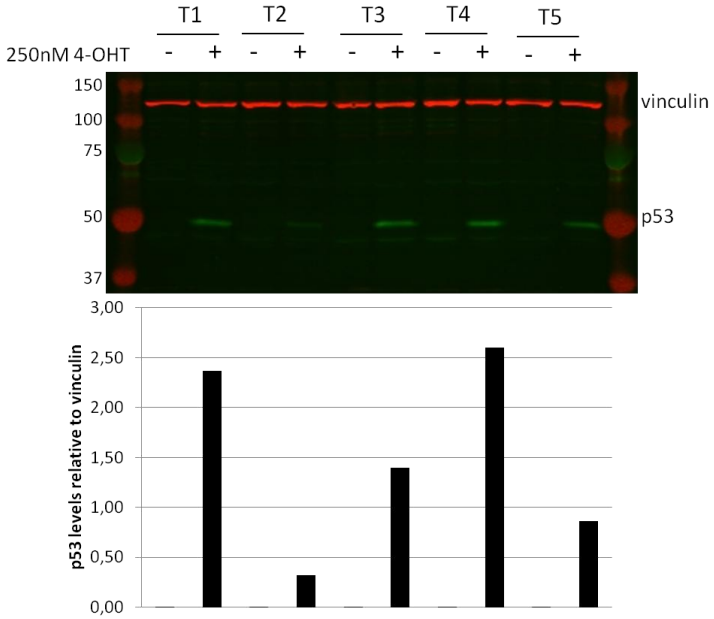

Fig. 37 - Western blot analysis of the p53 protein in Eμ-myc LSL-p53 lymphomas.
p53 stabilization is determined by quantitative infrared Western blotting in five different Eμ-*myc* LSL-p53 lymphomas (T) 8h after *in vitro* treatment with 250nM 4-OHT or vehicle. Densitometric quantification of p53 band is shown normalized to vinculin.

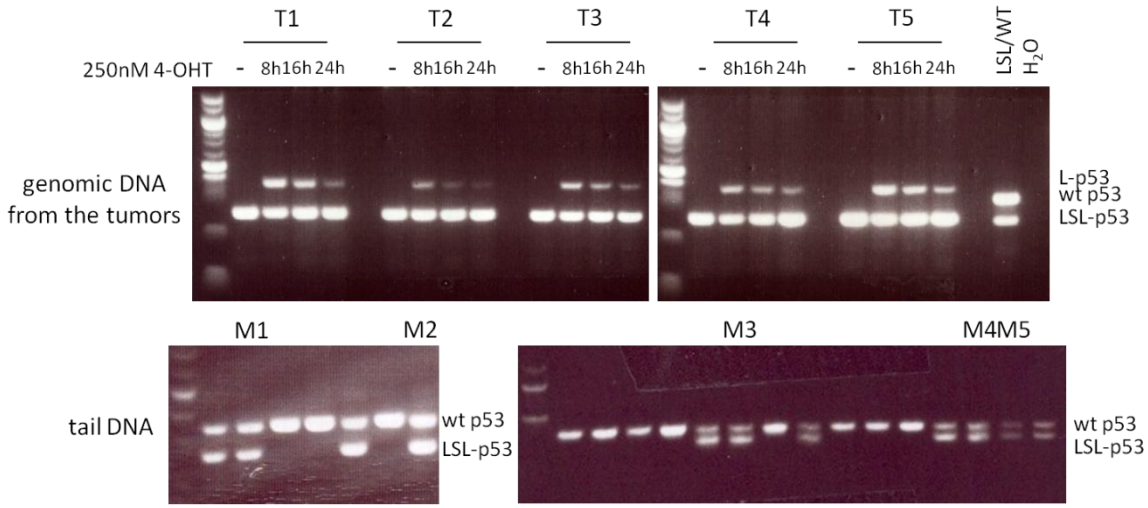

Fig. 38 - Excision of the STOP element in Eμ-myc LSL-p53 lymphomas.
Excision of the STOP element is determined by PCR on genomic DNA from five different Eμ-*myc* lymphomas (T) treated *in vitro* with 250 nM 4-OHT or vehicle using the same amount of starting material. Tail DNA from a LSL-p53 heterozygous mouse is included as positive control. Genotyping by PCR amplification of matched normal tail DNA (M) shows that Eμ-*myc* LSL-p53 tumors undergo LOH of the wild-type *Trp53* allele.

We analyzed the genomic distribution of p53 in three Eμ-*myc* LSL-p53 lymphomas eight hours after Cre activation by 4-OHT treatment. In vehicle-treated cells, we could identify very few peaks throughout the whole genome, likely false positive hits since they constituted the only few sites not overlapping the p53 consensus motif (Fig. 39). This evidence confirmed the efficiency of the STOP element in blocking *Trp53* expression and the specificity of the antibody in detecting p53. Upon 4-OHT-treatment, we detected around 1000 to 2000 p53 binding sites in the different lymphomas. Lymphoma 2 had the lowest number of p53 peaks, which constituted a fraction of the peaks in lymphoma 3 that in turn represented a fraction of the peaks in lymphoma 1 (Fig. 39, Fig. 40), correlating with the relative levels of p53 achieved in each of those lymphomas. p53 peaks in lymphoma 2 constituted the binding sites with the highest levels of enrichment in the other two lymphomas, suggesting that in this sample our sensivity in the detection of p53-DNA interactions was lower and therefore we identified only the high affinity sites. 90% of all binding sites overlapped with the p53-RE and approximately 60% were at intergenic sites, 30% at gene bodies and 10% at promoters. Differently from the Eμ-*myc* p53ER^{TAM} lymphomas, where we identified up to 9000 p53 binding sites, in Eμ-*myc* LSL-p53 lymphomas we detected fewer binding sites, but which all contained the p53-RE. Thus, in this experimental setting, we identified only the

high affinity p53 binding sites because our sensitivity in calling the peaks was decreased by the presence of undeleted clones.

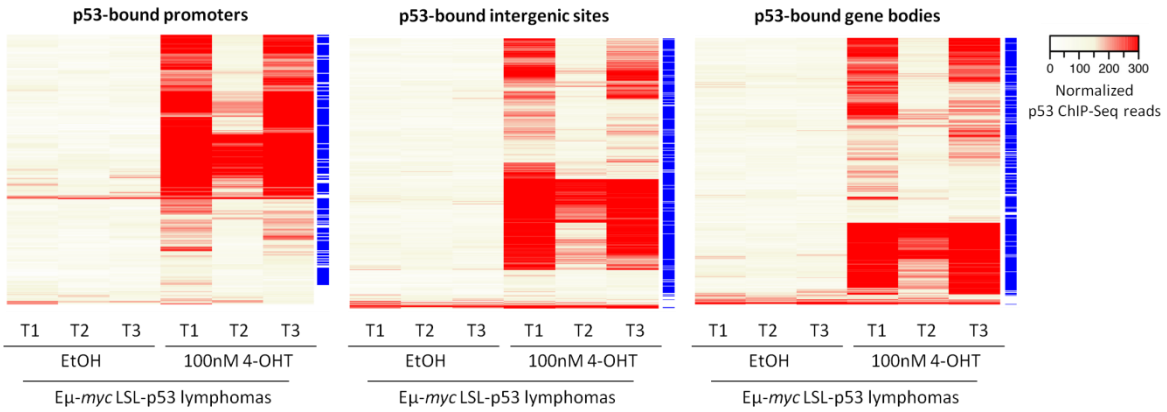

Fig. 39 - Heatmaps of p53 binding sites in vehicle- and 4-OHT-treated Eμ-myc LSL-p53 lymphomas.
Heatmaps showing library size-normalized ChIP-seq read counts for all p53-bound sites at promoters (-5/+2 kb from the TSS), gene bodies (+2 kb from the TSS through 3'UTR) and intergenic regions (everything else) in control and 4-OHT-treated Eμ-*myc* LSL-p53 lymphoma cells (T). Peaks are hierarchically clustered. The occurrence of the p53 motif at the genomic intervals analyzed is calculated by the FIMO algorithm (153) (p-value<1 x 10^{-5}) and indicated with blue lines on the right side of the heatmaps.

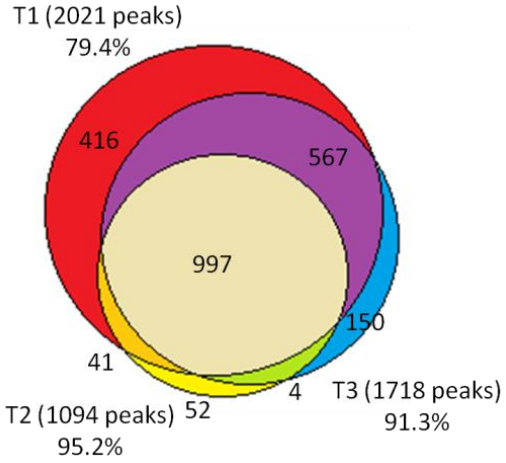

Fig. 40 - Overlap of p53 binding sites in three Eμ-myc LSL-p53lymphomas.
Venn diagram of p53 binding sites in 4-OHT-treated Eμ-*myc* LSL-p53 lymphoma cells (T). Percentages indicate the number of peaks for each lymphoma present in at least another sample.

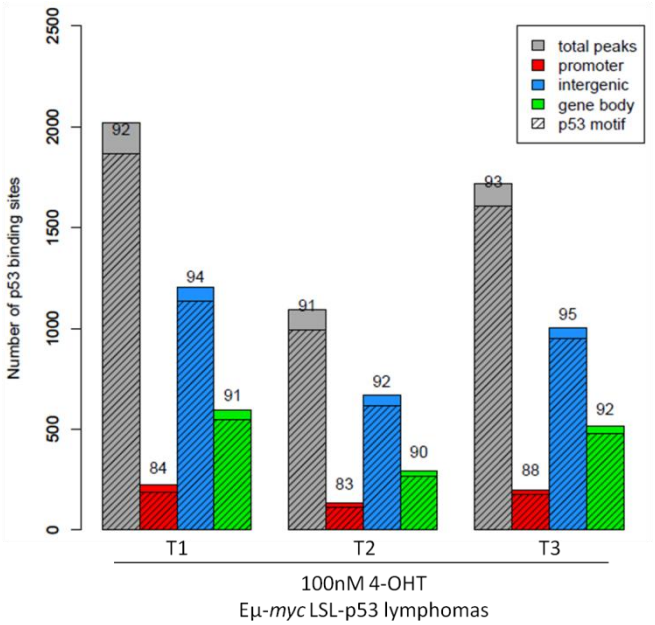

Fig. 41 - Motif analysis and genomic distribution of p53-binding sites in 4-OHT-treated Eμ-myc LSL-p53 lymphomas.
Characterization of all p53-bound sites at promoters (-5/+2 kb from the TSS, red bar), gene bodies (+2 kb from the TSS through 3'UTR, green bar) and intergenic regions (everything else, blue bar) in 4-OHT-treated Eμ-*myc* LSL-p53 lymphoma cells (T), for the occurrence of the p53 motif as calculated by the FIMO algorithm (p-value<1 x 10^{-5}). The percentage of p53-bound sites containing the p53-RE is reported.

4.2.4 p53 restoration in Eμ-*myc* lymphomas (iiI.): small molecules

Restoring p53 function in tumor cells is an attractive strategy in cancer therapy. In the clinic, this can be achieved using small molecules to reactivate wild-type p53, when present in tumors. This is the case, for example, in Eμ-*myc Arf*$^{-/-}$ *Trp53*$^{+/+}$ lymphomas, in which loss of Arf leads to enhanced degradation of p53, thereby alleviating the selective pressure to mutate the *Trp53* gene. Indeed, Eμ-*myc Arf*$^{-/-}$ *Trp53*$^{+/+}$ lymphomas spontaneously arise by LOH at the *Arf* locus in Eμ-*myc Arf* heterozygous mice (126,127). Therefore, as a third model of tumor regression, we investigated p53-dependent transcriptional responses induced in Eμ-*myc Arf*$^{-/-}$ *Trp53*$^{+/+}$ lymphomas following treatment with doxorubicin (also known as adriamycin), a genotoxic drug that triggers p53 activity, or Nutlin, a non-genotoxic molecule that interferes with the ability of Mdm2 to target p53 for degradation (163). Nutlin is a chiral molecule: (-)-Nutlin is 150 times more potent in binding Mdm2 than (+)-Nutlin (163). We thus decided to use the inactive enantiomer as a control for off-target effects.

We performed a time-course experiment to determine the best time point for our analysis. We observed that between three and four hours of treatment *in vitro* with both doxorubicin and (-)-

Nutlin cells stopped proliferating and started to die, correlating with p53 protein stabilization (Fig. 42, Fig. 43, Fig. 44, Fig. 45). Both compounds induced apoptosis of all lymphoma cells within twenty-four hours after treatment (data not shown). We chose to analyze the three hours time point because we could detect clear accumulation of the p53 protein, with no substantial induction of apoptosis.

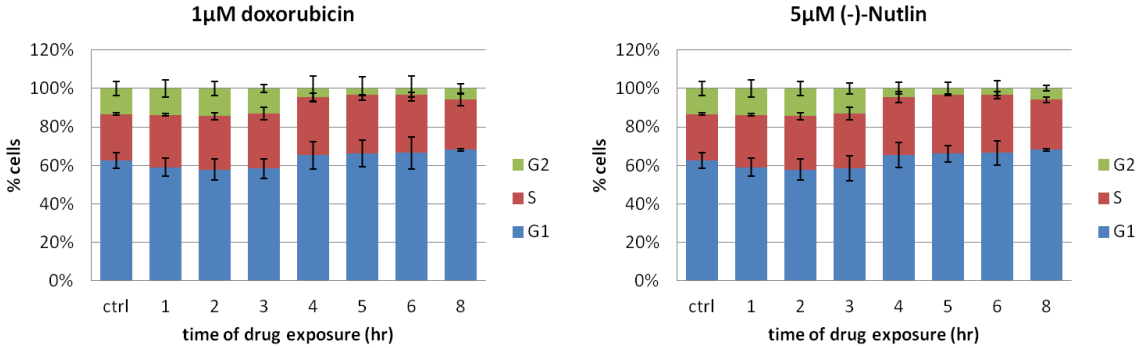

Fig. 42 - Four hours after drug exposure Eµ-myc Arf$^{-/-}$ Trp53$^{+/+}$ lymphoma cells stop proliferating.
The average percent of G_1-, S-, G_2-phase cells from three Eµ-*myc Arf*$^{-/-}$ *Trp53*$^{+/+}$ lymphomas treated with 1µM doxorubicin, 5µM (-)-Nutlin or vehicle is shown in a time-course experiment of cell cycle analysis by PI staining.

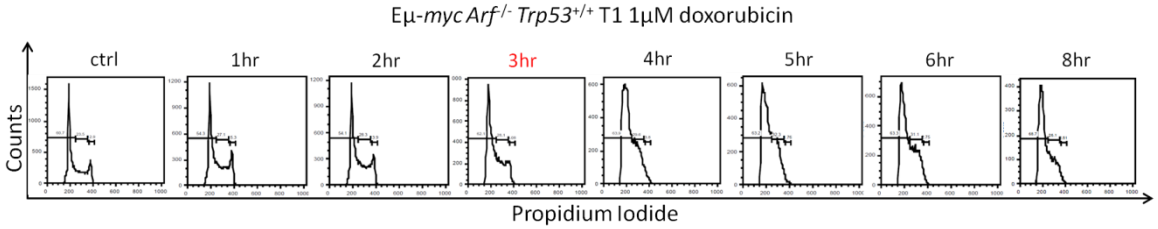

Fig. 43 - Between three and four hours after drug exposure, lymphoma cells stop proliferating.
Representative DNA content profile is shown.

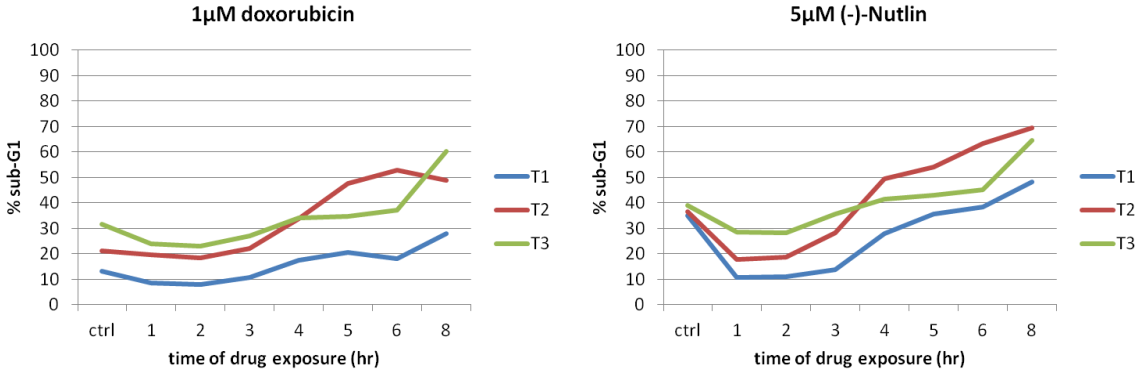

Fig. 44 - Four hours after drug exposure, cells start to die.
Time-course of accumulation of cells with sub-G1 DNA content in three Eµ-*myc Arf*$^{-/-}$ *Trp53*$^{+/+}$ lymphomas treated with 1µM doxorubicin, 5µM (-)-Nutlin or vehicle.

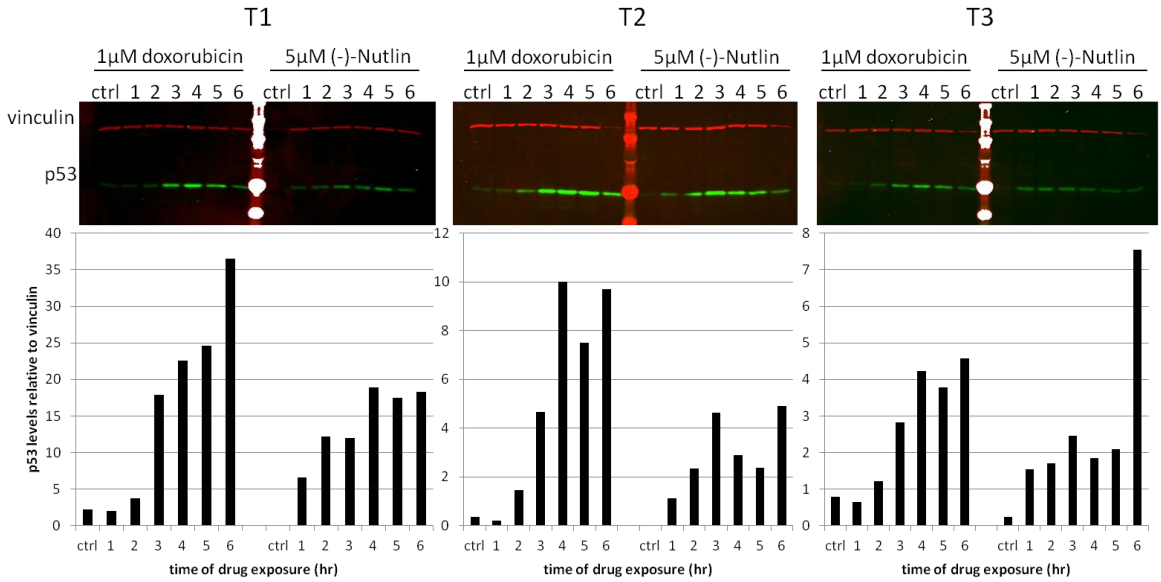

Fig. 45 - Time-course of p53 stabilization following drug exposure.
p53 stabilization is determined by quantitative infrared Western blotting. Densitometric quantification of p53 band is shown normalized to vinculin.

Previous published work stated that dimethylsulphoxide (DMSO), the solvent used to solubilize Nutlin, induced p53 binding to many sites (62), therefore we tested different conditions to choose the right controls for ChIP-Seq and RNA-Seq analysis. We observed that treatment with DMSO, H_2O or (+)-Nutlin didn't affect the p53 binding profile compared to untreated control, except for minor differences due to technical variability (Fig. 46), therefore the choice of one was equal to the other.

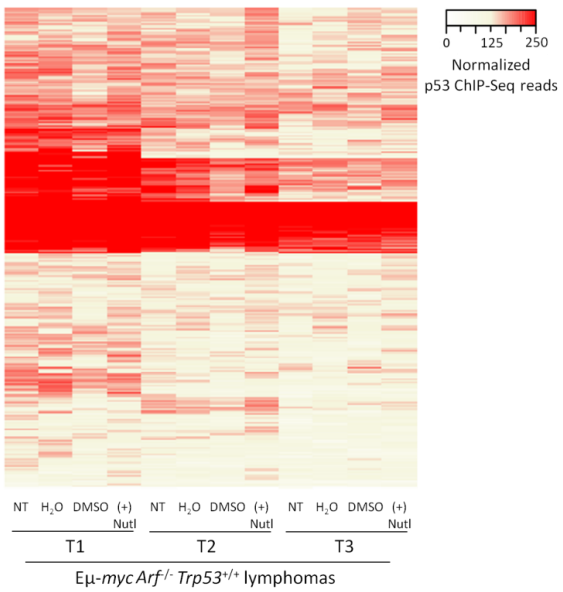

Fig. 46 - Heatmap of p53 binding sites in unperturbed Eμ-myc $Arf^{-/-}$ $Trp53^{+/+}$ lymphomas.
Heatmap showing library size-normalized ChIP-seq read counts for p53-bound genomic regions at chromosome 1, in three Eμ-*myc* $Arf^{-/-}$ $Trp53^{+/+}$ lymphomas cells (T) left untreated (NT) or treated for 3 hr with 0.1% H_2O, 0.05% DMSO or 5µM (+)-Nutlin. Peaks are hierarchically clustered.

Both (-)-Nutlin and doxorubicin treatment increased p53 chromatin occupancy and induced similar p53 binding profiles between the different lymphomas and to the ones triggered by the other drug, implying common features between these two different modes of activating p53 (Fig. 47, Fig. 48). All the peaks identified in control samples were present in the treated samples and were among the strongest binding sites (Fig. 47). Approximately 50-60% of the peaks identified upon p53 activation by small molecules were located in the promoter-proximal region, but only 10% of these binding sites contained the canonical p53 motif, suggesting that p53 was either bound to degenerate recognition sites, in a sequence-independent manner, or through protein-protein interactions (Fig. 49). The remaining peaks were distributed at distal intergenic locations and at gene bodies, where the p53-RE was more represented (Fig. 49). Peaks sitting on the consensus p53 motif showed higher p53 binding intensity compared to the ones where the p53-RE was not identified (Fig. 50).

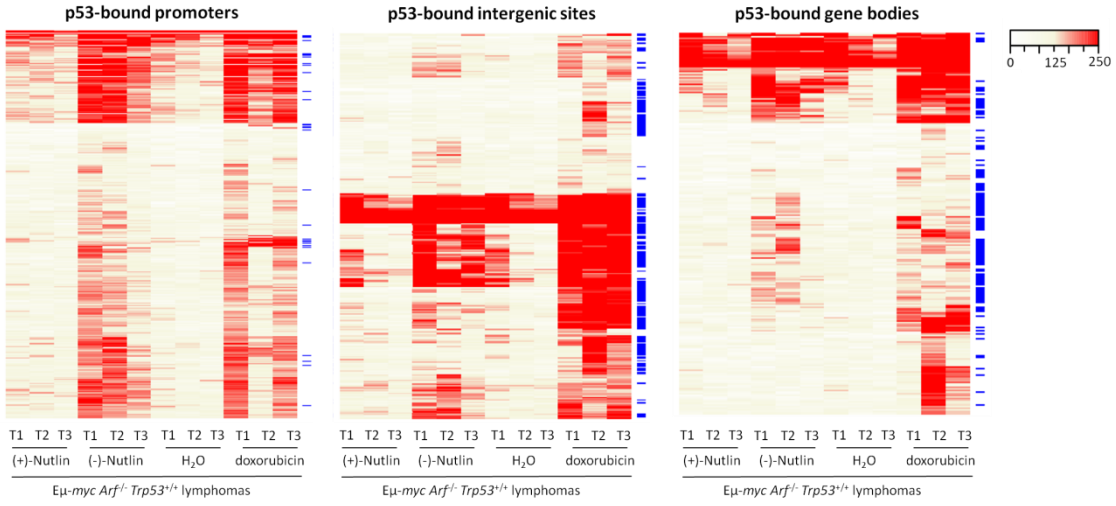

Fig. 47 - Heatmaps of p53 binding sites in control and drug treated-Eμ-myc Arf$^{-/-}$ Trp53$^{+/+}$ lymphomas. Heatmaps showing library size-normalized ChIP-seq read counts for all p53-bound promoters (-5/+2 kb from the TSS), gene bodies (+2 kb from the TSS through 3'UTR) and intergenic regions (everything else) at chromosome 1 in three Eμ-*myc Arf*$^{-/-}$ *Trp53*$^{+/+}$ lymphomas cells (T) treated for 3 hr with 5μM (+)-Nutlin, 5μM (-)-Nutlin, 0.1% H_2O or 1μM doxorubicin, as indicated. Peaks are hierarchically clustered. The occurrence of the p53 motif at the genomic intervals analyzed is calculated by the FIMO algorithm (153) (p-value<1 x 10^{-5}) and indicated with blue lines on the right side of the heatmaps.

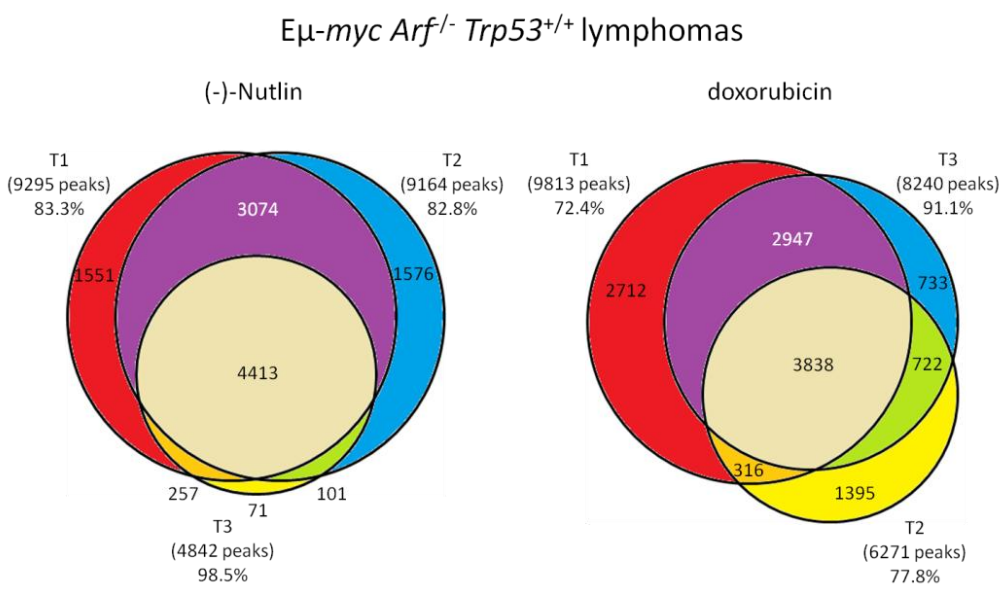

Fig. 48 - Overlap of p53 binding sites in three Eμ-myc Arf$^{-/-}$ Trp53$^{+/+}$ lymphomas (T) treated with 5μM (-)-Nutlin or 1μM doxorubicin.

Venn diagrams of p53 binding sites in three Eμ-*myc Arf*$^{-/-}$ *Trp53*$^{+/+}$ lymphoma cells (T) treated for 3 hr with 5μM (-)-Nutlin or 1μM doxorubicin. Percentages indicate the number of peaks for each lymphoma present in at least another sample.

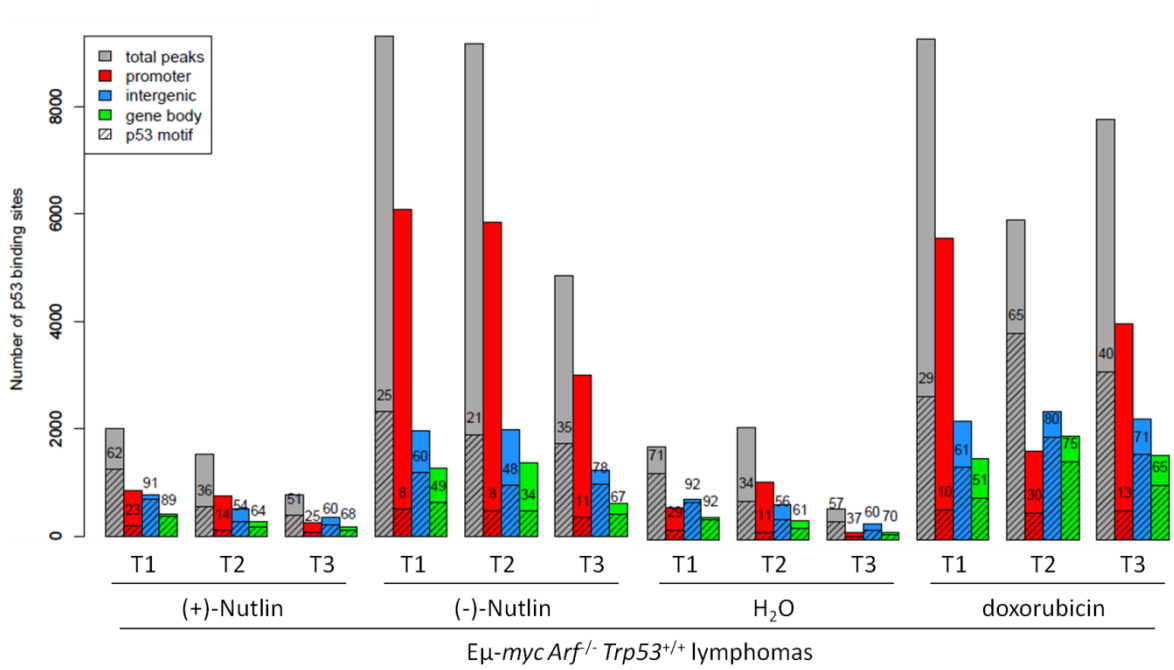

Fig. 49 - Motif analysis and genomic distribution of p53-binding sites in Eμ-myc Arf$^{-/-}$ Trp53$^{+/+}$ lymphomas following small molecules treatment.

Characterization of all p53-bound sites at promoters (-5/+2 kb from the TSS, red bar), gene bodies (+2 kb from the TSS through 3'UTR, green bar) and intergenic regions (everything else, blue bar) in three Eμ-*myc Arf*$^{-/-}$ *Trp53*$^{+/+}$ lymphomas cells (T) treated for 3 hr with 5μM (+)-Nutlin, 5μM (-)-Nutlin, 0.1% H_2O or 1μM doxorubicin, for the occurrence of the p53 motif as calculated by the FIMO algorithm (p-value<1 x 10^{-5}). The percentage of p53-bound sites containing the p53-RE is reported.

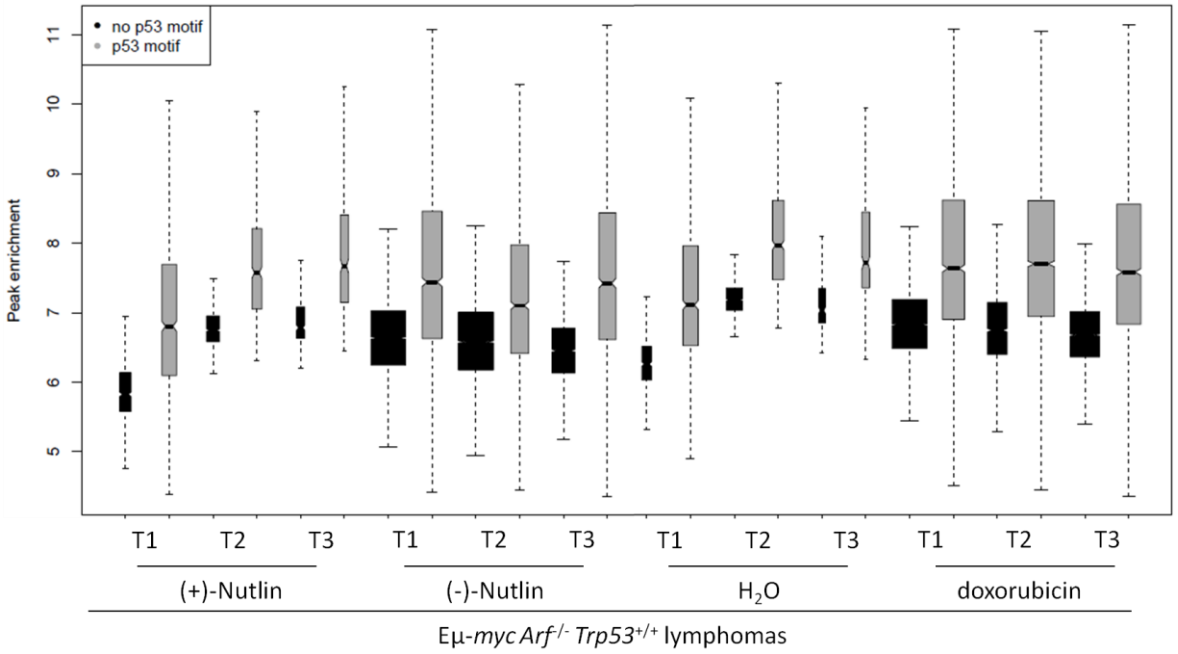

Fig. 50 - Stronger p53 binding sites are more likely to contain the consensus p53 motif.
Peak enrichment of p53 binding sites that contain (grey boxes) or not (black boxes) the p53 motif in three Eμ-*myc* $Arf^{-/-}$ $Trp53^{+/+}$ lymphomas cells (T) treated for 3 hr with 5μM (+)-Nutlin, 5μM (-)-Nutlin, 0.1% H_2O or 1μM doxorubicin.

4.2.5 Genome-wide analysis of p53 binding during tumor suppression and regression

Having established p53 binding patterns in control (C) and pre-tumoral Eμ-*myc* B cells (P) and with three modes of p53 restoration in tumors (T), we proceeded to compare these profiles. Both binding intensity and total number of p53 binding sites progressively increased from C and P to T (Fig. 51), consistent with the notion that the p53-dependent tumor suppressive response amplifies with increasing levels of oncogenic stress (132). In C and P, half of the p53 binding sites were at distal intergenic loci, and the remaining ones were equally distributed at promoters and gene bodies; the majority of the new p53 binding sites that appeared in tumors were instead located at promoter-proximal regions (Fig. 52). Most of these new p53 peaks at promoters didn't overlap with the p53 motif, suggesting that p53 was bound to weaker variant sites or recruited through protein-protein interactions (Fig. 51). Nevertheless, the specificity of all binding sites was supported by the fact that, when we considered all the peaks identified in each lymphoma model as a whole, we found that more than 80% of the peaks were present in at least two samples from different experimental models (Fig. 53). Upon p53 restoration in the Eμ-*myc* LSL-p53 lymphomas, we identified fewer peaks compared to the other lymphoma models and most of them were located at distal intergenic sites. In this experimental setting, our sensitivity in calling the peaks

was likely decreased by the incomplete recombination of the LSL cassette in the cell population and the quick outgrowth of undeleted clones. Moreover, the binding sites identified in the Eμ-*myc* LSL-p53 lymphomas were all present in the other samples, where they constituted some of the most enriched peaks, and almost all contained the p53 motif (Fig. 39). Therefore, the data produced in this experimental model helped in pointing out which where the high affinity sites in lymphomas upon p53 reactivation, leading to the observation that they were mainly distal sites. To characterize the binding sites identified, we checked for the presence of H3K4me3, H3K4me1 and H3K27ac using our recently published ChIP-Seq data (157). The Eμ-*myc* lymphomas used in this study were different from the ones analyzed in this thesis except for the T1 in reference (157), which was labeled as T2 Eμ-*myc* $Arf^{-/-}$ $Trp53^{+/+}$ lymphoma in this work. Since the location of these marks was substantially fixed in B cells and didn't change during tumor progression from C to P to T, we used them as reference to outline our p53 binding sites. These features marked all the p53-bound promoters, indicating that p53 localized at active regulatory regions. p53 binding sites with the chromatin signature characteristic of enhancers were similarly partitioned on intra- and intergenic regions and constituted a noteworthy fraction of the distal sites (Fig. 54). The remaining distal sites, including a big portion of the high affinity sites bound by p53 in all lymphomas, didn't enrich for any of the chromatin features investigated, and hence remain to be characterized, although the presence of the p53-RE and the absence of these peaks in C and P excluded sequencing artifact. We also checked for the presence of RNA-Seq reads in the surrounding region but we didn't detect any significant enrichment; moreover, we overlapped them with the regulatory elements identified in B cells by Busslinger and co-workers (164), without observing any co-localization. In the future, we plan to search for the co-occurrence of different proteins at these sites using publicly available data. Finally, some distal sites bear the H3K4me3 mark, suggesting that they may instead represent the promoters of unannotated transcripts or ncRNAs.

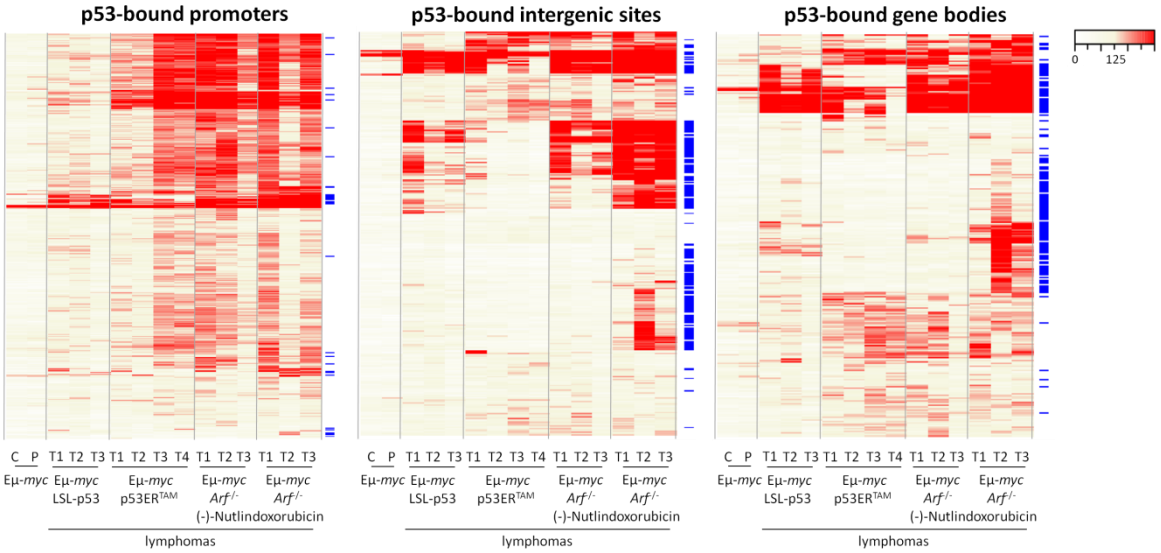

Fig. 51 - Comparison of p53 binding profiles during tumor suppression and regression.
Heatmaps showing library size-normalized ChIP-seq read counts for all p53-bound promoters (-5/+2 kb from the TSS), gene bodies (+2 kb from the TSS through 3'UTR) and intergenic regions (everything else) at chromosome 1 in C, P, three Eμ-*myc* LSL-p53 lymphomas and four Eμ-*myc* p53ER^{TAM} lymphomas upon 4-OHT treatment, and three Eμ-*myc* *Arf*$^{-/-}$ *Trp53*$^{+/+}$ treated with (-)-Nutlin or doxorubicin. Peaks are hierarchically clustered. The occurrence of the p53 motif at the genomic intervals analyzed is calculated by the FIMO algorithm (153) (p-value<1 x 10^{-5}) and indicated with blue lines on the right side of the heatmaps.

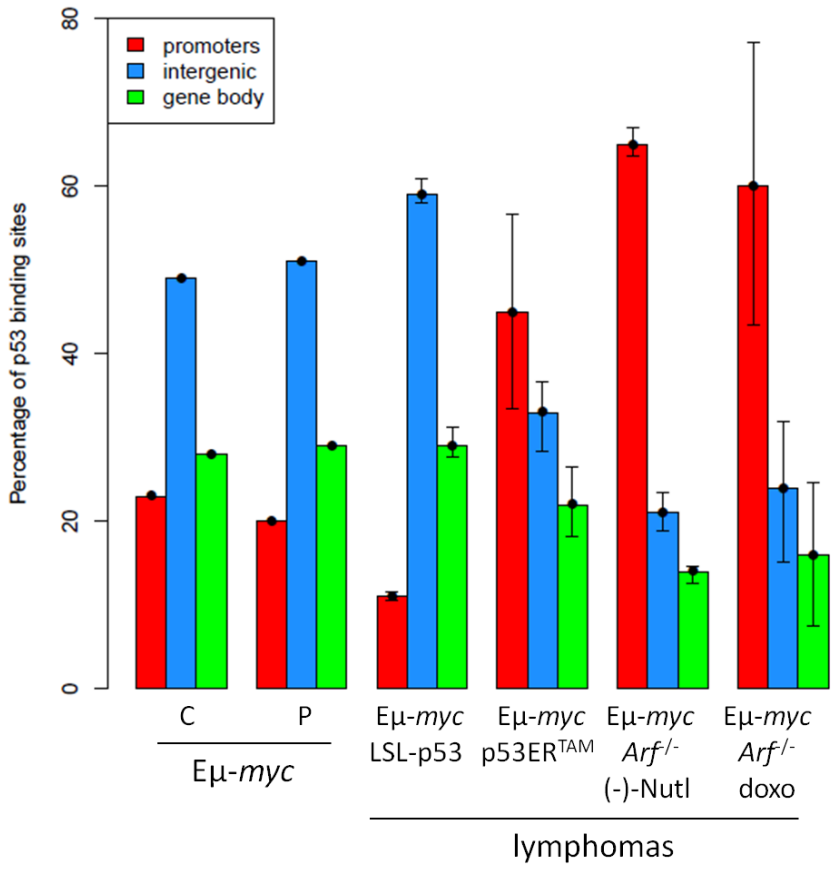

Fig. 52 - Genomic distribution of p53 binding sites.
Percentages of p53 binding sites at promoters (-5/+2 kb from the TSS, red bar), gene bodies (+2 kb from the TSS through 3'UTR, green bar) and intergenic regions (everything else, blue bar). The reported values represent the average of three or four biological replicates. Error bars stand for standard deviation.

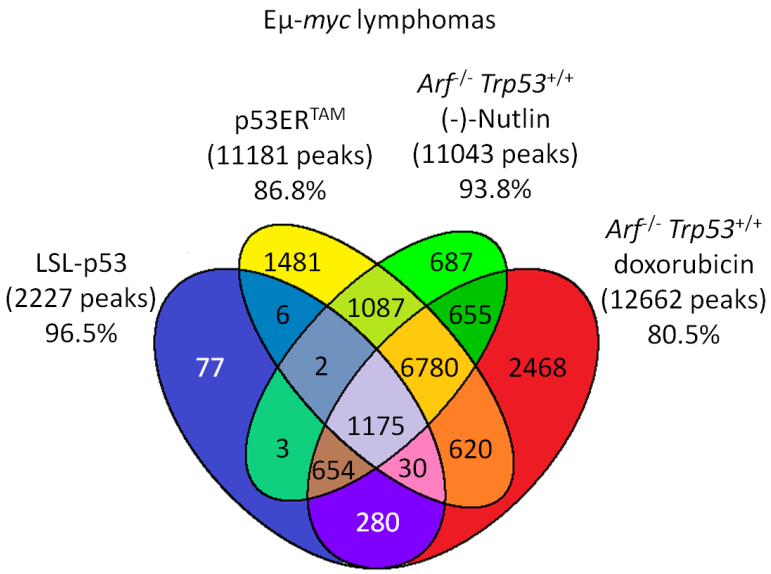

Fig. 53 - Identification of high-confidence p53 binding sites during tumor regression.
Venn diagram of p53 binding sites identified upon p53 restoration in Eμ-*myc* LSL-p53 lymphomas, Eμ-*myc* p53ER^{TAM} lymphomas, and Eμ-*myc* *Arf*$^{-/-}$ *Trp53*$^{+/+}$ treated with (-)-Nutlin or doxorubicin. Data shown for each condition represent the union of the p53 peaks identified in each lymphoma model. Percentages indicate the number of peaks shared with at least another model.

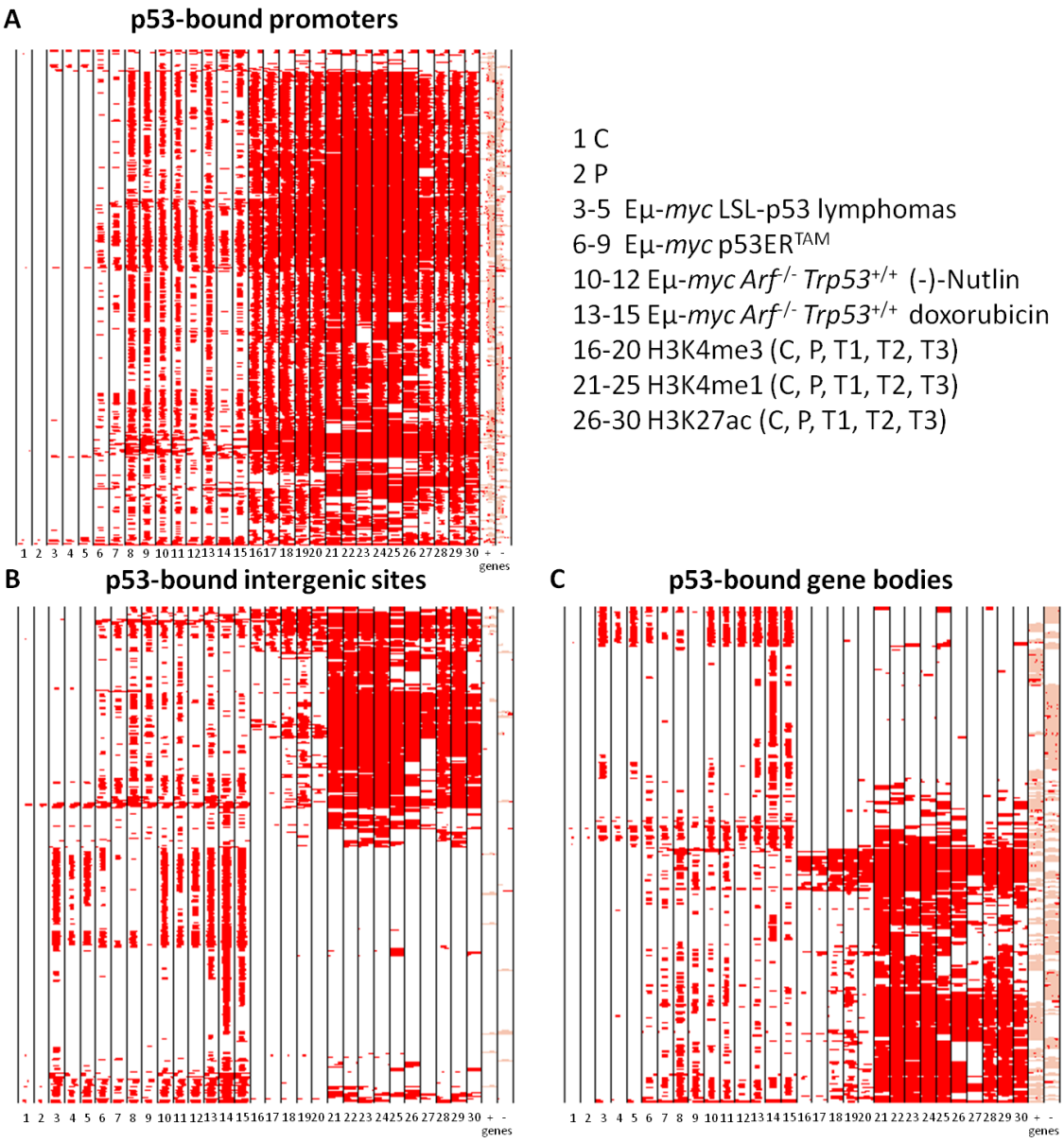

Fig. 54 - Distribution of p53 binding sites at annotated promoters and distal sites.
Heatmaps showing the distribution of p53 at annotated promoters (panel A), distal intergenic sites (panel B) and at gene bodies (panel C) in C, P and T, as indicated. Each row represents a different genomic interval (4 kb width centred on p53 peaks). The panels include every annotated promoter and every distant location in chromosome 1 that is identified as p53-associated by ChIP-seq in at least one of the experimental samples. For the same intervals, the distributions of H3K4me3, H3K4me1, H3K27ac and annotated genes (exons in red, introns in pink; + sense, - antisense strand) are also shown (157).

4.2.6 Expression profiling during tumor suppression and regression

To identify genes important for suppression of cancer development, we used RNA-Seq to profile changes in mRNA levels during tumor progression and regression upon restoration of p53 function. As described in our recent publication (157), the DEGs in Eμ-*myc* pre-tumor relative to control were mainly involved in metabolism, cell cycle and RNA processing, as expected from the comparison of mRNA levels in highly proliferating and less differentiated pre-tumoral B cells with

mature quiescent B cells. Thus, the transcriptional changes induced by p53 were confounded by the direct and indirect effects of Myc on gene expression. Moreover, it is most likely that the B cell population in pre-tumoral mice is a very heterogeneous population for p53 activation: at any time, only a small fraction of the cells may be experiencing oncogenic stress above the threshold required to activate the p53-driven apoptotic pathway (132), resulting in the dilution of the p53 signal and therefore impacting on our sensitivity in detecting p53 binding sites and transcriptional response. Nevertheless, we could identify 13 genes, all up-regulated (except *4933426M11Rik*), that had a p53 binding site at the promoter in the pre-tumoral sample (Table 8). The consensus p53 motif was found in the promoter-proximal region of all these genes, except *Phlda3.* A putative p53-RE was previously described overlapping the transcription initiation site of the *Phlda3* gene (5'-GAACATGTAAGGGCACATCC-3') (165), but was not identified by our motif search due to the absence of a G in position 17, indicating that some *bona fide* p53-RE may be missed in our analysis due to the stringency of our statistical criteria. This list of genes included well-known p53 targets, such as *Cdkn1a, Bbc3* and *Ccng1*, reinforcing its potential significance. Moreover, some of these genes were already validated tumor suppressors: both *Cdkn1a* and *Bbc3* deficiency were shown to accelerate tumorigenesis in tumor-prone mouse models (104,106,107,108), while recently, *Phlda3*, the p53-regulated repressor of Akt, was demonstrated to increase tumor growth when knocked-down in allograft tumor assays (109,165). Finally, we identified three ribosomal proteins *Rps27l, Rps19* and *Rpl24.* Myc-driven lymphomagenesis relies on protein biosynthesis and *Rpl24* haploinsufficiency was demonstrated to delay Myc-induced tumor progression (166). p53 may create an imbalance in ribosomal protein production to trigger the checkpoint sensing the integrity of ribosome biogenesis. The remaining genes constitute new candidates for functional validation.

Gene Symbol	log_2(FC)	Known p53 target	p53 motif	Official Full Name
Dyrk3	3.06		✓	dual-specificity tyrosine-(Y)-phosphorylation regulated kinase 3
Ckap2	2.32		✓	cytoskeleton associated protein 2
Psrc1	2.21	✓	✓	proline/serine-rich coiled-coil 1
Ogn	1.79		✓	osteoglycin
Rps27l	1.46	✓	✓	ribosomal protein S27-like
Phlda3	1.45	✓		pleckstrin homology-like domain, family A, member 3
Cdkn1a	1.41	✓	✓	cyclin-dependent kinase inhibitor 1A (p21, Cip1)
Bbc3	1.27	✓	✓	Bcl2 binding component 3
Klhdc4	0.72		✓	kelch domain containing 4
Rps19	0.69		✓	ribosomal protein S19
Rpl24	0.63		✓	ribosomal protein L24
Ccng1	0.48	✓	✓	cyclin G1
4933426M11Rik	-0.81		✓	

Table 8 - DEGs in Eμ-myc pre-tumor vs control bound by p53 at the promoter in P.
Log_2(FC) (log_2 of fold-change) values of DEGs in Eμ-*myc* pre-tumoral B cells (P) vs control (C), that have p53 bound on the p53-RE at the promoter in P.

To obtain a more comprehensive picture of the transcriptional programs induced by p53 activation, we compared the expression changes triggered by different modes of p53 restoration in tumors. Activation of the $p53ER^{TAM}$ chimera by 4-OHT administration in Eμ-*myc* $p53ER^{TAM}$ lymphomas yielded approximately 800 DEGs, while around 1500 and 4500 DEGs were observed with (-)-Nutlin and doxorubicin treatment in Eμ-*myc* $Arf^{-/-}$ $Trp53^{+/+}$ lymphomas, respectively. Upon $p53ER^{TAM}$ activation and (-)-Nutlin treatment, more than two-thirds of DEGs showed increased expression, while following doxorubicin treatment half of the DEGs were up-regulated and half down-regulated (Table 9). We observed that 65% of the genes induced upon p53 restoration in Eμ-*myc* $p53ER^{TAM}$ lymphomas also responded to both (-)-Nutlin and doxorubicin treatment in Eμ-*myc* $Arf^{-/-}$ $Trp53^{+/+}$ lymphomas and the remaining DEGs to doxorubicin treatment only; moreover, (-)-Nutlin-induced DEGs represented a fraction of the doxorubicin-induced ones (Fig. 55). The genes down-regulated by $p53ER^{TAM}$ restoration and (-)-Nutlin treatment were mainly different, with 20% and 10% in common, respectively, but they all constituted a fraction of doxorubicin-repressed genes. Transcriptional changes induced in Eμ-*myc* $p53ER^{TAM}$ lymphomas by p53 restoration were milder compared to the ones induced by drug treatment, with doxorubicin inducing the strongest changes (Fig. 56). Doxorubicin-induced transcriptional changes were

probably more intense because this small molecule triggered the DDR, which synergized with the Arf pathway to activate p53 (135). In line with this observation, Western blot analysis showed increased stabilization of p53 upon doxorubicin treatment compared to (-)-Nutlin treatment (Fig. 45). Despite the difference in magnitude of the transcriptional changes induced by p53 restoration in the various experimental models, they all followed consistent trends in the sense that we didn't identify genes down-regulated in one condition and up-regulated in the other. Since the transcriptional changes induced by (-)-Nutlin treatment and p53ER^{TAM} activation were weaker, some of the doxorubicin-induced DEGs were missed in these two models, in which the increases in mRNA steady state levels were not sufficient to reach the threshold of statistical significance. In all instances, the highest transcriptional changes were associated to gene induction (Fig. 56). p53 ChIP-seq studies had shown that in cancer cells treated with different agents, total p53-binding profiles were remarkably similar despite significant transcriptional differences (80,158). Here, we observed well-overlapping p53 genome-wide maps upon p53 restoration in different experimental settings (Fig. 51); however, also the gene expression changes were very homogeneous, consistent with the similarity in cell phenotypes observed. Smeenk *et al.* (80) and Nikulenkov *et al.* (158) instead used p53 activating drugs that resulted in either apoptosis or cell cycle arrest, revealing more substantial differences between DEGs.

	p53 restoration-induced DEGs	
	DEG up	DEG down
Eμ-*myc* p53ER^{TAM} lymphomas (4-OHT/EtOH)	527 (68%)	252 (32%)
Eμ-*myc Arf*$^{-/-}$ *Trp53*$^{+/+}$ lymphomas ((-)-Nutlin/ (+)-Nutlin)	1055 (68%)	503 (32%)
Eμ-*myc Arf*$^{-/-}$ *Trp53*$^{+/+}$ lymphomas (doxorubicin/ H_2O)	2436 (53%)	2167 (47%)

Table 9 - DEGs induced by three modes of p53 restoration in tumors.
Summary of total numbers and percentages of induced and repressed genes in Eμ-*myc* p53ER^{TAM} lymphomas following 4-OHT treatment, and in Eμ-*myc Arf*$^{-/-}$ *Trp53*$^{+/+}$ lymphomas following (-)-Nutlin and doxorubicin treatment relative to controls.

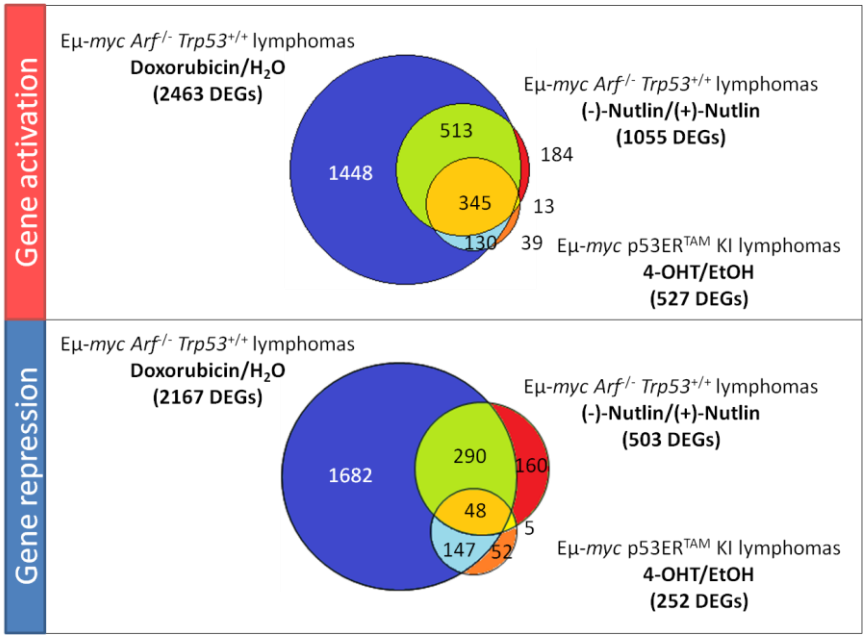

Fig. 55 - Comparison of genes that respond to p53 restoration in Myc-driven lymphomas.
Venn diagram showing the overlap between the DEGs identified in Eμ-*myc* p53ER^{TAM} lymphomas following 4-OHT treatment, and in Eμ-*myc* *Arf*$^{-/-}$ *Trp53*$^{+/+}$ lymphomas following (-)-Nutlin and doxorubicin treatment relative to controls.

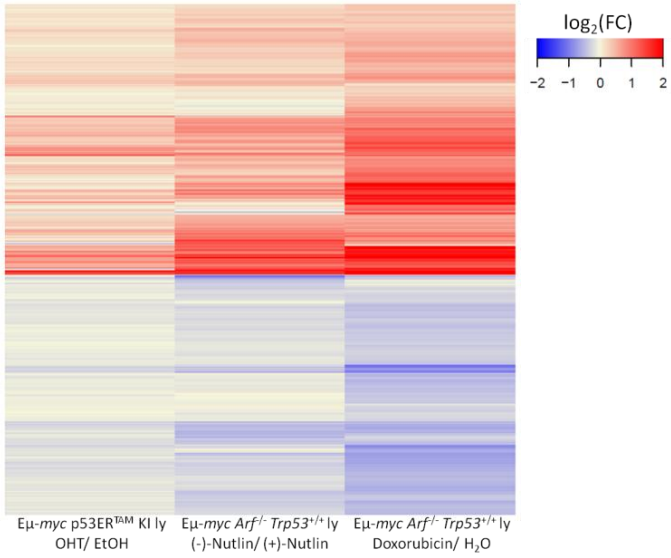

Fig. 56 - Different modes of p53 restoration in lymphomas lead to similar transcriptional changes, despite differences in magnitude.
Heatmap of the log2(FC) (log2 of fold-change) values of all up- and down-regulated genes (n=5055) upon p53 reactivation in Eμ-*myc* p53ER^{TAM} lymphomas following 4-OHT treatment, and in Eμ-*myc* *Arf*$^{-/-}$ *Trp53*$^{+/+}$ lymphomas following (-)-Nutlin and doxorubicin treatment relative to controls. The genes are clustered hierarchically on the basis of their differential expression.

To assess the p53 dependency of biological responses, we knocked down *Trp53* in Eμ-*myc* *Arf*$^{-/-}$ *Trp53*$^{+/+}$ lymphomas using a selectable retroviral vector expressing an shRNA against p53 (Fig. 57). Following (-)-Nutlin treatment, no DEG could be identified in lymphomas where p53 was silenced, indicating that the response measured was entirely p53-dependent (Fig. 58A). Doxorubicin treatment instead still caused significant regulation of 40 genes, and many more changed

transcripts levels even if not in a statistically significant manner and with smaller amplitude compared to wild-type cells. Thus, doxorubicin-induced changes were largely p53-dependent, but other factors contributed to the transcriptional regulation of most genes (Fig. 58B). The difference between the two p53-activating agents could probably be explained by the genotoxic effects of doxorubicin, which is not the case for (-)-Nutlin, and could then contribute to the expression changes via activation of DDR pathways.

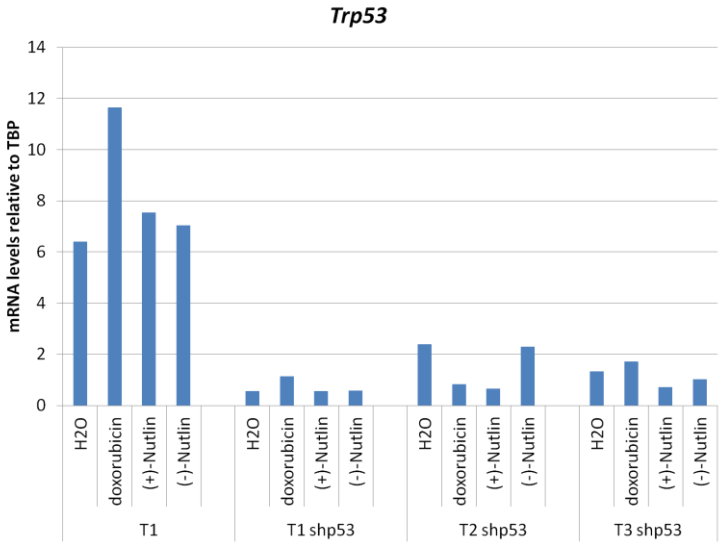

Fig. 57 - Efficiency of Trp53 knock-down.
qPCR analysis of *Trp53* mRNA levels in three Eμ-*myc* *Arf*$^{-/-}$ *Trp53*$^{+/+}$ lymphomas infected with a retroviral vector expressing an shRNA against p53 (shp53) and treated for 3 hr with 0.1% H_2O, 1μM doxorubicin, 5μM (+)-Nutlin or 5μM (-)-Nutlin, as indicated. *Trp53* expression in one uninfected lymphoma was analyzed as positive control.

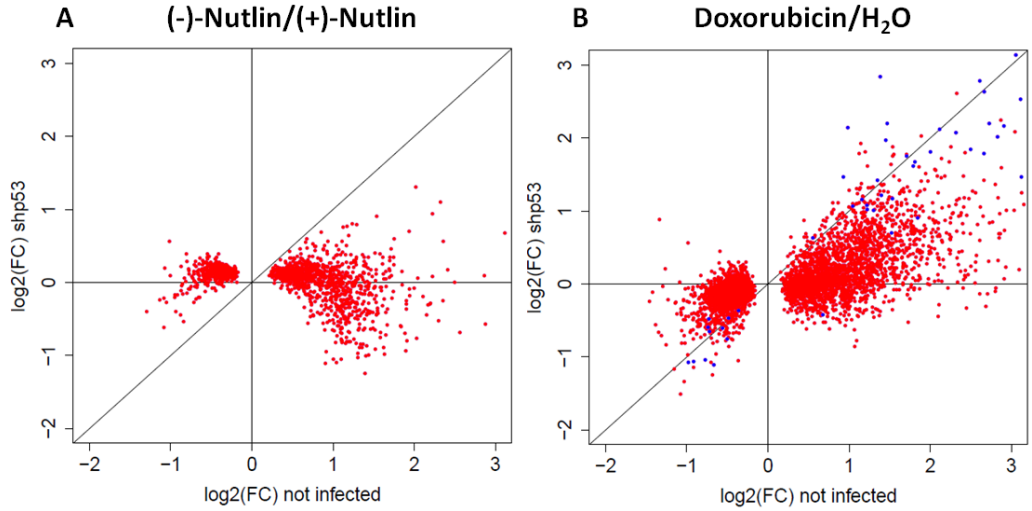

Fig. 58 - p53 dependency of transcriptional changes.
Scatter plot opposing the $\log_2$(FC) ($\log_2$ of fold-change) values of all DEGs as estimated by RNA-Seq analysis in Eμ-*myc* *Arf*$^{-/-}$ *Trp53*$^{+/+}$ lymphomas (not infected) following (-)-Nutlin (panel A) and doxorubicin treatment (panel B) relative to controls and the $\log_2$(FC) of the same genes in lymphoma cells infected with a retroviral vector expressing an shRNA against p53 (shp53). In case a gene is still differentially expressed in shp53 cells, it is marked with a blue dot.

4.2.7 p53-regulated transcriptional program during tumor regression

To identify which of the differentially expressed genes induced by p53 restoration in lymphomas were direct p53 targets, we combined p53 binding with gene expression profiles. In all instances, approximately half of the DEGs, both up- and down-regulated, had at least one p53 binding site in the promoter proximal region (Fig. 59, Fig. 60). Approximately 20% of the p53-bound up-regulated genes contained the p53 motif, which was instead less represented at the promoter of the repressed genes (Fig. 60), in line with what was previously observed in B and non-B cells from irradiated mice.

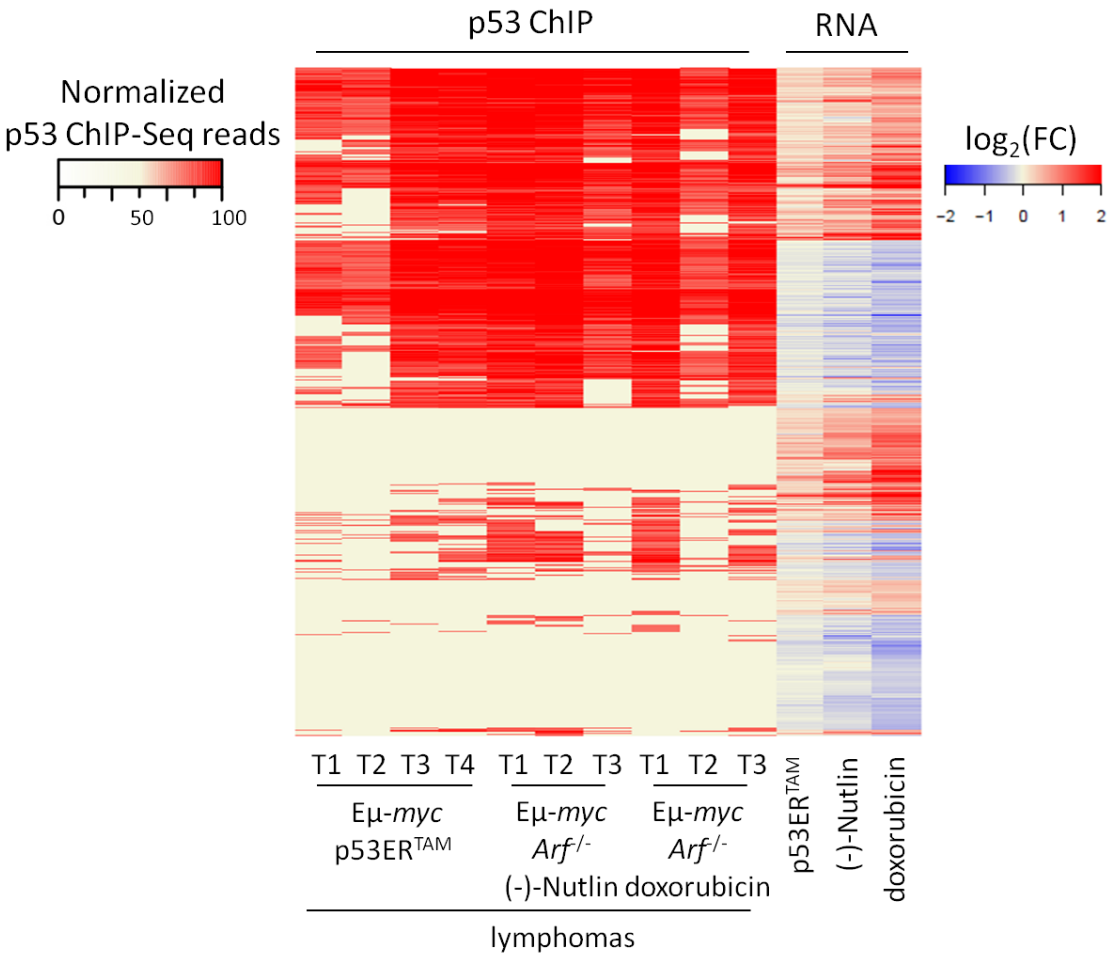

Fig. 59 - Heatmap of all DEGs upon p53 restoration in Eμ-myc lymphomas together with the indication about enrichment of p53 binding at the corresponding promoter.
Heatmap of the log_2(FC) (log_2 of fold-change) values of all DEGs (n=5055) as estimated by RNA-Seq analysis upon p53 restoration in Eμ-*myc* p53ER^{TAM} lymphomas following 4-OHT treatment, and in Eμ-*myc* *Arf*$^{-/-}$ *Trp53*$^{+/+}$ lymphomas following (-)-Nutlin and doxorubicin treatment relative to controls, together with the indication about enrichment of p53 binding at the corresponding promoter (-600/+400 bp from the TSS).

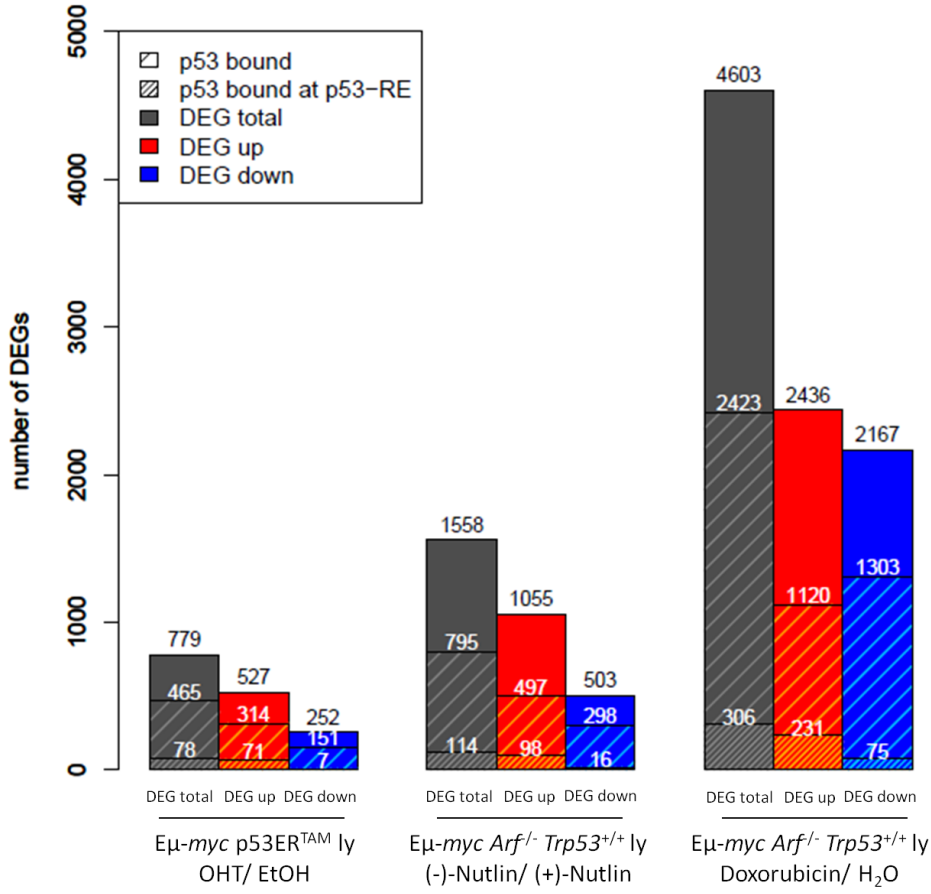

Fig. 60 - Absolute numbers of p53-bound DEGs.
Bar plot showing the number of DEGs (total, up and down) divided as p53-bound, -unbound and -bound on the p53-RE in Eμ-*myc* p53ER^{TAM} lymphomas following 4-OHT treatment, and in Eμ-*myc Arf*$^{-/-}$ *Trp53*$^{+/+}$ lymphomas following (-)-Nutlin and doxorubicin treatment relative to controls, as indicated. Genes are considered bound if a p53 peak is identified nearby the TSS in at least one of the corresponding ChIP-Seq samples.

To determine whether the presence of a p53 binding site was predictive of transcriptional activation of the corresponding gene, we determined the frequency of DEGs among the p53-bound genes, distinguishing them between those containing or not the p53-RE. As in B and non-B cells upon acute DNA damage, p53 binding on the p53 motif in the promoter region of genes was more predictive of gene regulation compared to mere p53 binding (Fig. 61). Moreover, binding intensity of the p53 peaks containing the p53 consensus motif correlated with activation of the corresponding genes, and this linkage was not observed for the remaining p53-bound genes not overlapping with the canonical p53-RE (Fig. 62). The genes that were bound by p53 on the p53-RE and that didn't change expression, may be induced in a minor fraction of the cells, as indicated by the lower peak enrichment, and therefore their activation at the steady state level may not be detectable yet (Fig. 62).

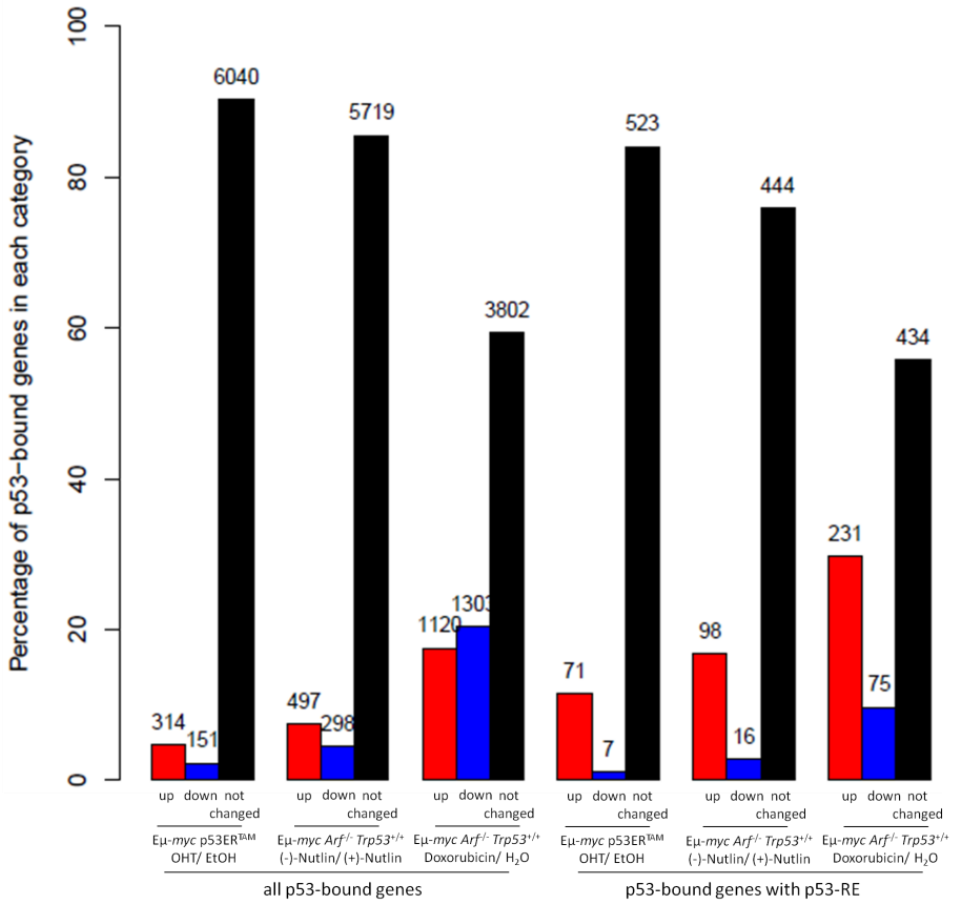

Fig. 61 - Expression changes of p53-bound genes upon p53 restoration in Eμ-myc lymphomas.
Bar plot showing the percentage and the absolute number of all p53 peaks and of p53 peaks containing the p53-RE at the promoters of genes in Eμ-*myc* p53ER^{TAM} lymphomas and in Eμ-*myc Arf*$^{-/-}$ *Trp53*$^{+/+}$ lymphomas that don't change expression (black bar), or that are up-regulated (red bar) or down-regulated (blue bar) following p53 restoration.

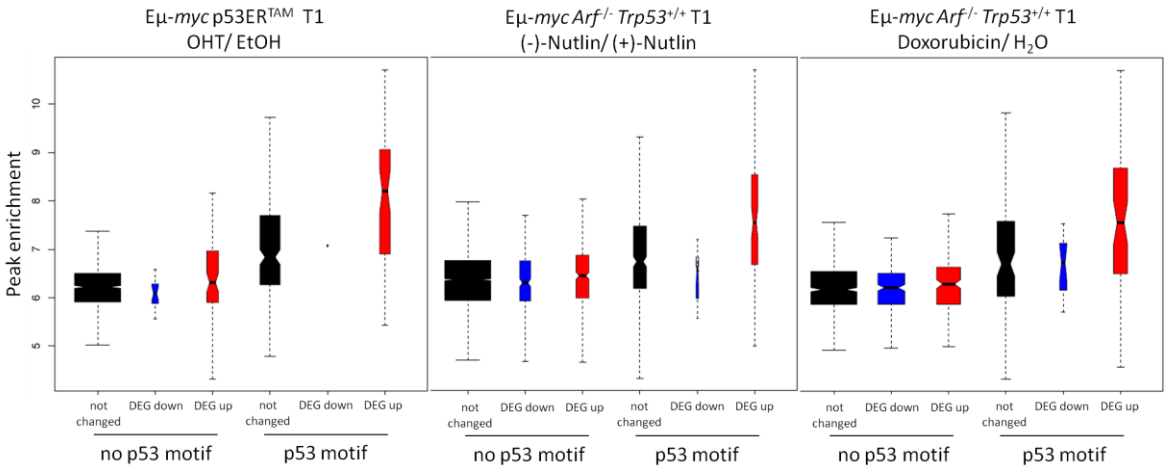

Fig. 62 - Higher p53 binding intensities are most frequently correlated with transcriptional activation.
Box plots showing the enrichment of p53 peaks in Eμ-*myc* p53ER^{TAM} lymphomas following 4-OHT treatment, in Eμ-*myc Arf*$^{-/-}$ *Trp53*$^{+/+}$ lymphomas following (-)-Nutlin and doxorubicin treatment at the promoter region of genes containing or not the p53-RE and that don't change expression (black box), or that are up-regulated (red box) or down-regulated (blue box) upon p53 reinstatement. The boxes are drawn with widths proportional to the square-roots of the number of observations in the groups. Results in lymphoma 1 for each experimental model are reported as representative of the other lymphomas.

A biological process GO analysis of the p53-bound genes containing the p53-RE indicated that they were involved in intracellular signal transduction, response to stress, apoptosis, negative regulation of growth and several other terms directly related to p53 activation. The remaining up-regulated genes, whether bound or not by p53, enriched for categories related to regulation of gene expression and cell development. Finally, the down-regulated genes following (-)-Nutlin and doxorubicin treatment enriched for terms associated to cell cycle, cell division and RNA processing. Moreover, (-)-Nutlin-repressed genes were also linked to cholesterol biosynthesis, and the doxorubicin-down-regulated ones to cellular catabolic processes. The repressed genes upon $p53ER^{TAM}$ activation didn't enrich for any categories in a statistically significant manner.

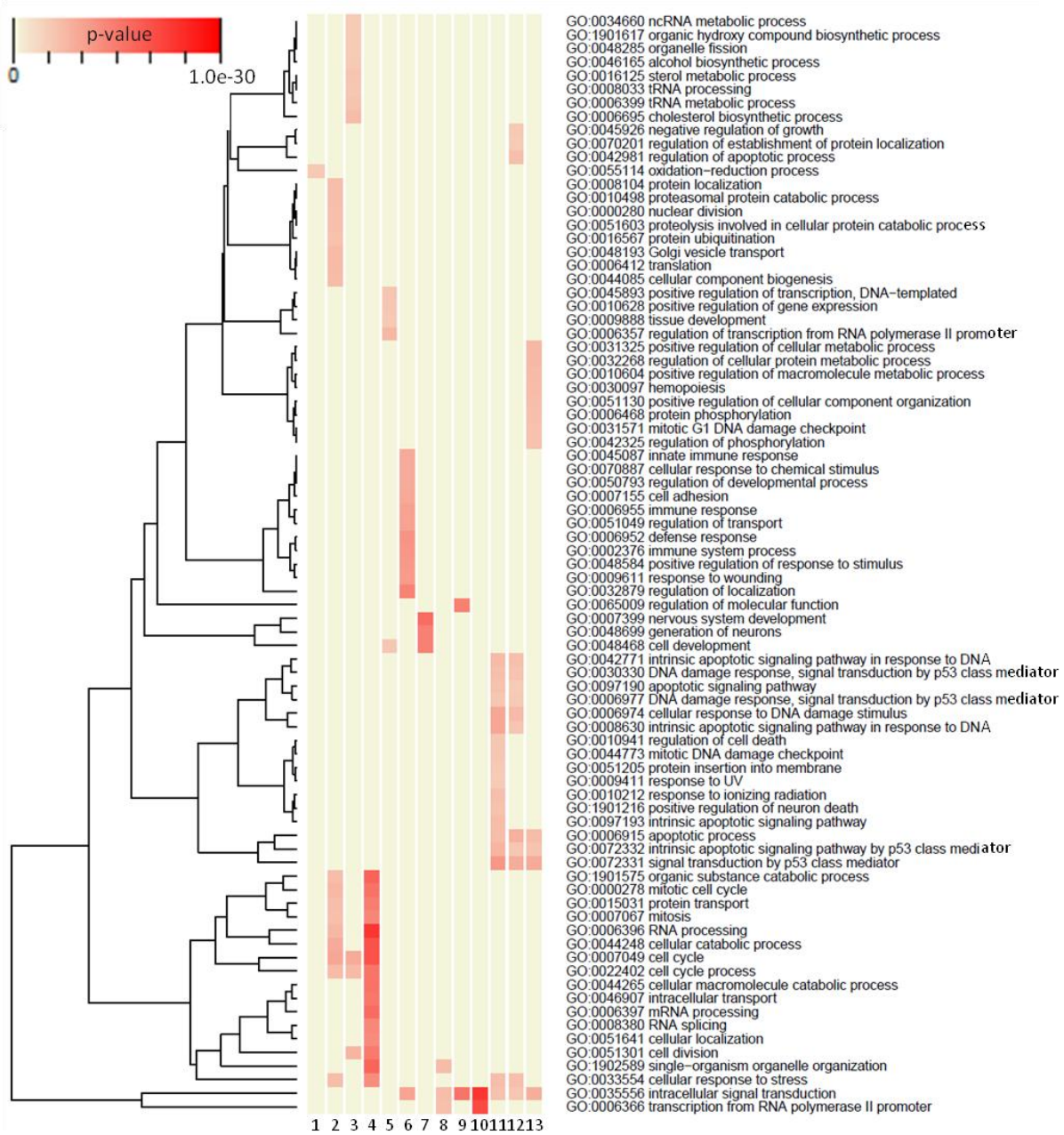

Fig. 63 Functional annotation of all DEGs in Eμ-myc lymphomas upon p53 restoration.
Gene Ontology terms enriched in up- and down-regulated genes upon p53 restoration in Eμ-*myc* p53ER^{TAM} lymphomas following 4-OHT treatment, and in Eμ-*myc Arf*$^{-/-}$ *Trp53*$^{+/+}$ lymphomas following (-)-Nutlin and doxorubicin treatment relative to controls, further distinguished in p53-bound and unbound and containing the p53-RE. GO terms significantly enriched (Fisher test p-value<1*10^{-5}) in at least one gene set are selected (rows in the heatmap) and the p-values for each GO term in each gene set (columns) are colour-coded as indicated. Only GO terms in the biological process ontology that are assigned to less than 2,000 and more than 10 genes in the mouse genome are considered.

Since the p53-bound genes containing the p53-RE were a minor fraction of all DEGs, we used IPA to try to identify the putative upstream regulators of the remaining DEGs. In doxorubicin-treated Eμ-*myc Arf*$^{-/-}$ *Trp53*$^{+/+}$ lymphomas the down-regulated genes were involved in cell cycle and mitosis, as in B and non-B cells exposed to acute DNA damage; therefore, IPA indicated as putative upstream regulators of these genes the *let-7* microRNA and the p21/Rb/E2f pathway (Table 10). For the down-regulated genes upon p53ER^{TAM} activation the p-value associated to the putative regulators identified were higher, due to the smaller number of DEGs analyzed, making the results more uncertain. Finally, among the putative regulators of the down-regulated genes upon (-)-Nutlin treatment, we noticed SREBF1 and 2. The SREBF transcription factors were described to cooperate with mutant p53 to induce the genes involved in sterol biosynthesis, contributing to the malignant phenotype in breast cancer cells (167). Here, we found indications that wild-type p53 could have the opposite effect of dampening the expression of SREBF target genes.

DEG down p53-dependent											
Eμ-*myc* p53ER^{TAM} lymphomas				Eμ-*myc* Arf$^{-/-}$ Trp53$^{+/+}$ lymphomas (-)-Nutlin				Eμ-*myc* Arf$^{-/-}$ Trp53$^{+/+}$ lymphomas doxorubicin			
p53-bound		non p53-bound		p53-bound		non p53-bound		p53-bound		non p53-bound	
Upstream Regulator	p-value	Upstream Regulator	p-value	Upstream Regulator	p-value	Upstream Regulator	p-value	Upstream Regulator	p-value	Upstream Regulator	p-value
HNF4A	8,13E-04	SPRED1	3,35E-03	SCAP	4,69E-10	let-7a-5p	1,85E-06	HNF4A	5,32E-37	HNF4A	4,38E-11
E2f	4,67E-03	ASF1B	3,35E-03	INSIG1	2,48E-09	HNF4A	6,06E-05	E2F4	1,57E-17	E2f	2,72E-04
miR-802	6,00E-03	miR-18a-3p	3,35E-03	SIRT2	3,81E-08	SIRT2	3,39E-04	XBP1	1,31E-11	KDM5B	3,77E-04
FADD	1,08E-02	CELF2	3,35E-03	SREBF2	1,03E-07	SCAP	7,49E-04	RICTOR	3,62E-09	miR-155-5p	4,54E-04
UXT	1,58E-02	CYFIP2	3,35E-03	SREBF1	1,29E-06	SREBF2	2,01E-03	E2F1	4,89E-09	HOXA9	5,12E-04
miR-291a-3p	1,60E-02	IP6K2	3,35E-03	HNF4A	5,84E-06	miR-96-5p	3,72E-03	RB1	5,46E-07	MAP4K4	1,17E-03
RAB1B	1,67E-02	ESX1	3,35E-03	FOXO4	9,81E-06	SPRED1	7,72E-03	let-7	8,52E-07	FOXO1	1,48E-03
miR-2682-5p	1,79E-02	TGFBR2	3,42E-03	PPARGC1B	1,66E-05	miR-521	7,72E-03	TP53	1,02E-06	RB1	1,76E-03
miR-376a-5p	1,79E-02	Cyclin B	6,70E-03	NPPB	2,28E-05	miR-18a-3p	7,72E-03	MYC	1,35E-06	RAE1	2,84E-03
EIF2AK3	1,96E-02	mir-375	6,70E-03	L1CAM	8,29E-05	GSX1	7,72E-03	miR-291a-3p	2,54E-06	TBX2	2,86E-03
OBSCN	2,38E-02	MID1	6,70E-03	NUPR1	9,36E-05	CYFIP2	7,72E-03	miR-16-5p	2,62E-06	GTF2H1	3,06E-03
TACSTD2	2,38E-02	NBN	6,70E-03	INSR	1,90E-04	ESX1	7,72E-03	CDKN1A	3,53E-06	ERBB2	3,77E-03
VSNL1	2,38E-02	Dynamin	1,00E-02	KDM5B	4,16E-04	CSHL1	9,76E-03	E2F8	7,32E-06	E2F4	5,42E-03
EP400	2,40E-02	CK1	1,00E-02	miR-16-5p	4,25E-04	OTX2	1,34E-02	FOXO4	9,11E-06	OBSCN	5,98E-03
ZBTB46	2,96E-02	EGR2	1,12E-02	MPZ	1,11E-03	GTF2E2	1,54E-02	BNIP3L	2,09E-05	NFYB	6,77E-03

Table 10 - Putative upstream regulators of down-regulated genes upon p53 restoration in Eμ-myc lymphomas.
IPA Upstream Regulator Analysis of down-regulated genes having or not a p53 binding site at the promoter containing the p53-RE in Eμ-*myc* p53ER^{TAM} lymphomas following 4-OHT treatment, and in Eμ-*myc Arf*$^{-/-}$ *Trp53*$^{+/+}$ lymphomas following (-)-Nutlin and doxorubicin treatment relative to controls. Statistical significance and p-values are determined by IPA using a Fisher's Exact Test.

As expected, p53 and its family members p63 and p73 were indicated as the most probable regulators of the p53-bound genes containing the p53-RE. For the remaining up-regulated genes,

IPA results were less clear: we couldn't identify any putative regulator in common between the different modes of p53 reactivation in tumors and none of the ones highlighted was a direct p53 target. However, even if not highlighted by IPA, among the p53 target genes containing the p53-RE we identified the transcription regulators *Foxo3, Notch1, Fos* (that dimerizes with *Jun* to form the AP-1 complex), and several zinc finger proteins (73,168,169). In the literature, there are already indications that Foxo3 plays a role in p53-dependent apoptosis (168,170), while AP-1 and Notch1 are known to control several processes, including cell proliferation and death, and may thus conceivably contribute to gene regulation downstream of p53.

DEG up p53-dependent																	
Eμ-*myc* p53ER^{TAM} lymphomas						Eμ-*myc* Arf$^{-/-}$ Trp53$^{+/+}$ lymphomas (-)-Nutlin						Eμ-*myc* Arf$^{-/-}$ Trp53$^{+/+}$ lymphomas doxorubicin					
p53-bound p53 motif		p53-bound no motif		non p53-bound		p53-bound p53 motif		p53-bound no motif		non p53-bound		p53-bound p53 motif		p53-bound no motif		non p53-bound	
Upstream Regulator	p-value	Upstream Regulator	p-value	Upstream Regulator	p-value	Upstream Regulator	p-value	Upstream Regulator	p-value	Upstream Regulator	p-value	Upstream Regulator	p-value	Upstream Regulator	p-value	Upstream Regulator	p-value
TP53	6,99E-19	NFYA	9,80E-06	ATOH1	9,52E-06	TP53	1,98E-19	EGR1	1,21E-05	TP53	5,61E-10	TP53	2,56E-21	RELA	2,15E-09	TP53	1,32E-07
TP63	1,23E-13	LMNA	2,90E-05	FOXC2	3,65E-04	TP63	5,05E-13	LMNA	2,60E-05	Tgf beta	2,90E-09	TP63	1,79E-13	NFKB1	2,52E-07	MYD88	8,01E-05
TP73	1,44E-11	EPHB1	9,10E-05	FOXC1	5,80E-04	TP73	1,51E-12	BAG1	5,01E-05	STAT3	1,36E-08	TP73	1,69E-11	IRAK4	2,58E-07	P38 MAPK	8,60E-05
TOPBP1	9,06E-11	TP73	2,30E-04	SMAD1/5	6,11E-04	BCL2L12	2,56E-09	SP3	5,33E-05	mir-223	3,54E-08	CHEK2	2,30E-09	NUPR1	4,32E-06	Bvr	1,25E-04
RPL22	2,32E-10	N4BP1	2,57E-04	KRIT1	6,11E-04	miR-221-3p	2,42E-08	RPS6KA5	6,74E-05	CEBPB	1,13E-07	ANXA2	5,67E-09	EPAS1	5,00E-06	PARP	1,93E-04
CHEK2	3,42E-10	ADRB	3,04E-04	CREB1	9,75E-04	TCP1	4,83E-08	Irs3	7,11E-05	TET2	1,15E-07	RPL22	3,16E-08	LMNA	5,43E-06	IKBKB	2,57E-04
BCL2L12	6,93E-10	RPS6KA5	3,33E-04	FBXW7	9,80E-04	TOPBP1	8,31E-08	ERK1/2	8,21E-05	KRT17	1,41E-07	TOPBP1	4,22E-08	TP73	1,15E-05	FOXC1	4,39E-04
PHF1	7,32E-09	KDM5B	7,69E-04	Insulin	1,11E-03	CHEK2	2,27E-07	Jnk	1,15E-04	MYD88	4,06E-07	BCL2L12	9,40E-08	MAPK9	1,89E-05	Mek	5,63E-04
ANXA2	1,31E-08	ELK1	8,07E-04	PTH	1,29E-03	REL	4,72E-07	MAP3K1	1,82E-04	ETS2	5,35E-07	TP53BP2	9,40E-08	PRKCB	1,92E-05	TET2	7,04E-04
BRD7	1,51E-08	ZBTB17	8,07E-04	SPARC	1,42E-03	BCAS2	4,80E-07	MAPK14	1,94E-04	JUN	1,04E-06	ACTL6A	1,24E-07	IKBKB	2,04E-05	DMD	1,03E-03
UIMC1	1,82E-08	ATF2	9,10E-04	MYOG	1,85E-03	RPL22	4,80E-07	BNIP3L	2,02E-04	IKBKB	1,21E-06	UIMC1	7,17E-07	Irs3	2,16E-05	RAB1B	1,05E-03
HMGB1	4,59E-08	NTRK1	9,35E-04	ACVRL1	2,03E-03	DMTF1	1,67E-06	RELA	3,56E-04	IRF8	1,26E-06	BRD7	2,00E-06	GFI1	2,24E-05	STAT3	1,12E-03
LETMD1	7,28E-08	EGR1	9,89E-04	NUPR1	2,33E-03	PHF1	2,41E-06	EPHB1	4,08E-04	Ifnar	1,49E-06	miR-221-3p	2,07E-06	TAF4B	3,13E-05	CDK2AP1	1,16E-03
MDM2	1,31E-07	SERCA	1,26E-03	IKZF1	2,86E-03	IRF8	4,95E-06	RPS6KA4	4,08E-04	Ras	1,68E-06	LETMD1	2,85E-06	REL	4,56E-05	SMAD7	1,35E-03
BCAS2	1,82E-07	HEXIM1	1,57E-03	TFAP4	3,09E-03	RELA	5,22E-06	MAPK8	5,67E-04	STK40	1,88E-06	PHF1	3,16E-06	TICAM1	1,09E-04	PIK3R1	1,38E-03

Table 11 - Putative upstream regulators of up-regulated genes upon p53 restoration in Eμ-myc lymphomas.
IPA Upstream Regulator Analysis of up-regulated genes having or not a p53 binding site at the promoter containing the p53-RE in Eμ-*myc* p53ER^{TAM} lymphomas following 4-OHT treatment, and in Eμ-*myc Arf*$^{-/-}$ *Trp53*$^{+/+}$ lymphomas following (-)-Nutlin and doxorubicin treatment relative to controls. Statistical significance and p-values are determined by IPA using a Fisher's Exact Test.

4.2.8 Comparison between the response of B and non-B cells to genotoxic stress and of Eμ-*myc* lymphoma cells to p53 restoration

In the previous paragraphs, we described the response of B and non-B cells to IR and of Eμ-*myc* lymphoma cells to p53 restoration. In both experimental settings, we characterized p53 binding sites and identified a p53-dependent program, both directly and indirectly regulated by p53. Initially, we proceeded to compare p53 binding patterns: all p53 binding sites identified in Eμ-*myc* lymphoma cells were also present in wild-type B and non-B cells upon IR (Fig. 64). p53 binding sites progressively increased from C to P to T to the irradiated samples, initially occupying

prevalently high affinity p53-REs and then progressively spreading to new sites not containing the p53 motif.

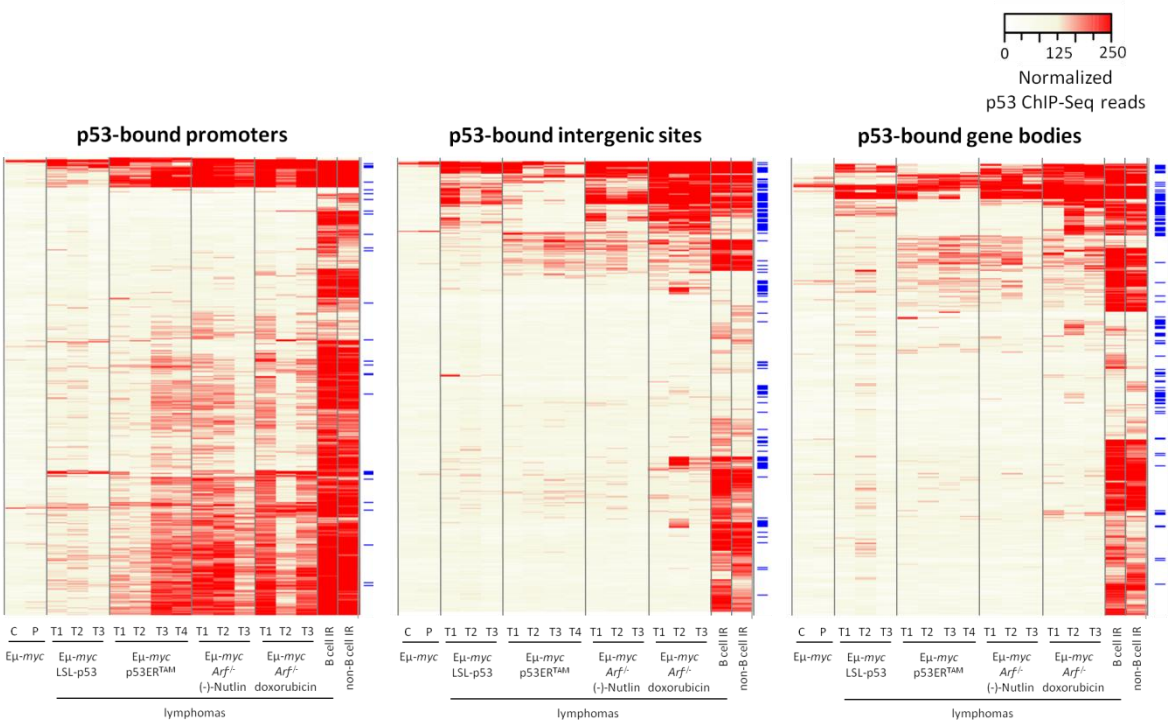

Fig. 64 - Comparison of p53 binding profiles during tumor suppression, regression and in response to acute DNA damage.
Heatmaps showing library size-normalized ChIP-seq read counts for all p53-bound promoters (-5/+2 kb from the TSS), gene bodies (+2 kb from the TSS through 3'UTR) and intergenic regions (everything else) at chromosome 1 in C, P, Eμ-*myc* LSL-p53 lymphomas and Eμ-*myc* p53ER^{TAM} lymphomas upon 4-OHT treatment, Eμ-*myc* *Arf*$^{-/-}$ *Trp53*$^{+/+}$ upon (-)-Nutlin or doxorubicin treatment, B and non-B cells from irradiated animals. Peaks are hierarchically clustered. The occurrence of the p53 motif at the genomic intervals analyzed is calculated by the FIMO algorithm (153) (p-value<1 x 10^{-5}) and indicated with blue lines on the right side of the heatmaps.

We previously described that the transcriptional response to p53 restoration in Eμ-*myc* lymphomas was very similar in the various models, despite differences in the magnitude of expression changes (Fig. 56). B and non-B cells response to IR was instead for a large part cell type-specific with many genes that preferentially responded in one cell type or the other, except for the p53-activated program that constituted the gene set with the highest percentage of common DEGs between B and non-B cells (Fig. 14, Table 2). When we looked at the whole transcriptional response in B and non-B cells following IR and compared it with the expression changes observed upon p53 restoration in Eμ-*myc* lymphoma cells, we noted a group of genes that was strongly up-regulated in all conditions, few genes that moved in opposite directions in lymphomas compared to wild-type cells and many genes that responded in one condition but not

in the other (Fig. 65A). When we removed the p53-independent DEGs from the analysis, we noted a group of genes involved in the response to DNA damage that was up-regulated independently of the cellular context and the upstream stress signal, genes involved in cell adhesion and migration specifically induced following ionizing radiation, while the most repressed genes were implicated in cell cycle and mitosis (Fig. 65B).

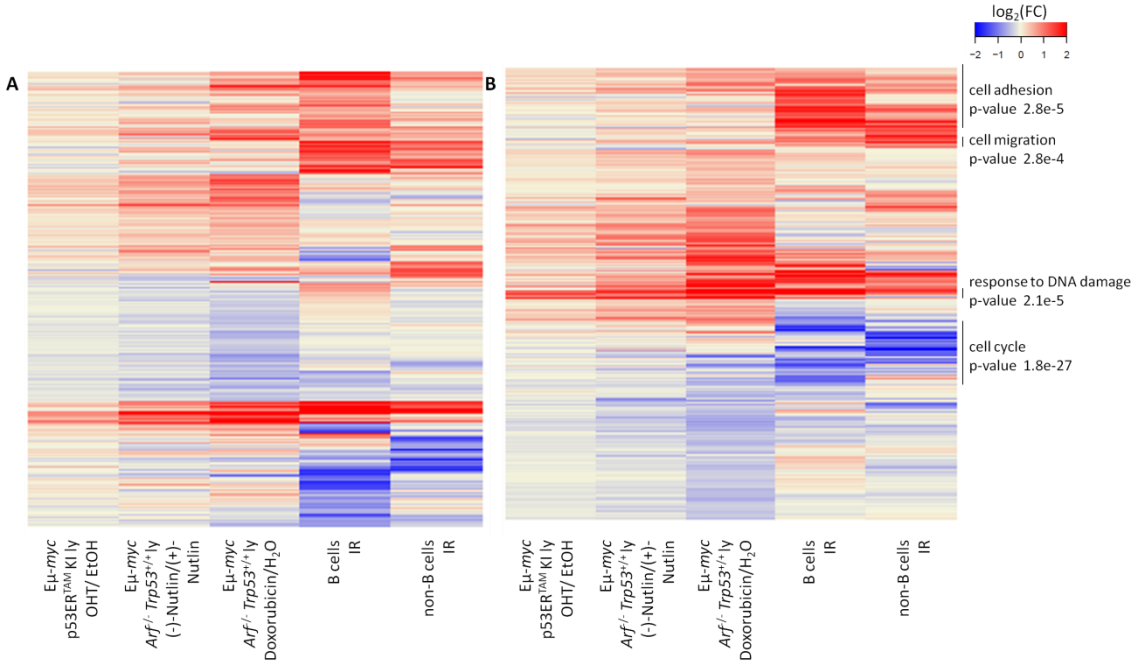

Fig. 65 - All DEGs upon different modes of p53 activation.
Heatmap of relative levels of total mRNA for all DEGs (panel A, n=8598) and all p53-dependent DEGs (panel B, n=7036) upon p53 reactivation in Eμ-*myc* p53ER^{TAM} lymphomas following 4-OHT treatment, in Eμ-*myc Arf*$^{-/-}$ *Trp53*$^{+/+}$ lymphomas following (-)-Nutlin and doxorubicin treatment, and in B and non-B cells following IR relative to controls. The genes are clustered hierarchically on the basis of their differential expression. Biological process GO terms with p-values as calculated by DAVID (154,155) using a modified Fisher exact test are reported.

To explore the directly regulated p53 response, we compared the p53-dependent DEGs that were bound by p53 on the p53-RE in the different experimental models and identified 23 genes that were induced independently of the activating stress and of the cell type, representing the 'default p53 program' (Fig. 66) (158). This list included genes involved in apoptosis, such as *Aen, Pmaip1, Bbc3* and *Lrdd,* cell cycle regulators, such as *Cdkn1a* and *Ccng1*, the negative regulator of p53 *Mdm2*, and several novel p53 target genes. Other genes preferentially responded to one condition and not the other, likely representing stress-specific effectors of the p53 response. All these genes constitute strong candidates to mediate tumor suppression.

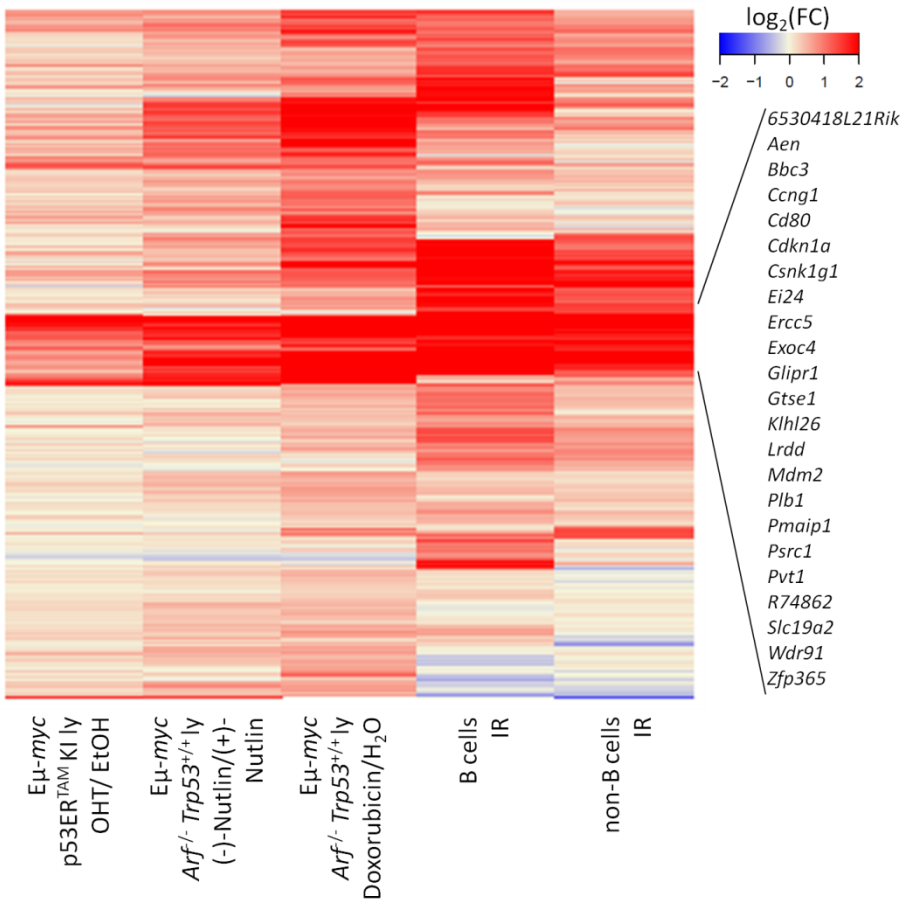

Fig. 66 - Heatmap of all p53-dependent DEGs that are bound by p53 on the p53-RE in Eμ-myc lymphomas upon p53 restoration and in B and non-B cells following IR.
Heatmap of the log_2(FC) (log_2 of fold-change) values of all DEGs (n=333) as estimated by RNA-Seq analysis upon p53 restoration in Eμ-*myc* p53ER^{TAM} lymphomas following 4-OHT treatment, in Eμ-*myc* *Arf*$^{-/-}$ *Trp53*$^{+/+}$ lymphomas following (-)-Nutlin or doxorubicin treatment, and in B and non-B cells following IR relative to controls. The genes identified as direct p53 targets in all experimental models are reported.

Currently, we are testing the impact of some of these p53 target genes on tumorigenesis with a shRNA screen *in vivo,* following the protocol established in the Lowe's lab (171) (Fig. 67). We selected genes that were not previously described as tumor suppressors, prioritizing the ones that were activated in our tumor progression and regression models. We designed an shRNA library using on-chip oligonucleotide synthesis and a barcoding strategy such that the shRNAs could be amplified from the mixture in pools of 55 shRNAs targeting 11 genes (5 shRNAs per gene) for a total of 30 pools. Pre-malignant hematopoietic stem and progenitor cells (HSPCs) from Eμ-*myc* fetal livers ED 12.5-14.5 will be infected with the pools and transplanted in sub-lethally irradiated recipient mice to screen for their ability to increase the lymphomagenic potential. We tested serial dilutions of cells transduced with a green fluorescent protein (GFP)-coupled shRNA against p53 and observed that 2000 transduced cells diluted with uninfected cells were sufficient to

accelerate lymphomagenesis and the resulting lymphomas were GFP positive (Fig. 68). By contrast, a control GFP-tagged scrambled shRNA did not accelerate lymphomagenesis. Once the mice will develop lymphomas, we will extract the DNA, PCR-amplify to isolate the shRNAs and sequence on the Illumina platform. shRNAs that will be kept in the tumor are candidate tumor suppressors and will be subsequently validated. The screening is currently ongoing and hopefully will identify new tumor suppressor genes, paving the way for their therapeutic application.

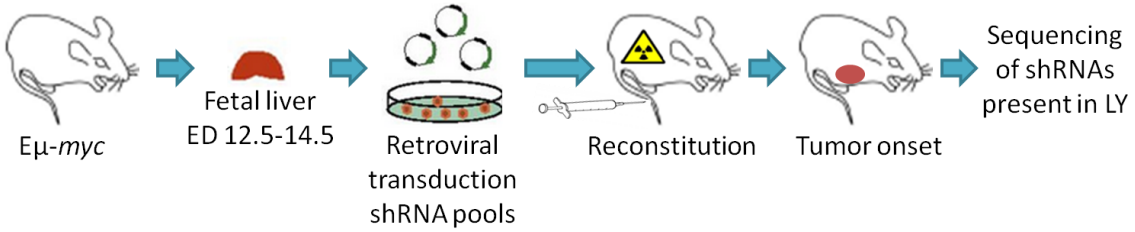

Fig. 67 - Functional screening of candidate gene set in vivo.
Pre-malignant hematopoietic stem and progenitor cells from Eμ-*myc* transgenic mice are infected with pools of shRNAs targeting candidate tumor suppressor genes and transplanted in sub-lethally irradiated recipient mice. The DNA from the resulting lymphomas is PCR-amplified to isolate the shRNAs and sequenced.

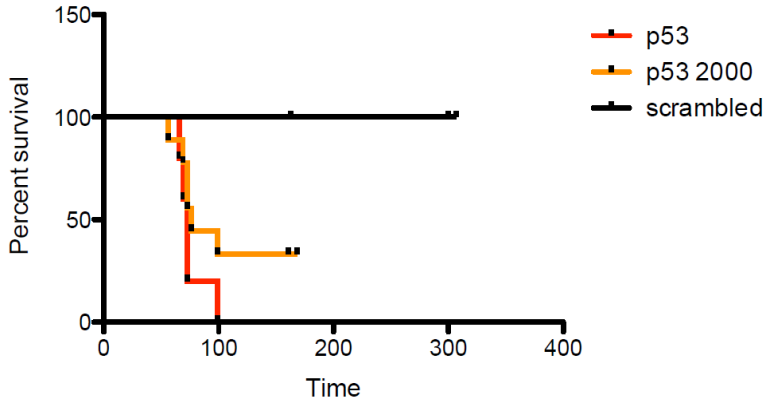

Fig. 68 - Setup of the experimental conditions for functional screening of candidate tumor suppressor genes in vivo.
Survival curves of mice transplanted with HSPCs infected with a neutral shRNA (scrambled, black, n=7), shp53 (p53, red, n=5), or diluted shp53 in order to tail vein inject only 2000 GFP-positive cells (p53 2000, orange, n=9).

5 Discussion

The genetic programs used by the p53 tumor suppressor to direct stress-specific biological responses remain to be clarified. Here, to gain novel insights into p53 function, we combined whole genome mapping of p53 binding and gene expression profiling to investigate the transcriptional circuitry employed by p53 in suppressing cancer development and in response to DNA damage. We studied the progression of Myc-induced lymphomas in Eμ-*myc* transgenic mice, as well as the regression of these lymphomas following restoration of p53 function, by either pharmacological or genetic means. In parallel, we determined the p53-dependent transcriptional program in splenic B and non-B cells of mice exposed to acute DNA damage. Our study revealed novel components of the p53-regulated network and indications of the regulatory mechanisms downstream of p53 activation.

5.1.1 p53 was bound to DNA in unstressed conditions

p53 was already bound to chromatin in unstressed cells, as observed in non-transgenic control mice (C) of the Eμ-*myc* colony and in non-irradiated C57/Bl6 mice. The binding of p53 to chromatin under basal conditions was previously reported in primary cells grown *in vitro* (64,69,78), but culture-associated stress may have constituted an activating stimulus; only recently p53 was shown to play a role under physiological conditions *in vivo* in developing kidney (83). Our data therefore confirmed that p53 was bound to DNA in the absence of any extrinsic stress *in vivo* and suggested that p53 was likely poised for activation at its response elements to provide a fast response to stress, as it had been previously shown for *Cdkn1a* (172,173). It is noteworthy that few p53-binding sites were detected in these conditions, implying that (i.) p53 was present at very low levels and/or (ii.) it was activated in a minority of the cells at any given time. Furthermore, not all of the genes bound by p53 in control conditions became differentially expressed in response to stress, implying a two-stage mechanism whereby p53 binding should be followed by a second layer of regulation, such as the recruitment of cofactors or PTMs, to result in differential expression. For example, acetylation of the DNA binding domain of p53 was shown to play a key role in modulating the expression of p53 target genes, and mutation of the modified

residues completely impaired p53's ability to induce apoptosis, cell cycle arrest and senescence in MEFs (111). Similarly, phosphorylation of p53 at Serine 46 has been proposed to be required for the expression of apoptotic genes (80). Numerous cofactors have been described that can modify the p53 transcriptional program: these binding partners can function either by altering p53 target gene selectivity, or by affecting the ability of p53 to recruit transcriptional co-activators at certain loci (32). The distribution of p53 modifications and cofactors in Myc-induced lymphomas remain to be addressed, and will add an additional layer of information to the data described here.

5.1.2 p53 was bound to a common set of sites irrespective of the type of stimulus and the cellular context

We observed that p53 was bound to the same sites in B cells from control (C) and Eμ-*myc* pre-tumoral mice (P), yet, with higher intensity in the latter. It is most likely that B cells in pre-tumoral mice are a very heterogeneous population for p53 activation: at any time, only a small fraction of the cells may be experiencing oncogenic stress above the threshold required to activate the p53-driven apoptotic pathway (132) and this fraction increases from C to P. Nevertheless, this results in the dilution of the p53 signal, impacting on our sensitivity in detecting p53 binding sites. The number and the binding intensity of p53 peaks increased in tumors in which p53 was experimentally re-activated (T), consistent with the notion that the p53 response amplifies with increasing levels of oncogenic stress (132). The overall p53 binding profiles in the various T samples were very similar, even if we used very different modes to restore p53 function, such as genetic activation, inhibition of Mdm2 with (-)-Nutlin and doxorubicin-induced genotoxic stress. Moreover, almost all of the binding sites in T were retrieved in wild-type B and non-B cells following IR, supporting the hypothesis previously raised by others of a 'default set' of p53 binding sites not influenced by the activating stimulus or the cellular context (67,80,158). On the other hand, these data contradicted a previous study, which observed that p53 in normal cells (IMR90 fibroblasts), was recruited to genomic locations that were significantly different from those occupied in transformed cells (HCT116 colorectal cancer cell and U2OS osteosarcoma cells) (82),

albeit it should be noted that those normal and transformed lines originated from totally different tissues.

Most p53 peaks in C and P contained the canonical p53 motif; the same was observed in Eμ-*myc* LSL-p53 lymphomas where we could identify only the high affinity sites because our sensitivity in detecting p53 binding was affected by the incomplete recombination of the LSL casette. In the remaining tumor samples, as in B and non-B cells following IR, the number of binding sites increased and the p53-RE was less represented. Altogether these ChIP-seq data suggested that endogenous p53 was initially bound to high affinity sites, characterized by the presence of the p53 motif, and then progressively spread to weaker variant sites through DNA scanning or interaction with other DNA binding proteins.

5.1.3 p53 was bound to many distal loci.

In all conditions tested, we observed the presence of p53 binding sites at distant loci. In C, P and Eμ-*myc* LSL-p53 lymphomas, the majority of p53 peaks was located at distal sites, indicating that a large fraction of high affinity p53 sites was not in the promoter-proximal region. A portion of these p53 peaks showed the characteristic features of enhancers (high H3K4me1 and low H3K4me3). Enhancers have been shown to play a central role in p53-mediated gene regulation: on one hand, p53 was described to interfere with enhancer activity to repress the expression of target genes in mESC (78); on the other, it was shown to induce the expression of enhancer RNA to activate target genes in fibroblasts (79). In support of an activating rather than a repressing role of p53 at enhancers, Espinosa and co-workers described the transcription of eRNA from proximal sites (<25 kb from a gene) associated with direct p53-induced genes (86). A more extensive characterization of the role played by p53 at enhancers would advance our understanding of the regulatory mechanisms employed by p53 to regulate tumor suppression: however, this would entail a precise assignment of the enhancers elements identified in B cells to specific genes, through long-range association studies, which is currently being pursued in our group through dedicated collaborations.

Finally, it is noteworthy that not all distant p53 binding sites showed the characteristic chromatin signature of enhancers: we also identified strong p53 peaks in regions devoid of H3K4me3, H3K4me1, or H3K27ac. These sites were high affinity sites, as supported by the identification of the consensus p53 motif, but neither overlapped with previously characterized regulatory regions in B cells (164), nor enriched for RNA-Seq reads. The role played by p53 at these sites is still under investigation: in particular, we hope to obtain some clues by searching for the co-occurrence of other proteins in B cells or other cell types.

5.1.4 p53 binding on the p53-RE nearby the TSS of a gene was predictive of p53-dependent gene regulation.

p53 binding on the p53 motif was systematically present only at the promoters of p53-dependent genes; however, only a fraction of these p53-bound genes was differentially regulated in response to stress. These genes may not be clearly regulated at the time point investigated or require the recruitment of specific cofactors or PTMs for a complete activation.

The observation that p53 binding on the p53-RE nearby the TSS of a gene was predictive of p53-dependent gene regulation, may sound very obvious as the presence of the p53 protein on its RE has been traditionally used as a criteria to define p53 target genes (63). However, these distinctions became evident only upon analysis of ChIP-Seq data with enough sequencing depth, leading to the accurate detection of low-intensity peaks not associated to the canonical p53 motif. For example, without this distinction, we would have missed that p53-mediated repression was likely indirect (discussed below) and that the strongest binding was coupled with the activation of gene expression. In the future, we plan to relax the stringency in searching the p53 motif to study how non-canonical or slightly variant sequences contribute to the p53 response. Binding affinity could allow for a fine-tuning of the response through the regulation of p53 protein levels: for example, it has been shown that the choice between regulating cell cycle arrest and apoptosis is dictated by the presence of high and low affinity sites at the promoter of target genes, respectively (67).

5.1.5 p53-regulated gene network

Combining ChIP-Seq and RNA-Seq analysis, we identified a set of genes directly and indirectly regulated by p53 in Eμ-*myc* lymphomas upon p53 restoration through genetic activation of p53ER^{TAM}, doxorubicin or (-)-Nutlin treatment, and in B and non-B cells following IR. A minor fraction of the p53-dependent genes was bound by p53 on the p53-RE, thus likely representing direct p53 targets; among them, some were induced independently of the activating stress and of the cell type, thereby constituting the 'default p53 program'. However, since most of the p53-dependent response was indirectly regulated, other transcription factors, under direct control of p53, should cooperate to expand the regulatory network. We identified transcriptional regulators, such as *Foxo3*, *Notch1*, *Fos* and several zinc finger proteins that were directly regulated by p53 in Eμ-*myc* lymphomas. FoxO3 belongs to a family of transcription factors involved in longevity and tumor suppression (174,175) and was shown to control the expression of genes involved in apoptosis, cell cycle arrest and DNA repair, including known p53 target genes (174,176). Moreover, FoxO3 itself was described as a p53 target (168). Finally, abrogation of FoxO function using a dominant-negative form of FoxO factors accelerated Myc-driven lymphomagenesis by blocking p53-dependent apoptosis (170). All these evidences suggest that FoxO3 and p53 likely cooperate to achieve tumor suppression. *Fos* and *Notch1* are also known p53 targets (73,169), however less is known about their possible involvement as mediator of the p53 response. Therefore, it would be extremely interesting to characterize if and how FoxO3, Fos and Notch1 contribute to the p53-activated programs in our experimental models. The regulation of p53-dependent genes not directly bound by p53 at the promoter level could be otherwise achieved through enhancers, as previously discussed.

5.1.6 p53-mediated gene repression was largely indirect.

While the role of p53 as a transcriptional activator has been extensively studied, how p53 represses transcription is still a matter of debate. The different modes of p53-dependent transcriptional repression described so far can be grouped in direct (DNA binding-dependent) and indirect (DNA binding-independent) mechanisms. The first ones have been proposed to include

either displacement by p53 of specific activators from promoters due to the presence of overlapping binding sites, interference of p53 with distal enhancer elements, the binding of p53 to unique “repression” response elements, or recruitment by p53 of chromatin-modifying factors, such as histone deacetylases, which then block gene expression (35,78). Our data indicated that repression induced through p53 binding on the p53-RE is not a major component of the global p53 transcriptional program.

p53 may also suppress transcription indirectly by regulating the expression of microRNAs and long non-coding RNAs (177). Our analysis indicated that gene repression of cell cycle and mitosis genes was likely mediated by transactivated gene products such as microRNAs and *Cdkn1a/*p21, which inhibited Cdks, resulting in Rb hypophosphorylation and repression of E2f targets. Moreover, the repression of genes involved in sterol biosynthesis was likely achieved through the impairment of the transcription factors SREBF1 and 2, which were shown to cooperate with mutant p53 to activate the expression of the mevalonate pathway genes, leading to a more invasive and malignant phenotype in breast cancer cells (167). This observation could represent another example of mutant and wild-type p53 opposing functions.

5.1.7 Identification of new putative tumor suppressor genes.

Targeting p53 for tumor eradication is not always possible, therefore the identification of p53 targets that could be activated to restore p53 tumor suppressive function in tumors constitutes a promising new route for cancer therapy. Here, we identified a set of novel p53 target genes that are strong candidates for mediating tumor suppression. A valuable tool to test if these new components of the p53 transcriptional program are important to prevent tumor development is provided by functional genetic screens. RNAi-based experimental tools allow stable gene silencing and can be exploited to mimic gene loss during tumorigenesis in mice, leading to the identification of genes whose knock-down can promote cancer development. We decided to carry out a large scale, phenotype-based screen to examine the consequences of depleting some of the genes we identified on lymphomagenesis. These tools have been already successfully applied to test the impact of silencing candidate tumor suppressors on tumorigenesis (171). Hopefully, this

functional genetic screen will highlight new cancer preventing genes, paving the way for their therapeutic application.

References

1. Hanahan D, Weinberg R. Hallmarks of cancer: the next generation. Cell. 2011; 144(5): p. 646-74.
2. Kress M, May E, Cassingena R, May P. Simian virus 40-transformed cells express new species of proteins precipitable by anti-simian virus 40 tumor serum. J Virol. 1979;(31): p. 472-83.
3. Lane D, Crawford L. T antigen is bound to a host protein in SV40-transformed cells. Nature. 1979; 278(5701): p. 261-3.
4. Linzer D, Maltzman W, Levine A. The SV40 A gene product is required for the production of a 54,000 MW cellular tumor antigen. Virology. 1979; 98(2): p. 308-18.
5. Melero J, Stitt D, Mangel W, Carroll R. Identification of new polypeptide species (48-55K) immunoprecipitable by antiserum to purified large T antigen and present in SV40-infected and -transformed cells. Virology. 1979; 93(2): p. 466-80.
6. Smith A, Smith R, Paucha E. Characterization of different tumor antigens present in cells transformed by simian virus 40. Cell. 1979; 18(2): p. 335-46.
7. DeLeo A, Jay G, Appella E, Dubois G, Law L, Old L. Detection of a transformation-related antigen in chemically induced sarcomas and other transformed cells of the mouse. 1979; 76(5).
8. Rotter V. p53, a transformation-related cellular-encoded protein, can be used as a biochemical marker for the detection of primary mouse tumor cells. Proc Natl Acad Sci U S A. 1983; 80(9): p. 2613-7.
9. Baker S, Fearon E, Nigro J, Hamilton S, Preisinger A, Jessup J, et al. Chromosome 17 deletions and p53 gene mutations in colorectal carcinomas. Science. 1989; 244(4901): p. 217-21.
10. Nigro J, Baker S, Preisinger A, Jessup JHRCK, Bigner S, Davidson N, et al. Mutations in the p53 gene occur in diverse human tumour types. Nature. 1989; 342(6250): p. 705-8.
11. Levine A, Oren M. The first 30 years of p53: growing ever more complex. Nature Reviews

Cancer. 2009; 9(10): p. 749-58.

12. Bargonetti J, Friedman P, Kern S, Vogelstein B, Prives C. Wild-type but not mutant p53 immunopurified proteins bind to sequences adjacent to the SV40 origin of replication. Cell. 1991; 65(6): p. 1083-91.
13. Kern S, Kinzler K, Bruskin A, Jarosz D, Friedman P, Prives C, et al. Identification of p53 as a sequence-specific DNA-binding protein. Science. 1991; 252(5013): p. 1708-11.
14. Farmer G, Bargonetti J, Zhu H, Friedman P, Prywes R, Prives C. Wild-type p53 activates transcription in vitro. Nature. 1992; 358(6381): p. 83-6.
15. Funk W, Pak D, Karas R, Wright W, Shay J. A transcriptionally active DNA-binding site for human p53 protein complexes. Mol Cell Biol. 1992; 12(6): p. 2866-71.
16. Stenger J, Mayr G, Mann K, Tegtmeyer P. Formation of stable p53 homotetramers and multiples of tetramers. Mol Carcinog. 1992; 5(2): p. 102-6.
17. Li F, Fraumeni JJ. Soft-tissue sarcomas, breast cancer, and other neoplasms. A familial syndrome? Ann Intern Med. 1969; 71(4): p. 747-52.
18. Malkin D, Li F, Strong L, Fraumeni JJ, Nelson C, Kim D, et al. Germ line p53 mutations in a familial syndrome of breast cancer, sarcomas, and other neoplasms. Science. 1990; 30(250): p. 1233-8.
19. Srivastava S, Zou Z, Pirollo K, Blattner W, Chang E. Germ-line transmission of a mutated p53 gene in a cancer-prone family with Li-Fraumeni syndrome. Nature. 1990; 348(6303): p. 747-9.
20. Malkin D. Li-fraumeni syndrome. Genes Cancer. 2011; 2(4): p. 475-84.
21. Jacks T, Remington L, Williams B, Schmitt E, Halachmi S, Bronson R, et al. Tumor spectrum analysis in p53-mutant mice. Current Biology. 1994; 4(1): p. 1-7.
22. Donehower L, Harvey M, Slagle B, McArthur M, Montgomery C, Butel J, et al. Mice deficient for p53 are developmentally normal but susceptible to spontaneous tumors. Nature. 1992; 356(6366): p. 215-21.

23. Purdie C, Harrison D, Peter A, Dobbie L, White S, Howie S, et al. Tumour incidence, spectrum and ploidy in mice with a large deletion in the p53 gene. Oncogene. 1994; 9(2): p. 603-9.

24. Petitjean A, Mathe E, Kato S, Ishioka C, Tavtigian S, Hainaut P, et al. Impact of mutant p53 functional properties on TP53 mutation patterns and tumor phenotype: lessons from recent developments in the IARC TP53 database. Hum Mutat. 2007; 28(6): p. 622-9.

25. Brosh R, Rotter V. When mutants gain new powers: news from the mutant p53 field. Nature Reviews Cancer. 2009; 9(10): p. 701-13.

26. Joerger A, Ferscht A. Structural Biology of the Tumor Suppressor p53 and Cancer-Associated Mutants. Advances in Cancer Research. 2007; 97: p. 1-23.

27. Gu W, Shi X, Roeder R. Synergistic activation of transcription by CBP and p53. Nature. 1997; 387(6635): p. 819-23.

28. Gamper A, Roeder R. Multivalent binding of p53 to the STAGA complex mediates coactivator recruitment after UV damage. Mol Cell Biol. 2008; 28(8): p. 2517-27.

29. Momand J, Zambetti G, Olson D, George D, Levine A. The mdm-2 oncogene product forms a complex with the p53 protein and inhibits p53-mediated transactivation. Cell. 1992; 69(7): p. 1237-45.

30. Toledo F, Lee C, Krummel K, Rodewald L, Liu C, Wahl G. Mouse mutants reveal that putative protein interaction sites in the p53 proline-rich domain are dispensable for tumor suppression. Mol Cell Biol. 2007; 27(4): p. 1425-32.

31. Toledo F, Krummel K, Lee C, Liu C, Rodewald L, Tang M, et al. A mouse p53 mutant lacking the proline-rich domain rescues Mdm4 deficiency and provides insight into the Mdm2-Mdm4-p53 regulatory network. Cancer Cell. 2006; 9(4): p. 273-85.

32. Vousden K, Prives C. Blinded by the light: the growing complexity of p53. Cell. 2009; 137(3): p. 413-31.

33. Walker D, Bond J, Tarone R, Harris C, Makalowski W, Boguski M, et al. Evolutionary conservation and somatic mutation hotspot maps of p53: correlation with p53 protein

structural and functional features. Oncogene. 1999; 18(1): p. 211-8.

34. Bieging K, Mello S, Attardi L. Unravelling mechanisms of p53-mediated tumour suppression. Nature Reviews Cancer. 2014; 14(5): p. 359-70.

35. Beckerman R, Prives C. Transcriptional regulation by p53. Cold Spring Harb Perspect Biol. 2010; 2(8): p. 1-18.

36. Hock A, Vousden K. The role of ubiquitin modification in the regulation of p53. Biochim Biophys Acta. 2014; 1843(1): p. 137-49.

37. Oliner J, Pietenpol J, Thiagalingam S, Gyuris J, Kinzler K, Vogelstein B. Oncoprotein MDM2 conceals the activation domain of tumour suppressor p53. Nature. 1993; 362(6423): p. 857-60.

38. Haupt Y, Maya R, Kazaz A, Oren M. Mdm2 promotes the rapid degradation of p53. Nature. 1997; 387(6630): p. 296-9.

39. Honda R, Tanaka H, Yasuda H. Oncoprotein MDM2 is a ubiquitin ligase E3 for tumor suppressor p53. FEBS Lett. 1997; 420(1): p. 25-7.

40. Kubbutat M, Jones S, Vousden K. Regulation of p53 stability by Mdm2. Nature. 1997; 387(6630): p. 299-303.

41. Wu X, Bayle J, Olson D, Levine A. The p53-mdm-2 autoregulatory feedback loop. Genes Dev. 1993; 7(7A): p. 1126-32.

42. Picksley S, Lane D. The p53-mdm2 autoregulatory feedback loop: a paradigm for the regulation of growth control by p53? Bioessays. 1993; 15(10): p. 689-90.

43. Wade M, Li Y, Wahl G. MDM2, MDMX and p53 in oncogenesis and cancer therapy. Nat Rev Cancer. 2013: p. 83-96.

44. Weber J, Taylor L, Roussel M, Sherr C, Bar-Sagi D. Nucleolar Arf sequesters Mdm2 and activates p53. Nat Cell Biol. 1999; 1(1): p. 20-6.

45. Zhou X, Liao J, Liao W, Lu H. Scission of the p53-MDM2 Loop by Ribosomal Proteins. Genes

Cancer. 2012; 3(3-4): p. 298-310.

46. Jones S, Roe A, Donehower L, Bradley A. Rescue of embryonic lethality in Mdm2-deficient mice by absence of p53. Nature. 1995; 378(6553): p. 206-8.

47. Montes de Oca Luna R, Wagner D, Lozano G. Rescue of early embryonic lethality in mdm2-deficient mice by deletion of p53. Nature. 1995; 378(6553): p. 203-6.

48. Parant J, Chavez-Reyes A, Little N, Yan W, Reinke V, Jochemsen A, et al. Rescue of embryonic lethality in Mdm4-null mice by loss of Trp53 suggests a nonoverlapping pathway with MDM2 to regulate p53. Nat Genet. 2001; 29(1): p. 92-5.

49. Tollini L, Jin A, Park J, Zhang Y. Regulation of p53 by Mdm2 E3 ligase function is dispensable in embryogenesis and development, but essential in response to DNA damage. Cancer Cell. 2014; 26(2): p. 235-47.

50. Caelles C, Helmberg A, Karin M. p53-dependent apoptosis in the absence of transcriptional activation of p53-target genes. Nature. 1994; 370(6486): p. 220-3.

51. Haupt Y, Rowan S, Shaulian E, Vousden K, Oren M. Induction of apoptosis in HeLa cells by trans-activation-deficient p53. Genes Dev. 1995; 9(17): p. 2170-83.

52. Comel A, Sorrentino G, Capaci V, Del Sal G. The cytoplasmic side of p53's oncosuppressive activities. FEBS Letters. 2014; 588(16): p. 2600-2609.

53. Vaseva A, Mol lU. The mitochondrial p53 pathway. Biochim Biophys Acta. 2009; 1787(5): p. 414-20.

54. Green D, Kroemer G. Cytoplasmic functions of the tumor suppressor p53. Nature. 2009; 458(7242): p. 1127-30.

55. Vaseva A, Marchenko N, Ji K, Tsirka S, Holzmann S, Moll U. p53 opens the mitochondrial permeability transition pore to trigger necrosis. Cell. 2012; 149(7): p. 1536-48.

56. Brenner C, Moulin M. Physiological Roles of the Permeability Transition Pore. Circulation Research. 2012; 111: p. 1237-47.

57. Berkers C, Maddocks O, Cheung E, Mor I, Vousden K. Metabolic regulation by p53 family members. Cell Metab. 2013; 18(5): p. 617-33.

58. Jiang P, Du W, Wang X, Mancuso A, Gao X, Wu M, et al. p53 regulates biosynthesis through direct inactivation of glucose-6-phosphate dehydrogenase. Nat Cell Biol. 2011; 13(3): p. 310-6.

59. Vousden K, Ryan K. p53 and metabolism. Nat Rev Cancer. 2009; 9(10): p. 691-700.

60. Zhao Y, Chaiswing L, Velez J, Batinic-Haberle I, Colburn N, Oberley T, et al. p53 translocation to mitochondria precedes its nuclear translocation and targets mitochondrial oxidative defense protein-manganese superoxide dismutase. Cancer Res. 2005; 65(9): p. 3745-50.

61. el-Deiry W, Kern S, Pietenpol J, Kinzler K, Vogelstein B. Definition of a consensus binding site for p53. Nat Genet. 1992; 1(1).

62. Menendez D, Nguyen T, Freudenberg J, Mathew V, Anderson C, Jothi R, et al. Diverse stresses dramatically alter genome-wide p53 binding and transactivation landscape in human cancer cells. Nucleic Acids Res. 2013; 41(15): p. 7286-301.

63. Riley T, Sontag E, Chen P, Levine A. Transcriptional control of human p53-regulated genes. Nat Rev Mol Cell Biol. 2008; 9(5): p. 402-12.

64. Lee K, Li M, Michalowski A, Zhang X, Liao HCL, Xu Y, et al. A genomewide study identifies the Wnt signaling pathway as a major target of p53 in murine embryonic stem cells. Proc Natl Acad Sci U S A. 2010; 107(1): p. 69-74.

65. Mathelier A, Zhao X, Zhang A, Parcy F, Worsley-Hunt R, Arenillas D, et al. JASPAR 2014: an extensively expanded and updated open-access database of transcription factor binding profiles. Nucleic Acids Res. 2014; 42: p. D142-7.

66. Inga A, Storici F, Darden T, Resnick M. Differential transactivation by the p53 transcription factor is highly dependent on p53 level and promoter target sequence. Mol Cell Biol. 2002; 22(24): p. 8612-25.

67. Schlereth K, Heyl C, Krampitz A, Mernberger M, Finkernagel F, Scharfe M, et al.

Characterization of the p53 cistrome--DNA binding cooperativity dissects p53's tumor suppressor functions. PLoS Genet. 2013; 9(8): p. 1-15.

68. Zeron-Medina J, Wang X, Repapi E, Campbell M, Su D, Castro-Giner F, et al. A polymorphic p53 response element in KIT ligand influences cancer risk and has undergone natural selection. Cell. 2013; 155(2).

69. Kenzelmann-Broz D, Spano Mello S, Bieging K, Jiang D, Dusek R, Brady C, et al. Global genomic profiling reveals an extensive p53-regulated autophagy program contributing to key p53 responses. Genes & Dev. 2013; 27.

70. Zhao R, Gish K, Murphy M, Yin Y, Notterman D, Hoffman W, et al. Analysis of p53-regulated gene expression patterns using oligonucleotide arrays. Genes Dev. 2000; 14(8): p. 981-93.

71. Cawley S, Bekiranov S, Ng H, Kapranov P, Sekinger E, Kampa D, et al. Unbiased mapping of transcription factor binding sites along human chromosomes 21 and 22 points to widespread regulation of noncoding RNAs. Cell. 2004; 116(4): p. 499-509.

72. Jen K, Cheung V. Identification of novel p53 target genes in ionizing radiation response. Cancer Res. 2005; 65(17): p. 7666-73.

73. Wei C, Wu Q, Vega V, Chiu K, Ng P, Zhang T, et al. A global map of p53 transcription-factor binding sites in the human genome. Cell. 2006; 124(1).

74. Smeenk L, van Heeringen S, Koeppel M, van Driel M, Bartels S, Akkers R, et al. Characterization of genome-wide p53-binding sites upon stress response. Nucleic Acids Res. 2008; 36(11): p. 3639-54.

75. Hermeking H. MicroRNAs in the p53 network: micromanagement of tumour suppression. Nat Rev Cancer. 2012; 12(9): p. 613-26.

76. Huarte M, Guttman M, Feldser D, Garber M, Koziol M, Kenzelmann-Broz D, et al. A large intergenic noncoding RNA induced by p53 mediates global gene repression in the p53 response. Cell. 2010; 142(3): p. 409-19.

77. Guttman M, Amit I, Garber M, French C, Lin M, Feldser D, et al. Chromatin signature reveals

over a thousand highly conserved large non-coding RNAs in mammals. Nature. 2009; 458(7235): p. 223-7.

78. Li M, He Y, Dubois W, Wu X, Shi J, Huang J. Dinstinct regulatory mechanisms and functions of p53-activated genes and p53-repressed DNA damage response genes in embryonic stem cells. Molecular Cell. 2012; 46(1): p. 30-42.

79. Melo C, Drost J, Wijchers P, van de Werken H, de Wit E, Oude Vrielink JER, et al. eRNAs are required for p53-dependent enhancer activity and gene transcription. Mol Cell. 2013; 49(3): p. 524-35.

80. Smeenk L, van Heeringen S, Koeppel M, Gilbert B, Janssen-Megens E, Stunnenberg H, et al. Role of p53 serine 46 in p53 target gene regulation. PLoS One. 2011; 6(3): p. 1-14.

81. Zaccara S, Tebaldi T, Pederiva C, Ciribilli Y, Bisio A, Inga A. p53-directed translational control can shape and expand the universe of p53 target genes. Cell Death Differ. 2014; 21(10): p. 1522-34.

82. Botcheva K, McCorkle S, McCombie W, Dunn J, CW A. Distinct p53 genomic binding patterns in normal and cancer-derived human cells. Cell Cycle. 2011; 10(24): p. 4237-49.

83. Li Y, Liu J, McLaughlin N, Bachvarov D, Saifudeen Z, El-Dahr S. Genome-wide analysis of the p53 gene regulatory network in the developing mouse kidney. Physiol Genomics. 2013; 45(20): p. 948-64.

84. Dimitrova N, Zamudio J, Jong R, Soukup D, Resnick R, Sarma K, et al. LincRNA-p21 activates p21 in cis to promote Polycomb target gene expression and to enforce the G1/S checkpoint. Mol Cell. 2014; 54(5): p. 777-90.

85. Benson E, Mungamuri S, Attie O, Kracikova M, Sachidanandam R, Manfredi J, et al. p53-dependent gene repression through p21 is mediated by recruitment of E2F4 repression complexes. Oncogene. 2014; 33(30): p. 3959-69.

86. Allen M, Andrysik Z, Dengler V, Mellert H, Guarnieri A, Freeman J, et al. Global analysis of p53-regulated transcription identifies its direct targets. eLife. 2014; 3: p. 1-29.

87. Harvey M, McArthur M, Montgomery CJ, Bradley A, Donehower L. Genetic background alters the spectrum of tumors that develop in p53-deficient mice. FASEB J. 1993; 7(10): p. 938-43.

88. Sah V, Attardi L, Mulligan G, Williams B, Bronson R, Jacks T. A subset of p53-deficient embryos exhibit exencephaly. Nat Genet. 1995; 10(2): p. 175-80.

89. Armstrong J, Kaufman M, Harrison D, Clarke A. High-frequency developmental abnormalities in p53-deficient mice. Curr Biol. 1995; 5(8): p. 931-6.

90. Hu W, Feng Z, Teresky A, Levine A. p53 regulates maternal reproduction through LIF. Nature. 2007; 450(7170): p. 721-4.

91. Brady C, Attardi L. p53 at a glance. J Cell Sci. 2010; 123(15): p. 2527-32.

92. Lane D. Cancer. p53, guardian of the genome. Nature. 1992; 358(6381): p. 15-6.

93. Lowe S, Schmitt E, Smith S, Osborne B, Jacks T. p53 is required for radiation-induced apoptosis in mouse thymocytes. Nature. 1993; 362(6423): p. 847-9.

94. Clarke A, Purdie C, Harrison D, Morris R, Bird C, Hooper M, et al. Thymocyte apoptosis induced by p53-dependent and independent pathways. Nature. 1993; 362(6423): p. 849-52.

95. Symonds S, Krall L, Remington L, Saenz-Robles M, Lowe S, Jacks T, et al. p53-dependent apoptosis suppresses tumor growth and progression in vivo. Cell. 1994; 78(4): p. 703-11.

96. Liu G, Parant J, Lang G, Chau P, Chavez-Reyes A, El-Naggar A, et al. Chromosome stability, in the absence of apoptosis, is critical for suppression of tumorigenesis in Trp53 mutant mice. Nature genetics. 2004; 36(1): p. 63-8.

97. Timofeev O, Schlereth K, Wanzel M, Braun A, Nieswandt B, Pagenstecher A, et al. p53 DNA binding cooperativity is essential for apoptosis and tumor suppression in vivo. Cell Rep. 2013; 3(5): p. 1512-25.

98. Deng C, Zhang P, Harper J, Elledge S, Leder P. Mice lacking p21CIP1/WAF1 undergo normal development, but are defective in G1 checkpoint control. Cell. 1995; 82(4): p. 675-84.

99. Brugarolas J, Chandrasekaran C, Gordon J, Beach D, Jacks T, Hannon G. Radiation-induced

cell cycle arrest compromised by p21 deficiency. Nature. 1995; 377(6549): p. 552-7.

100. Martín-Caballero J, Flores J, García-Palencia P, Serrano M. Tumor susceptibility of p21(Waf1/Cip1)-deficient mice. Cancer Res. 2001; 61(16): p. 6234-8.

101. Hollander M, Sheikh M, Bulavin D, Lundgren K, Augeri-Henmueller L, Shehee R, et al. Genomic instability in Gadd45a-deficient mice. Nat Genet. 1999; 23(2): p. 176-84.

102. Jeffers J, Parganas E, Lee Y, Yang C, Wang J, Brennan J, et al. Puma is an essential mediator of p53-dependent and -independent apoptotic pathways. Cancer Cell. 2003; 4(4): p. 321-8.

103. Villunger A, Michalak E, Coultas L, Müllauer F, Böck G, Ausserlechner M, et al. p53- and drug-induced apoptotic responses mediated by BH3-only proteins puma and noxa. Science. 2003; 302(5647): p. 1036-8.

104. Hemann M, Zilfou J, Zhao Z, Burgess D, Hannon G, Lowe S. Suppression of tumorigenesis by the p53 target PUMA. Proc Natl Acad Sci U S A. 2004; 101(25): p. 9333-8.

105. Egle A, Harris A, Bouillet P, Cory S. Bim is a suppressor of Myc-induced mouse B cell leukemia. Proc Natl Acad Sci U S A. 2004; 101(16): p. 6164-9.

106. Michalak E, Jansen E, Happo L, Cragg M, Tai L, Smyth GSA, et al. Puma and to a lesser extent Noxa are suppressors of Myc-induced lymphomagenesis. Cell Death Differ. 2009; 16(5): p. 684-96.

107. Garrison S, Jeffers J, Yang C, Nilsson J, Hall M, Rehg J, et al. Selection against PUMA gene expression in Myc-driven B-cell lymphomagenesis. Mol Cell Biol. 2008; 28(17): p. 5391-402.

108. Barboza J, Liu G, Ju Z, El-Naggar A, Lozano G. p21 delays tumor onset by preservation of chromosomal stability. Proc Natl Acad Sci U S A. 2006; 103(52): p. 19842-7.

109. Brady C, Jiang D, Mello S, Johnson T, Jarvis L, Kozak M, et al. Distinct p53 transcriptional programs dictate acute DNA-damage responses and tumor suppression. Cell. 2011; 145(4).

110. Jiang D, Brady C, Johnson T, Lee E, Park E, Scott M, et al. Full p53 transcriptional activation potential is dispensable for tumor suppression in diverse lineages. Proc Natl Acad Sci U S A. 2011; 108(41).

111. Li T, Kon N, Jiang L, Tan M, Ludwig T, Zhao Y, et al. Tumor suppression in the absence of p53-mediated cell-cycle arrest, apoptosis, and senescence. Cell. 2012; 149(6): p. 1269-83.

112. Valente L, Gray D, Michalak E, Pinon-Hofbauer J, Egle A, Scott C, et al. p53 efficiently suppresses tumor development in the complete absence of its cell-cycle inhibitory and proapoptotic effectors p21, Puma, and Noxa. Cell Rep. 2013; 3(5): p. 1339-45.

113. Sheiness D, Fanshier L, Bishop J. Identification of nucleotide sequences which may encode the oncogenic capacity of avian retrovirus MC29. J Virol. 1978; 28(2): p. 600-10.

114. Meyer N, Penn L. Reflecting on 25 years with MYC. Nat Rev Cancer. 2008; 8(12): p. 976-90.

115. Kamijo T, Weber J, Zambetti G, Zindy F, Roussel M, Sherr C. Functional and physical interactions of the ARF tumor suppressor with p53 and Mdm2. Proc Natl Acad Sci U S A. 1998; 95(14): p. 8292-7.

116. Zindy F, Eischen C, Randle D, Kamijo T, Cleveland J, Sherr C, et al. Myc signaling via the ARF tumor suppressor regulates p53-dependent apoptosis and immortalization. Genes Dev. 1998; 12(15): p. 2424-33.

117. Chen D, Kon N, Zhong J, Zhang P, Yu L, Gu W. Differential effects on ARF stability by normal versus oncogenic levels of c-Myc expression. Mol Cell. 2013; 51(1): p. 46-56.

118. Askew D, Ashmun R, Simmons B, Cleveland J. Constitutive c-myc expression in an IL-3-dependent myeloid cell line suppresses cell cycle arrest and accelerates apoptosis. Oncogene. 1991; 6(10): p. 1915-22.

119. Evan G, Wyllie A, Gilbert C, Littlewood T, Land H, Brooks M, et al. Induction of apoptosis in fibroblasts by c-myc protein. Cell. 1992; 69(1): p. 119-28.

120. Adams J, Harris A, Pinkert C, Corcoran L, Alexander W, Cory S, et al. The c-myc oncogene driven by immunoglobulin enhancers induces lymphoid malignancy in transgenic mice. Nature. 1985; 318(12): p. 533-8.

121. Shen-Ong G, Keath E, Piccoli S, Cole M. Novel myc oncogene RNA from abortive immunoglobulin-gene recombination in mouse plasmacytomas. Cell. 1982; 31(2 Pt 1): p. 443-

52.

122. Crews S, Barth R, Hood L, Prehn J, Calame K. Mouse c-myc oncogene is located on chromosome 15 and translocated to chromosome 12 in plasmacytomas. Science. 1982; 218(4579): p. 1319-21.

123. Dalla-Favera R, Bregni M, Erikson J, Patterson D, Gallo R, Croce C. Human c-myc onc gene is located on the region of chromosome 8 that is translocated in Burkitt lymphoma cells. Proc Natl Acad Sci U S A. 1982; 79(24): p. 7824-7.

124. Neel B, Jhanwar S, Chaganti R, Hayward W. Two human c-onc genes are located on the long arm of chromosome 8. Proc Natl Acad Sci U S A. 1982; 79(24): p. 7842-6.

125. Taub R, Kirsch I, Morton C, Lenoir G, Swan D, Tronick S, et al. Translocation of the c-myc gene into the immunoglobulin heavy chain locus in human Burkitt lymphoma and murine plasmacytoma cells. Proc Natl Acad Sci U S A. 1982; 79(24): p. 7837-41.

126. Eischen C, Weber J, Roussel M, Sherr C, Cleveland J. Disruption of the ARF-Mdm2-p53 tumor suppressor pathway in Myc-induced lymphomagenesis. Genes Dev. 1999; 13(20): p. 533-8.

127. Schmitt C, McCurrach M, de Stanchina E, Wallace-Brodeur R, Lowe S. INK4a/ARF mutations accelerate lymphomagenesis and promote chemoresistance by disabling p53. Genes Dev. 1999; 13(20): p. 2670-7.

128. Strasser A, Harris A, Bath M, Cory S. Novel primitive lymphoid tumours induced in transgenic mice by cooperation between myc and bcl-2. Nature. 1990; 348(6299): p. 331-3.

129. Schmitt C, Fridman J, Yang M, Baranov E, Hoffmann R, Lowe S. Dissecting p53 tumor suppressor functions in vivo. Cancer Cell. 2002; 1(3): p. 289-98.

130. Post S, Quintás-Cardama A, Terzian TSC, Eischen C, Lozano G. p53-dependent senescence delays Emu-myc-induced B-cell lymphomagenesis. Oncogene. 2010; 29(9): p. 1260-9.

131. Reimann M, Lee S, Loddenkemper C, Dörr J, Tabor V, Aichele P, et al. Tumor stroma-derived TGF-beta limits myc-driven lymphomagenesis via Suv39h1-dependent senescence. Cancer Cell. 2010; 17(3): p. 262-72.

132. Murphy D, Junttila M, Pouyet L, Karnezis A, Shchors K, Bui D, et al. Distinct thresholds govern Myc's biological output in vivo. Cancer Cell. 2008; 14(6): p. 447-57.

133. Halazonetis T, Gorgoulis V, Bartek J. An oncogene-induced DNA damage model for cancer development. Science. 2008; 319(5868): p. 1352-5.

134. Shreeram S, Hee W, Demidov O, Kek C, Yamaguchi H, Fornace AJ, et al. Regulation of ATM/p53-dependent suppression of myc-induced lymphomas by Wip1 phosphatase. J Exp Med. 2006; 203(13): p. 2793-9.

135. Campaner S, Amati B. Two sides of the Myc-induced DNA damage response: from tumor suppression to tumor maintenance. Cell Div. 2012; 7(1): p. 1-10.

136. Martins C, Brown-Swigart L, Evan G. Modeling the therapeutic efficacy of p53 restoration in tumors. Cell. 2006; 127(7): p. 1323-34.

137. Macias E, Jin A, Deisenroth C, Bhat K, Mao H, Lindström M, et al. An ARF-independent c-MYC-activated tumor suppression pathway mediated by ribosomal protein-Mdm2 Interaction. Cancer Cell. 2010; 18(3): p. 231-43.

138. Muthalagu N, Junttila M, Wiese K, Wolf E, Morton J, Bauer B, et al. BIM Is the Primary Mediator of MYC-Induced Apoptosis in Multiple Solid Tissues. Cell Rep. 2014; 8(5): p. 1347-53.

139. Ventura A, Kirsch D, McLaughlin M, Tuveson D, Grimm J, Lintault L, et al. Restoration of p53 function leads to tumor regression in vivo. Nature. 2007; 445(8): p. 661-5.

140. Xue W, Zender L, Miething C, Dickins R, Hernando E, Krizhanovsky V, et al. Senescence and tumour clearance is triggered by p53 restoration in murine liver carcinomas. Nature. 2007; 445(7128): p. 656-60.

141. Christophorou M, Martin-Zanca D, Soucek L, Lawlor E, Brown-Swigart L, Verschuren E, et al. Temporal dissection of p53 function in vitro and in vivo. Nature Genetics. 2005; 37(7).

142. Tazawa H, Kagawa S, Fujiwara T. Advances in adenovirus-mediated p53 cancer gene therapy. Expert Opin Biol Ther. 2013; 13(11): p. 1569-83.

143. Khoo K, Verma C, Lane D. Drugging the p53 pathway: understanding the route to clinical efficacy. Nat Rev Drug Discov. 2014; 13(3): p. 217-36.

144. Bykov V, Wiman K. Mutant p53 reactivation by small molecules makes its way to the clinic. FEBS Lett. 2014; 588(16): p. 2622-2627.

145. Kamijo T, Zindy F, Roussel M, Quelle D, Downing J, Ashmun R, et al. Tumor suppression at the mouse INK4a locus mediated by the alternative reading frame product p19ARF. Cell. 1997; 91(5): p. 649-59.

146. Oskarsson T, Essers M, Dubois N, Offner S, Dubey C, Roger C, et al. Skin epidermis lacking the c-Myc gene is resistant to Ras-driven tumorigenesis but can reacquire sensitivity upon additional loss of the p21Cip1 gene. Genes Dev. 2006; 20(15): p. 2024-9.

147. Fellmann C, Hoffmann T, Sridhar V, Hopfgartner B, Muhar M, Roth M, et al. An optimized microRNA backbone for effective single-copy RNAi. Cell Reports. 2013; 5.

148. Li H, Durbin R. Fast and accurate short read alignment with Burrows-Wheeler transform. Bioinformatics. 2009; 25(14): p. 1754-60.

149. Zhang Y, Liu T, Meyer C, Eeckhoute J, Johnson D, Bernstein B, et al. Model-based analysis of ChIP-Seq (MACS). Genome Biol. 2008; 9(9): p. R137.

150. Gentleman R, Carey V, Bates D, Bolstad B, Dettling M, Dudoit S, et al. Bioconductor: open software development for computational biology and bioinformatics. Genome Biol. 2004; 5(10): p. R80.

151. Machanick P, Bailey T. MEME-ChIP: motif analysis of large DNA datasets. Bioinformatics. 2011; 27(12): p. 1696-7.

152. Gupta S, Stamatoyannopoulos J, Bailey T, Noble W. Quantifying similarity between motifs. Genome Biol. 2007; 8(2): p. R24.

153. Grant C, Bailey T, Noble W. FIMO: scanning for occurrences of a given motif. Bioinformatics. 2011; 27(7): p. 1017-8.

154. Huang D, Sherman B, Lempicki R. Systematic and integrative analysis of large gene lists using

DAVID Bioinformatics Resources. Nature Protoc. 2009; 4(1).

155. Huang D, Sherman B, Lempicki R. Bioinformatics enrichment tools: paths toward the comprehensive functional analysis of large gene lists. Nucleic Acids Res. 2009; 37(1).

156. McLean C, Bristor D, Hiller M, Clarke S, Schaar B, Lowe C, et al. GREAT improves functional interpretation of cis-regulatory regions. Nat. Biotechnol. 2010; 28(5).

157. Sabò A, Kress T, Pelizzola M, de Pretis S, Gorski M, Tesi A, et al. Selective transcriptional regulation by Myc in cellular growth control and lymphomagenesis. Nature. 2014; 511(7510): p. 488-92.

158. Nikulenkov F, Spinnler C, Li H, Tonelli C, Shi Y, Turunen M, et al. Insights into p53 transcriptional function via genome-wide chromatin occupancy and gene expression analysis. Cell Death Differ. 2012; 19(12).

159. Polager S, Ginsberg D. p53 and E2f: partners in life and death. Nat Rev Cancer. 2009; 9(10): p. 738-48.

160. Drost J, Mantovani F, Tocco F, Elkon R, Comel A, Holstege H, et al. BRD7 is a candidate tumour suppressor gene required for p53 function. Nat Cell Biol. 2010; 12(4): p. 380-9.

161. Ryan K, Ernst M, Rice N, Vousden K. Role of NF-kappaB in p53-mediated programmed cell death. Nature. 2000; 404(6780): p. 892-7.

162. Maltzman W, Czyzyk L. UV irradiation stimulates levels of p53 cellular tumor antigen in nontransformed mouse cells. Mol Cell Biol. 1984; 4(9): p. 1689-94.

163. Vassilev L, Vu B, Graves B, Carvajal D, Podlaski F, Filipovic Z, et al. In vivo activation of the p53 pathway by small-molecule antagonists of Mdm2. Science. 2004; 303(5659): p. 844-8.

164. Revilla-I-Domingo R, Bilic I, Vilagos B, Tagoh H, Ebert A, Tamir I, et al. The B-cell identity factor Pax5 regulates distinct transcriptional programmes in early and late B lymphopoiesis. EMBO J. 2012; 31(14): p. 3130-46.

165. Kawase T, Ohki R, Shibata T, Tsutsumi S, Kamimura N, Inazawa J, et al. PH domain-only protein PHLDA3 is a p53-regulated repressor of Akt. Cell. 2009; 163(3): p. 535-50.

166. Barna M, Pusic A, Zollo O, Costa M, Kondrashov N, Rego E, et al. Suppression of Myc oncogenic activity by ribosomal protein haploinsufficiency. Nature. 2008; 456(7224): p. 971-5.

167. Freed-Pastor W, Mizuno H, Zhao X, Langerød A, Moon S, Rodriguez-Barrueco R, et al. Mutant p53 disrupts mammary tissue architecture via the mevalonate pathway. Cell. 2012; 148(1-2): p. 244-58.

168. Renault V, Thekkat P, Hoang K, White J, Brady C, Kenzelmann Broz D, et al. The pro-longevity gene FoxO3 is a direct target of the p53 tumor suppressor. Oncogene. 2011; 30(29): p. 3207-21.

169. Elkeles A, Juven-Gershon T, Israeli D, Wilder S, Zalcenstein A, Oren M. The c-fos proto-oncogene is a target for transactivation by the p53 tumor suppressor. Mol Cell Biol. 1999; 19(4): p. 2594-600.

170. Bouchard C, Lee S, Paulus-Hock V, Loddenkemper C, Eilers M, Schmitt C. FoxO transcription factors suppress Myc-driven lymphomagenesis via direct activation of Arf. Genes Dev. 2007; 21(21): p. 2775-87.

171. Scuoppo C, Miething C, Lindqvist L, Reyes J, Ruse C, Appelmann I, et al. A tumour suppressor network relying on the polyamine-hypusine axis. Nature. 2012; 487(7406): p. 244-8.

172. Tang H, Zhao K, Pizzolato J, Fonarev M, Langer J, Manfredi J. Constitutive expression of the cyclin-dependent kinase inhibitor p21 is transcriptionally regulated by the tumor suppressor protein p53. J Biol Chem. 1998; 273(44): p. 29156-63.

173. Espinosa J, Verdun R, Emerson B. p53 functions through stress- and promoter-specific recruitment of transcription initiation components before and after DNA damage. Mol Cell. 2003; 12(4): p. 1015-27.

174. Greer E, Brunet A. FOXO transcription factors at the interface between longevity. Oncogene. 2005; 24(50): p. 7410-25.

175. Paik J, Kollipara R, Chu G, Ji H, Xiao Y, Ding Z, et al. FoxOs are lineage-restricted redundant

tumor suppressors and regulate endothelial cell homeostasis. Cell. 2007; 128(2): p. 309-23.

176. Janky R, Verfaillie A, Imrichová H, Van de Sande B, Standaert L, Christiaens V, et al. iRegulon: from a gene list to a gene regulatory network using large motif and track collections. PLoS Comput Biol. 2014; 10(7).

177. Rinn J, Huarte M. To repress or not to repress: this is the guardian's question. Trends Cell Biol. 2011; 21(6): p. 344-53.